LA-5830-T
Thesis

C.3

UC-34c
Reporting Date: December 1974
Issued: January 1975

Radiochemical Studies of some Low- and Medium-Energy Nuclear Reactions Produced by Accelerated Tritons, Deuterons, and Protons

by

Vito R. Casella*

*Present address: Chemistry Department, Brookhaven National Laboratory, Upton, NY.

los alamos
scientific laboratory
of the University of California
LOS ALAMOS, NEW MEXICO 87544

UNITED STATES
ATOMIC ENERGY COMMISSION
CONTRACT W-7405-ENG. 36

This report is derived from a dissertation submitted to the University of Wyoming, Laramie, WY, in partial fulfillment of the requirements for the Degree of Doctor of Philosophy in Chemistry. The report is the independent work of the author; it has not been edited by the Technical Information Staff.

Work done in LASL's Group CNC-11 with personal support for the author provided by the Associated Western Universities, Inc.

Printed in the United States of America. Available from
National Technical Information Service
U.S. Department of Commerce
5285 Port Royal Road
Springfield, VA 22151
Price: Printed Copy $7.60 Microfiche $2.25

TABLE OF CONTENTS

LIST OF TABLES

LIST OF FIGURES

Abstract

Radiochemical Studies of Some Low- and Medium-Energy Nuclear Reactions Produced by Accelerated Tritons, Deuterons, and Protons

Part I

Excitation functions have been measured for the production of ^{196g}Au, ^{196m}Au, ^{198g}Au, ^{198m}Au, ^{199}Au, ^{195g}Hg, ^{195m}Hg, ^{197g}Hg, ^{197m}Hg and ^{199m}Hg by 6- to 24-MeV deuteron and triton bombardments of stable ^{197}Au. The bombardments employed the stacked-foil technique and were carried out at the Los Alamos Van de Graaff Facility; the radioactive products were determined by measurement of their characteristic gamma-rays on a Ge(Li) detector-pulse height analyzer system. The experimental results have been compared with results of compound-nucleus calculations incorporating pre-equilibrium particle emission.

Part II

E3 isomeric states of ^{93}Y and ^{101}Ag have been discovered. Their half-lives are 0.8 ± 0.04 seconds and 3.12 ± 0.12 seconds, respectively. These activities were produced by short bursts of beam on isotopically enriched targets; the decay γ-rays were measured with a Ge(Li) detector-PHA system operated by a computer arrangement. Hindrance factors for the E3 transitions were calculated and discussed.

Part III

Chemical procedures have been developed for the isolation of spallation-produced radio-yttrium and radiopotassium from molybdenum and vanadium targets, respectively. These procedures incorporate precipitation, solvent extraction, and ion exchange techniques. An overall chemical yield of 96 ± 4% was achieved for yttrium, while the potassium overall chemical yield was 91 ± 3%.

The interaction of 800-MeV protons with a thin vanadium target was studied, and cross sections for the formation of ^{42}K and ^{43}K were measured to be 11 mb and 6 mb, respectively, with an estimated 15% error limit.

PART I

Excitation Functions of Nuclear Reactions of 6-24 MeV Deuterons and Tritons with ^{197}Au.

I. Introduction

The present work was undertaken to measure the total cross sections for formation of products of the reactions of deuterons and tritons with gold at energies from 6-24 MeV. The relationship between the cross section for a nuclear reaction and incident particle energy is called an excitation function. This information has both a practical and a theoretical value. Since gold is frequently used in accelerator systems, for example as beam stops or for beam apertures, the knowledge of reactions produced in it by charged particles is very important. From a fundamental viewpoint, the measured excitation functions can be used to test nuclear reaction theories, which form the basis for calculation of these excitation functions.

Isomerism occurs in nuclei when there is a large angular momentum difference between an upper and a lower state which hinders electromagnetic decay of the former to the point where its half-life becomes appreciable. Although more than one isomeric excited state may be found in a nucleus, usually only one major state with significant half-life is found close to the ground state and is called the metastable isomer.

A new high-spin 2.3-day isomer of ^{198}Au was recently discovered by Cunnane and Daly[1] using deuteron bombardments on enriched ^{200}Hg to produce ^{198m}Au by a (d,α) reaction. Pakkanen, et. al.,[2] published their findings of a 115.2-KeV

transition in ^{198m}Au from ^{197}Au(d,p) and ^{198}Hg(n,p) reactions. These recent discoveries helped generate an interest in medium-energy reactions on gold using deuterons up to 24 MeV (Pakkanen used 12.5-MeV deuterons), and using tritons producing the ^{197}Au(t,d) reaction, which had never been reported previously. The high spins of ^{198m}Au and ^{196m}Au (both have J=12) offer an opportunity to test the effect of angular momentum on product cross section.

There are two models that attempt to predict what happens in those events in which an incident particle reacts with a target nucleus. The compound-nucleus model assumes that an incident particle is captured, and its energy is eventually randomly shared among the nucleons in the compound nucleus, which then de-excites by evaporation of particles and emission of gamma-rays. The direct-interaction model assumes that the incident particle collides with the target nucleus without significantly disturbing its overall structure; only one, or at most a few, nucleons are transferred from projectile to target or vice versa. That is, part of the incident particle is absorbed by the nucleus while the remainder continues on after being deflected. This is known as a stripping reaction. The inverse of stripping, called a pick-up reaction, may also occur. In this case, an incident particle (e.g. a proton) interacts with a nucleon or group of nucleons in the target nucleus forming a complex

particle (e.g. a deuteron), which leaves the target nucleus. These two models, compound-nucleus and direct interaction, represent extremes of nuclear behavior. Evidence from nuclear reaction studies indicate that the actual course of events is usually intermediate between these extremes, and in recent years the compound-nucleus (statistical) models have been modified to take into account pre-compound reactions.[3,4]

Although the experimental measurements were the primary concern of this work, the data obtained were also compared with excitation functions calculated from a compound-nucleus (hybrid) model. Reactions such as $^{197}Au(d,2n)^{197}Hg$ and $^{197}Au(t,3n)^{197}Hg$ would be expected to be fairly well predicted from a compound-nucleus model, while reactions such as $^{197}Au(d,p)^{198}Au$ and $^{197}Au(t,d)^{198}Au$ should be predominantly stripping reactions and have much higher cross sections than predicted by this model.

Some previous cross section measurements of reactions of deuterons with gold have been reported. The earliest published excitation function was by Vandenbosch et. al.[5] for the $^{197}Au(d,2n)^{197}Hg$ reaction for deuteron energies up to 22 MeV. The excitation function for the $^{197}Au(d,p)^{198}Au$ reaction for deuteron energies up to 28 MeV was subsequently reported by Sandoval et. al.[6] and by Nassiff et. al.[7] A more recent determination of the excitation functions for the $^{197}Au(d,2n)^{197}Hg$ and $^{197}Au(d,p)^{198}Au$ reactions for

deuteron energies up to 40 MeV was published by Chevarier et. al.,[8] and they also determined the $^{197}Au(d,4n)^{195}Hg$ and $^{197}Au(d,p2n)^{196}Au$ excitation functions for deuteron energies above 25 MeV. Excitation functions have very recently been measured for $^{197}Au(d,xnyp)$ reactions in the energy range 25 to 86 MeV by Jahn et. al.[9]

An incident particle energy of up to 24 MeV was used in this work, and only the $^{197}Au(d,2n)^{197}Hg$ and $^{197}Au(d,p)^{198}Au$ reactions have been studied over this deuteron energy range. The Los Alamos Van de Graaff Facility provides a capability of accelerating tritons to energies over 20 MeV that is unique in the world. This fact helps explain why no excitation functions of tritons with gold have been previously reported.

II. Experimental

A. Apparatus and Materials

The stacked-foil technique was used to measure total cross sections for all reactions. Very pure gold foil, usually from foil or leaf stock 4-8 mg/cm^2 thick, was cut into discs 1.000 ± 0.002 inches in diameter and weighed to the nearest 0.01 mg. Variations in the weights of foils from adjacent cuts were of the order of 0.5%. Variations of

thickness within a given foil may have been larger, but the diffuseness of the beam on the target greatly reduced these effects by averaging them out. Results of spectrochemical analysis of the foil, performed by Group CMB-1 of the Los Alamos Scientific Laboratory, are presented in Table I.

Stacks of foils were bombarded with deuterons or tritons at selected incident energies. An aluminum catcher foil was placed after each gold foil to absorb reaction products from the preceding gold foil in the stack. The thickness of these catcher foils was chosen so that the energy of the beam would be degraded by a desired amount, and the energy of the incident beam would be appropriate for the next foil following.

The foil stacks were held in a combination target holder and Faraday cup (shown in Figure 1), which was mounted at the end of a beam line from the Los Alamos Van de Graaff Facility (Figure 2). The current from the Faraday cup was fed into a LASL 1000 beam integrator connected to a digital readout. A bias of +300 volts was applied to the suppressor, so that secondary radiations (principally electrons) escaping from the target would not cause an error in the measured beam current. Power dumped in the target holder was typically of the order of 10 watts; this heat load was removed by passing compressed air through the cooling system of the holder. The accelerated ion beam, magnetically and electrostatically focused, struck a more or less uniform area about

Table I

Spectrochemical Analysis of the Gold Foil Used for the Deuteron and Triton Irradiations

Element	Concentration (ppm)	Element	Concentration (ppm)
Ag	200	Mn	<2
Al	15	Mo	<2
B	<6	Na	<100
Ba	<2	Ni	2
Be	2	Pb	<6
Bi	<4	Pd	<10
Ca	10	Pt	<10
Cd	<6	Rh	<10
Co	<2	Ru	<10
Cr	<2	Si	6
Cu	30	Sn	<6
Fi	5	Sr	<2
Ir	<10	Ti	<2
K	<20	V	<2
Li	<2	Zn	<60
Mg	<2		

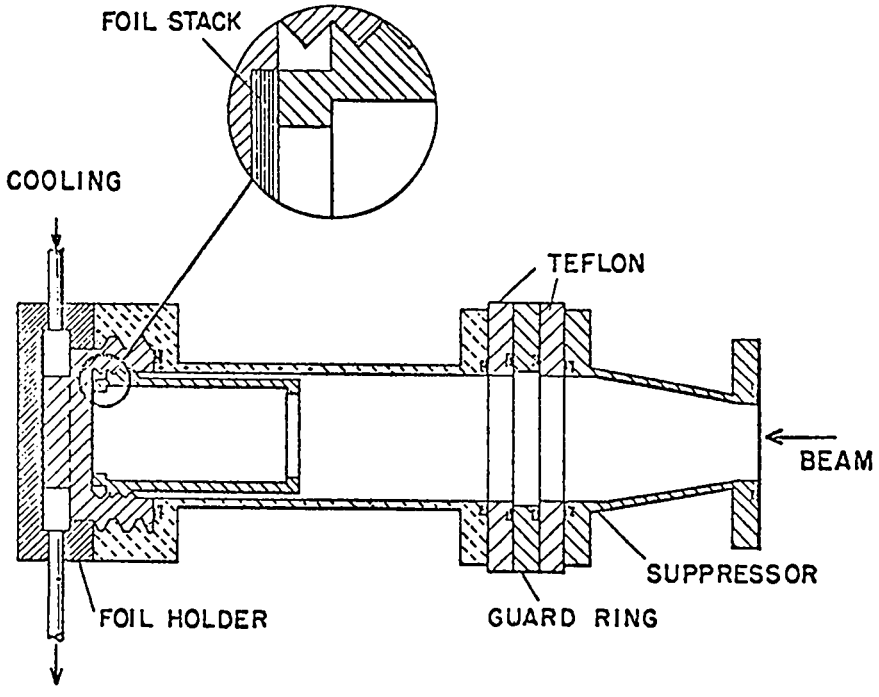

Figure 1. Target Arrangement for Bombardment of a Gold Foil Stack

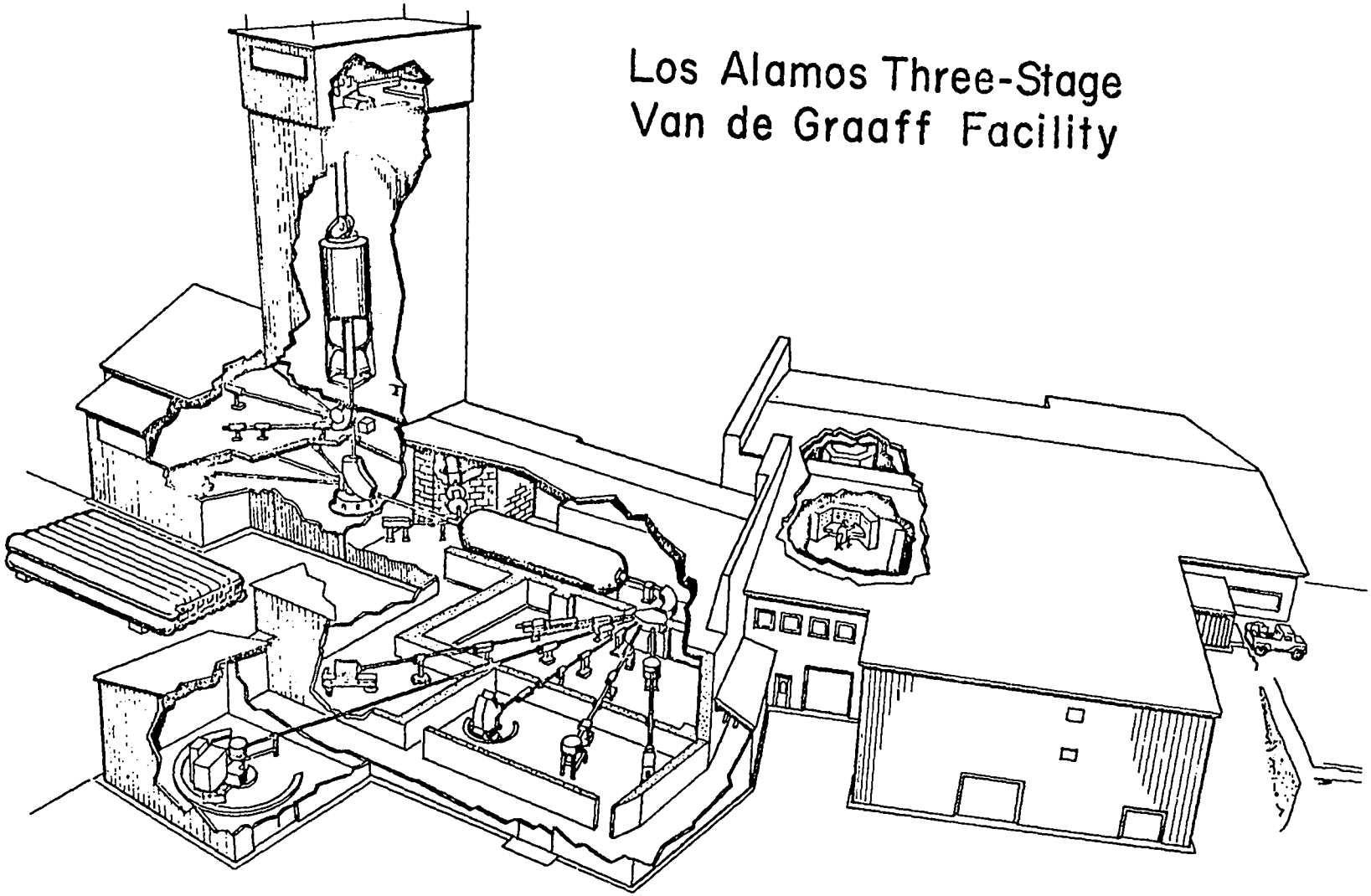

Figure 2. Los Alamos Three-Stage Van de Graaff Facility, Showing Both Vertical and Horizontal (Tandem) Accelerators

3 mm. in diameter on the front of the foil stack. Before each bombardment, the foil holder was replaced by a quartz window which glowed upon irradiation from the incident beam, and a camera-TV remote vision system was set up, such that one could see where the beam was located while tuning was underway.

For energies up to 16 MeV, the Los Alamos horizontal Tandem Van de Graaff accelerator was used; for the 24.5 MeV irradiations the vertical electrostatic accelerator (built at Los Alamos) was used to inject the negative ions into the Tandem Van de Graaff, constituting so-called "3-stage" operation.

B. Counting Equipment and Procedures

1. Cross Section Measurements

Each of the six foil stacks exposed contained from 9 to 12 gold foils and was irradiated with about 0.2 to 0.5 micro-Ampere hours ($\sim 10^{-3}$ Coulombs) of beam. The foils were removed from their holder and centered on rectangular aluminum plates for counting by gamma ray spectrometry on a semiconductor system. All the radionuclides measured were detected by their characteristic x-rays or gamma rays. The detector system consisted of a Canberra closed-end coaxial, cylindrical Ge(Li) crystal of 31 cm^3 active volume. At the ^{60}Co 1.3325 MeV photopeak, this detector has a resolution of 2.07 KeV FWHM, a relative efficiency of 14% (relative to NaI) and

a 41:1 Peak/Compton Ratio. Also included in the spectrometer system were a Geoscience Nuclear Model 7000 multichannel analyzer, and a Canberra Model 8060 analog-to digital converter. The spectra were stored on a magnetic tape by a PDP-9 computer, which also controlled the production of plots by a Calcomp 565 plotter.

The tape-recorded gamma spectra were analyzed on a CDC 6600 computer with the computer program BRUTAL.[10] The computer analysis provided energy and activity information on all statistically significant gamma-ray peaks, and from this data the zero-time activities were calculated.

The zero-time activities for the samples were obtained from a least-squares analysis of the decay data with the computer code SKITZO, which resolved the various decay components in each sample. This code was originally written by Moore and Zeigler,[11] but the program used was a more recent version written by Ford.[12] The function

$$Y_i = \frac{1}{S_i} \sum_{j=1}^{K/2} \frac{A_j(0)}{\lambda_j} \left(e^{-\lambda_j t_i} - e^{-\lambda_j (t_i + S_i)} \right),$$

is fitted to the data by least squares, where t_i is the time the count begins, S_i is the count length, Y_i is the corrected average counting rate observed during the ith counting interval, K is the total number of parameters (half-lives and zero-time activities), and $A_j(0)$ and λ_j are the

zero-time activity and decay constant to be determined for each radioactive species j. Chosen in this way, the function takes into account the decay during each counting interval.

The total number of particles hitting the target was determined by a digital beam integrator connected to the target holder. Table II gives the number of particles calculated for each bombardment.

The relationship of gamma detector efficiency to photon energy was determined for each of several source-detector distances by use of International Atomic Energy Agency standards (Set 64) and Isotope Product Laboratory standards (Set 1235 and Set 14103). The standard gamma-emitter discs were centered on rectangular aluminum plates and counted in the same geometry as the gold foils. The areas of the appropriate gamma spectrum peaks were determined by the computer code BRUTAL,[10] and the efficiency calculations were carried out in the usual way. That is, the efficiency at a given energy, V_γ, is equal to the measured gamma detection rate divided by the gamma emission rate of the source. A representative efficiency vs. energy curve is shown in Figure 3. A least squares fit of the logarithm of gamma efficiency versus the logarithm of gamma energy was performed in the region 200-2000 KeV, using the computer code CAK,[13] which fit this relationship to the formula $V = xE^y$, where V = efficiency, E = energy of photon and x and y are constants. The standard deviation in the least squares fit was

Table II

The Number of Incident Deuterons or Tritons Striking the Foil Stack for Each Bombardment Energy

Energy MeV	Incident Particle	Number of Particles Striking Target
12.000	deuterons	3.0572×10^{16}
12.000	tritons	1.2464×10^{16}
16.000	deuterons	4.8016×10^{15}
16.000	tritons	1.3827×10^{15}
24.400	deuterons	2.4921×10^{15}
24.600	tritons	2.4313×10^{15}

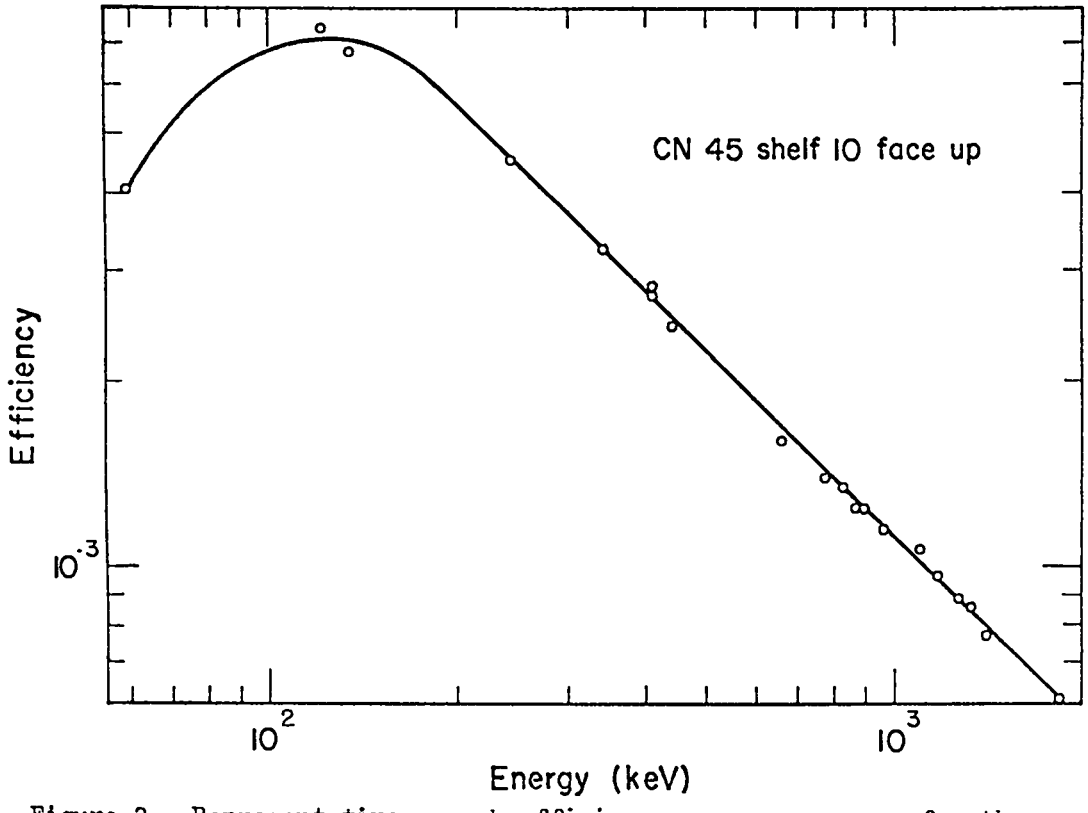

Figure 3. Representative γ-peak efficiency vs energy curve for the germanium detector used in this study at a source distance of 8.90 cm.

calculated as a function of energy between 200 and 2000 KeV, using the following formula, which combines independent and correlated errors:

$$S_V = \sqrt{\left(\frac{\partial V}{\partial x}\right)^2 S_x^2 + \left(\frac{\partial V}{\partial y}\right)^2 S_y^2 + 2\rho_{xy}\left(\frac{\partial V}{\partial x}\right)\left(\frac{\partial V}{\partial y}\right)S_x S_y}$$

The partial derivatives of the equation $V = xE^y$ are $\frac{\partial V}{\partial x} = E^y = \frac{V}{x}$ and $\frac{\partial V}{\partial y} = x(\ln E)E^y$. Since $\rho_{xy}S_xS_y$ is the correlation coefficient, then the standard deviation is calculated as follows:

$$S_V = V\sqrt{\left(\frac{S_x}{x}\right)^2 + (\ln E)^2 S_y^2 + 2\ln E/x\ (C.C.)}$$

The percent error was determined using the equation, % error = 100 S_V/V (68% confidence level). A representative error plot is shown in Figure 4.

This analysis gave the following expressions for the efficiencies of the Ge(Li) detector over the energy range E_γ = 200 - 2000 KeV:

Shelf 15: $V_\gamma = 1.92910 \times 10^{-1}\ E^{-0.96273}$

Shelf 10: $V_\gamma = 1.03611\ E^{-0.98901}$

Shelf 7: $V_\gamma = 4.30938\ E^{-1.04148}$

Shelf 5: $V_\gamma = 1.16473 \times 10^{1}\ E^{-1.09558}$

Shelf 1: $V_\gamma = 4.06952 \times 10^{1}\ E^{-1.14874}$

The cross section (σ) for production of a given reaction following collision of an incident projectile with a target nucleus may be defined in terms of the effective area presented by the target nucleus. Since generally such

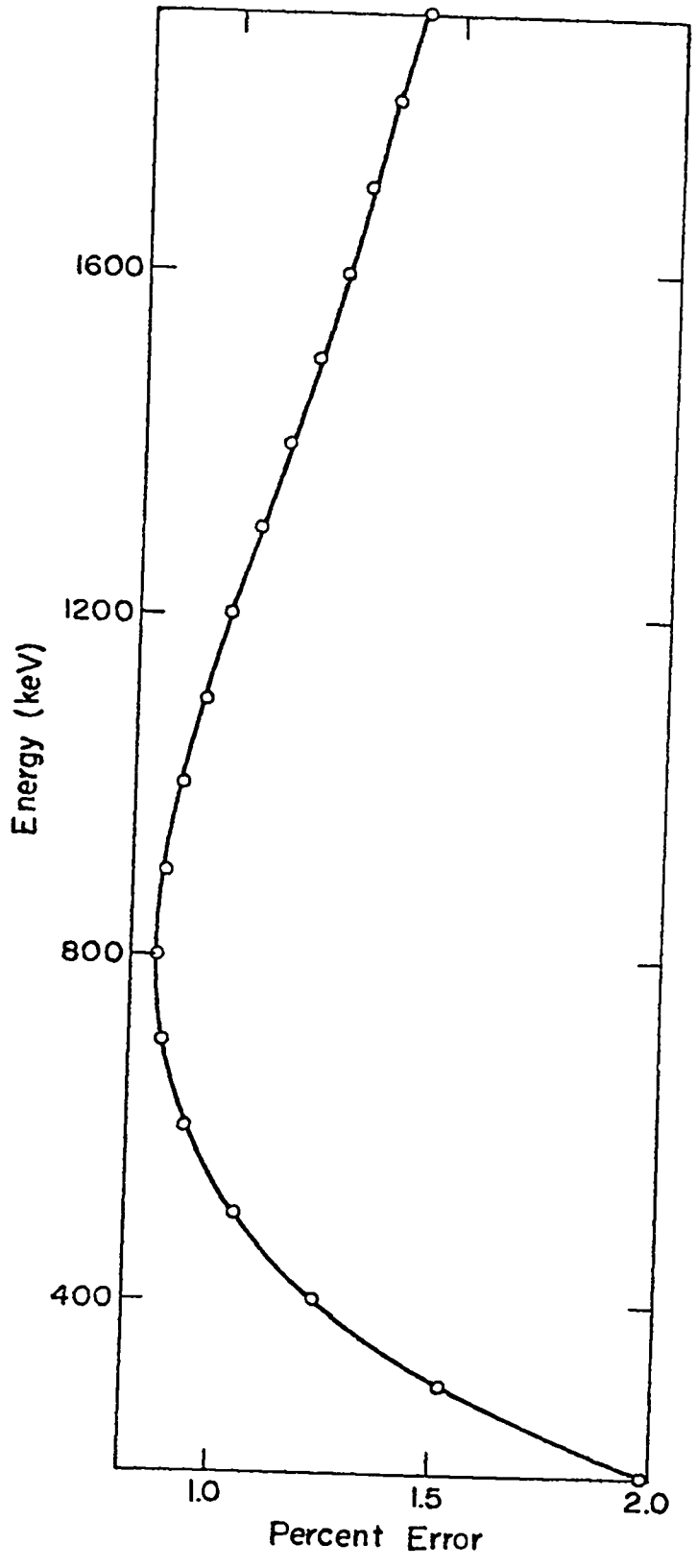

Figure 4. Representative Energy vs Percent Error for efficiencies over the range 200-2000 KeV for a source distance of 8.90 cm.

collisions can give rise to several different kinds of nuclear reactions ("reaction channels"), each kind of reaction has its own cross section at an individual incident particle energy. The total cross section for all reactions is commonly of the order of about 10^{-24} cm^2 = 1 barn. The thin-target cross section is defined by the equation:

$$\sigma = N_p/N_t(It),$$

where N_p is the number of nuclei of a particular isotope produced, N_t is the number of nuclei per square centimeter of the target normal to the beam, and (It) is the total number of incident particles. The amount of a product made is computed from the measured activity:

$$N_p = A_o/\lambda Va,$$

where A_o is the zero-time counts per minute, λ is the decay constant of the nuclide produced, V is the detector efficiency of the gamma ray emitted from the nuclide produced and a (abundance) is the number of photons emitted per decay. The cross section can be calculated by combining the two previous formulas, such that

$$\sigma = A_o/\lambda VaN_t(It).$$

As an example, if one considers the $^{197}Au(d,p)^{198g}Au$ reaction at 11.92 MeV, the cross section for this reaction can be calculated using the 411.8 KeV gamma ray emitted during decay of ^{198g}Au. The activity at zero-time for this gamma ray was determined using the program SKITZO to be

7.5825×10^4 (c/m), the number of target nuclei per cm^2 was 2.409×10^{19}, the number of incident particles was measured to be 1.2464×10^{16}, the efficiency of the detector was 1.5909×10^{-2} and the constants λ and c have been measured to be 1.7841×10^{-4} min^{-1} and 0.9542, respectively. Substituting these values into the previous formula gives a cross section of 9.324×10^{-26} cm^2; i.e., 93.24 millibarns.

For the purpose of simplicity, the zero-time for production of the radioactive species, except ^{199m}Hg, was taken to be the midpoint of the bombardment, and the error introduced was less then 1%. The zero-time activities of ^{199m}Hg were calculated by correcting the activity at the end of bombardment for decay during the irradiation. This correction factor for decay during an irradiation of constant intensity and of duration τ is given as follows:

$$C = \frac{0.693\ \tau/t_{\frac{1}{2}}}{1 - e^{-(0.693\ \tau/t_{\frac{1}{2}})}}$$

2. Energy of ^2H and ^3H in Gold

The midpoint energy of the incident beam for each foil was determined using the Tables of Range and Stopping Power of Chemical Elements for Charged Particles of Energy 0.5 to 500 MeV by Williamson, Boujot and Picard.[14] The range (mg/cm^2) of the incident particles on gold and aluminum are given, and if one subtracts the thickness of the foil (mg/cm^2), these tables can be interpolated to find the energy corresponding to this new thickness (range). This energy is obviously, the average energy of the beam particles

after passing through the foil. The midpoint energy is just the average of the beam energies before and after going through the foil.

As an example of this calculation, consider the case where 11.829 MeV tritons are incidental upon a gold foil of 7.88 mg/cm^2 thickness. The table lists the range for 12.00 MeV tritons as 258.6 mg/cm^2 and for 11.00 MeV tritons as 227.8 mg/cm^2. The energy after passing through this foil is then calculated by interpolation.

$$R_{in} = [(258.6 - 227.8)(.829) + 227.8] = 253.33 \text{ mg/cm}^2$$

$$R_{out} = (253.33 - 7.88) \text{ mg/cm}^2 = 245.45 \text{ mg/cm}^2$$

$$E_{out} = (245.45 - 227.8)/30.8 + 11.0 = 11.573 \text{ MeV}$$

$$E_{MP} = (E_{in} + E_{out})/2 = (11.829 + 11.573)/2 = 11.701 \text{ MeV}$$

3. Determination of ^{197m}Hg and ^{197g}Hg Activities

Since the gamma rays detected for ^{197g}Hg and ^{197m}Hg resulted from rather weak electron-capture decay branches as shown in Figure 5 (^{197m}Hg : 6.3% and ^{197g}Hg : 2.1%), the abundance of these gamma rays, in photons per decay, as based on published decay scheme data could be subject to significant error. Therefore, an additional Van de Graaff irradiation of 16 MeV tritons on gold (7 mg/cm^2) was performed to produce samples of these mercury activities which could be assayed by absolute gamma counting.

After bombardment, the mercury was separated from the gold target using a modification of the method of Friedlander and Wu.[15] A gold foil was dissolved in aqua regia, and after addition of a few milligrams of mercuric carrier, the solution was evaporated to 0.5 ml. on a steam bath. The solution was taken up to 10 ml. in distilled water and extracted twice with 10 ml. volumes of ethyl acetate. The organic phase was stripped twice with 10 ml. aliquots of 3N HCl; this aqueous phase was washed with 20 mls. of fresh ethyl acetate to which 3 drops of 6N HCl had been added. Hydrogen sulfide gas was bubbled through the aqueous solution producing the black precipitate mercuric sulfide. The sulfide precipitate was washed thoroughly with a hard stream of distilled water, which was then decanted. About 10 mls. of 1M HNO_3 was added to the precipitate and heat was applied until boiling began.

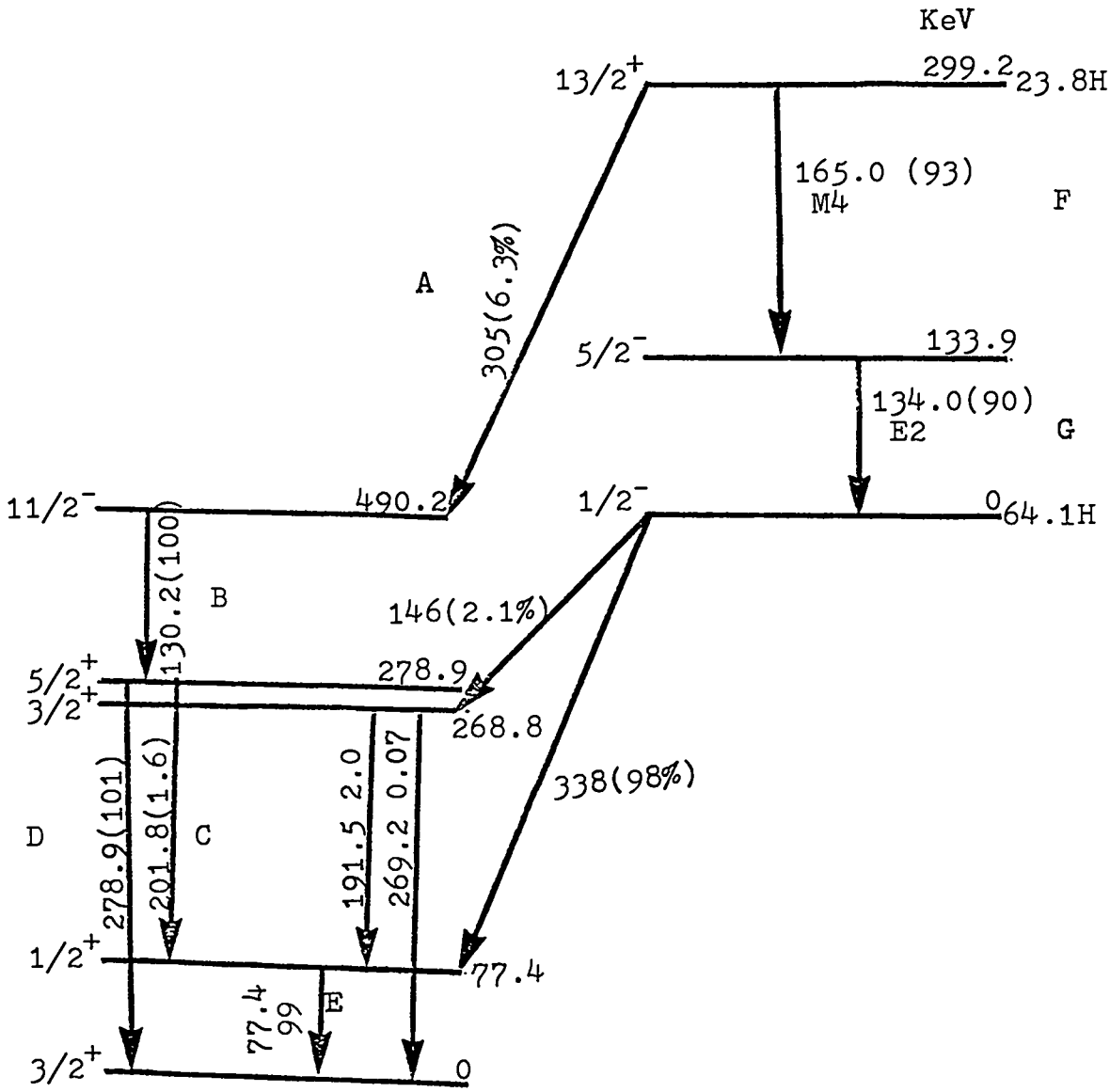

Figure 5. Decay Scheme for ^{197m}Hg and ^{197g}Hg
Transitions Labeled A → G were used for the NaI
Efficiency Calculation of ^{197m}Hg (page 24)

After boiling for about one minute, the solution was centrifuged, and the supernatant was decanted. The precipitate was washed with distilled water and filtered onto a 0.8μ Millipore filter disc. Gamma ray analysis of the precipitate showed that the gold concentration was less than 0.02%.

A portion of the HgS precipitate was placed on a piece of filter paper. This paper was wrapped in Scotch tape and inserted inside a piece of Tygon tubing which was then heat sealed. This sample, containing only mercury activity, was gamma counted, first on the semiconductor system used for all previous counting and then on a "4π" scintillation counter consisting of 5" x 5" NaI well detector and a RIDL 400 channel analyzer, Model 34-12B. The sample was counted for two weeks (about twice a day), and the two-component decay curve was resolved with the computer code CLSQ.[16]

To determine the numbers of ^{197m}Hg and ^{197g}Hg decays, it was necessary to know the detection efficiencies for these transitions with regard to both the energy of the photons observed and from decay scheme considerations. The relationship of total detection efficiency to photon energy had been calculated for the scintillation crystal by a Monte Carlo calculation; this relationship is shown in Figure 6. A small correction was made for the hole in the 4π counter in which the sample was inserted.

The main advantage of using this NaI detector was that the abundances of the mercury activities could be determined

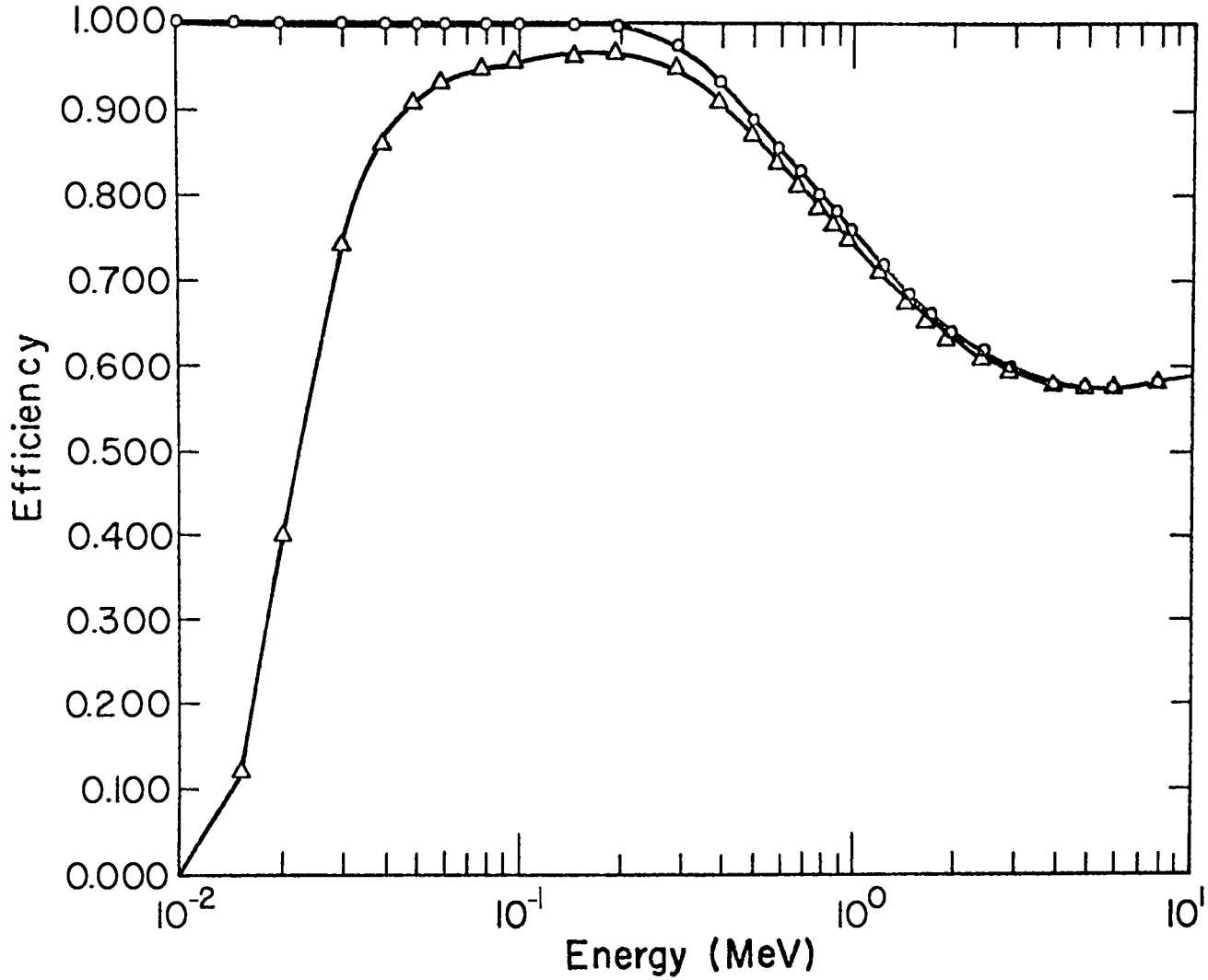

Figure 6. Absolute Total Efficiency vs Photon Energy for 5 x 5 NaI Well Where O Represents the Crystal Efficiency With No Absorber and Δ Represents the Crystal Efficiency With an Aluminum Absorber of .265 Grams/Sq.Cm.

with a minimal amount of decay scheme information, and a very high counting efficiency is usually observed. If one considers a decay event which only yields a single gamma ray, but may be internally converted, then the probability of counting a decay is:

$$P = \frac{1}{1 + \alpha} V_\gamma + \frac{\alpha_K}{1 + \alpha} \omega_K V_K \ ,$$

where α_K and α are the conversion coefficients for K shell conversions and total conversion of the gamma transition, V_γ and V_K are the detector photon efficiencies for the gamma ray and K x-rays emitted, and ω_K is the fluorescence yield of the K x-ray. The first term represents the probability of counting the gamma ray, and the second term represents the probability of counting the K x-ray if the transition is converted (L, M, etc., x-rays are not energetic enough to be detected). For a cascade of two or three gamma rays the probability of counting a decay is equal to one minus the probability of missing all gammas in the cascade, which is one minus the product of the probabilities of not counting each gamma ray in the cascade. If the probabilities of counting each gamma ray in a cascade are represented by P_a, P_b, P_c, etc., then for a two photon cascade the probability, P_T, of counting a decay equals

$$P_T = 1 - (1 - P_a)(1 - P_b) = P_a + P_b - P_a P_b \ ,$$

and correspondingly for a three photon cascade,

$$\begin{aligned} P_T &= 1 - (1 - P_a)(1 - P_b)(1 - P_c) \\ &= P_a + P_b + P_c + P_a P_b - P_a P_c - P_b P_c + P_a P_b P_c . \end{aligned}$$

In the case where a decay occurs by electron capture the probability of observing a K x-ray is:

$$P_{EC} = \frac{K_{capt}}{\text{total capt}} \omega_K V_K \ ,$$

where ω_K is the fluorescence yield of the K x-ray, V_K is the detector photon efficiency and K/total is the ratio of K x-rays to total x-rays emitted (K + L + M + N. . .).

As an example of these calculations the probability of detecting ^{197m}Hg decay, $E(^{197m}Hg)$, with the 5" x 5" NaI detector, considering the photon energy and decay scheme of the isomer (Figure 5) is calculated as follows:

$$E(^{197m}Hg) = 0.063 \left[1 - (1 - P_A)(1 - P_B)(1 - P_{CD})\right] + 0.937 \left[1 - (1 - P_F)(1 - P_G)\right]$$

where, $P_A = \frac{K_{capt}}{\text{total capt}} \omega_K V_K$,

$$P_B = \frac{1}{1 + \alpha_{130}} V_{130} + \frac{K130}{1 + \alpha_{130}} \omega_K V_K,$$

$$P_{CD} = 0.016 \left[1 - (P_C + P_E - P_C P_E)\right] + 0.984 \left[1 - P_D\right]$$

$$P_C = \frac{1}{1 + \alpha_{202}} V_{202} + \frac{K202}{1 + \alpha_{202}} \omega_K V_K$$

$$P_D = \frac{1}{1 + \alpha_{279}} V_{279} + \frac{K279}{1 + \alpha_{279}} \omega_K V_K$$

$$P_E = \frac{1}{1 + \alpha_{77}} V_{77} + \frac{K77}{1 + \alpha_{77}} \omega_K V_K$$

$$P_F = \frac{1}{1 + \alpha_{165}} V_{165} + \frac{K165}{1 + \alpha_{165}} \omega_K V_K$$

$$P_G = \frac{1}{1 + \alpha_{134}} V_{134} + \frac{K134}{1 + \alpha_{134}} \omega_K V_K$$

The values used in this equation were gotten from Bambynek, et. al.[17] and from Nuclear Data Sheets.[18] The probability of seeing a ^{197m}Hg decay was found to be 0.624, and the probability of seeing a ^{197g}Hg decay was calculated in the same manner to be 0.759.

Both parent and daughter mercury activities were detected by scintillation counting, while only the daughter (^{197g}Hg) activity was detected for the 191.5 KeV transition by semiconductor counting. The general equation which describes the case where a radioactive daughter was formed in the decay of its parent is derived[19] to be

$$A_2 = \left[\frac{\lambda_2}{\lambda_2 - \lambda_1} A_1^o a_1 V_1 e^{-\lambda_1 t} + \left(-\frac{\lambda_2}{\lambda_2 - \lambda_1} A_1^o + A_2^o\right) a_2 V_2 e^{-\lambda_2 t}\right]$$

where A_1^o, a_1, V_1 and λ_1 are the detected activity in cpm, abundance (photos/decay), detector efficiency for a particular energy photon and decay constant (min^{-1}) of the parent activity, respectively. The subscript 2 refers to the same quantities for the daughter activity. This equation applies when only a daughter activity is observed as in the case of detecting the 191.5 KeV ^{197g}Hg peak. However, both daughter and parent mercury activities were detected with the scintillation counter, and for this case, the first term of the previous equation becomes $\left(E_1 A_1^o + E_2(.93)\frac{\lambda_2}{\lambda_2 - \lambda_1} A_1^o\right) e^{-\lambda_1 t}$, where A_1 and A_2 are the detected activities of ^{197m}Hg and ^{197g}Hg, E_1 and E_2 are the probabilities of detecting the

^{197m}Hg and ^{197g}Hg decays, which were previously determined to be 0.624 and 0.759, and 0.93 is included since only 93% of the ^{197m}Hg decays directly to ^{197g}Hg.

The abundances of the observed mercury transitions were determined using the relationships of the previous equations. The metastable state abundance was found to be .0424 photons/decay for the 279 KeV transition, and the ground state abundance was found to be .00803 photons/decay for the 191.5 KeV transition. Values calculated from decay scheme data are .0449 and .00922, respectively. The values of the ^{197m}Hg abundance calculated from decay scheme data and determined in this work agree very well, but a very significant difference is seen in these values for ^{197g}Hg. This is to be expected, since the 191.5 KeV transition of ^{197g}Hg decay is produced by a 2.1% electron capture branch of the total decay, and the transition is highly converted (α = 1.17). The determination of the abundance of ^{197g}Hg(191.5 KeV) in this work provided a much more accurate value than could be gotten from decay scheme data.

4. Error Analysis

The following experimental errors contributed to the total error in the excitation function measurements. Total charge measurements using the Faraday cup and beam integrator are of the order of 1-2%. The original Van de Graaff bombardment energies were known to about .003 MeV, and errors for the incident particle energy within the stacks are

estimated to be ±.03 MeV. Errors in the weights and diameter of the foils were less than 1%, but the nonuniformity of the foil in the area where the beam struck will probably increase the error for the foil thickness to about 1-2%. Gamma ray peak analysis, using the computer program BRUTAL,[10] resulted in errors of 1-2% for the peaks which had good counting statistics and were well resolved; however, for low counting statistics and/or poorly resolved peaks, this error may have been as high as 5-20%. Since each foil was counted many times resulting in many determinations of each gamma ray peak, and these determinations were analyzed by a least squares fit to calculate the zero-time activities, the error in the final zero-time activities is significantly less than for one peak area determination. In general, the detector efficiencies were known to be better than 3% for the gamma ray peaks used. The beam attenuation for all irradiations was estimated to be less than 0.5%.

The experimental errors generally amounted to about 8-10%. Only for the most unfavorable cases of low counting statistics and poor γ-ray resolution, the experimental errors were about 20%. The absolute errors for these measurements depend on the decay scheme data used which are given in Table III of the next section.

The amount of competing (n,xn) reactions, which are due to the presence of high-energy neutrons and lead to the same final nuclei as the corresponding charged particle reactions,

was believed to be small. At a deuteron energy of 6.54 MeV, the cross section for producing ^{196g}Au is only 0.075 mb., which implies that very little (n,2n) reaction took place in the foil stack.

III. Calculation of Theoretical Excitation Functions Produced by Compound-Nucleus Reactions

A. Optical Model Calculations

In the single particle model (shell model) of the nucleus, each nucleon is considered to move in a potential well which is generated from the average interaction of all nuclei in the nucleus. The motion of any nucleon is assumed to be undisturbed by the presence of all other nucleons to the extent that they are collectively responsible for the very existence of the potential well. The direct interaction of an incident particle with a scattering nucleus uses this concept. When a target is bombarded with a beam of particles, some of the particles cause a nucleon in the target nucleus to be promoted to a higher energy (inelastic scattering), in other cases the target nucleons are left unchanged (elastic scattering), while other incident particles are absorbed in the target nucleus forming compound nuclei. If a potential well of depth U(MeV) represents the interaction of the particle with the nucleus, only elastic scattering can occur. This is shown in most elementary texts[20] by substituting the potential U into the one dimentional Schrodinger equation,

resulting in no absorption. Therefore, to include all other types of processes together with elastic scattering a potential well having both a real and an imaginary part is necessary.

The new potential is described by the formula

$$U = U_0 + iW_0,$$

where U_0 represents the real part of the potential and W_0 represents the imaginary part of the potential. The value of W_0 is directly related to absorption; such that, a large value of W_0 corresponds to a short mean free path of the incident particles (of a particular kinetic energy) in the target nucleus resulting in strong absorption.

Usually a very sophisticated potential is used to describe the optical-model potential, and optical-model parameters are included, which can be varied to obtain a better fit to experimental data. If all the parameters entering such a complicated potential were treated as free, most experiments could be fitted, and the fit would be meaningless. Therefore, it has become customary to carry out analysis with somewhat restricted forms of the potential.

The optical-model parameters used to calculate the total reaction formation cross sections as a function of energy were taken from the work of Fricke and Satchler[21] The computer code OPTIC[22] was used to calculate these cross sections up to an energy of 25 MeV.

The optical model is used to calculate reaction formation cross sections. To determine what residual product nuclei are produced in the reaction, it is necessary to follow how the excited compound nucleus dissipates its initial excitation energy.

B. Pre-Equilibrium-Statistical (Hybrid) Model

A hybrid combination of existing statistical (compound-nucleus) and pre-equilibrium models was used to calculate the reaction cross sections of deuterons and tritons with gold. The statistical model assumes that an incident particle is captured, and its energy is randomly shared among the nucleons in the compound nucleus, which then de-excites by evaporation of particles and emission of gamma rays. A pre-equilibrium process was proposed by Griffin[23] to describe the compound-nucleus before equilibrium is reached.

In this model the incident particle and the target nucleus are assumed to form a complex state. This state is characterized by the total number of protons, neutrons and holes sharing the excitation energy, which is known as the initial exciton number (Figure 7). The system is assumed to equilibrate through a series of two-body collisions allowed by the Pauli principle. As a result of these collisions, the total exciton number can remain unaltered or change by two units corresponding to the creation or annihilation of a particle-hole pair. The probability for particle emission

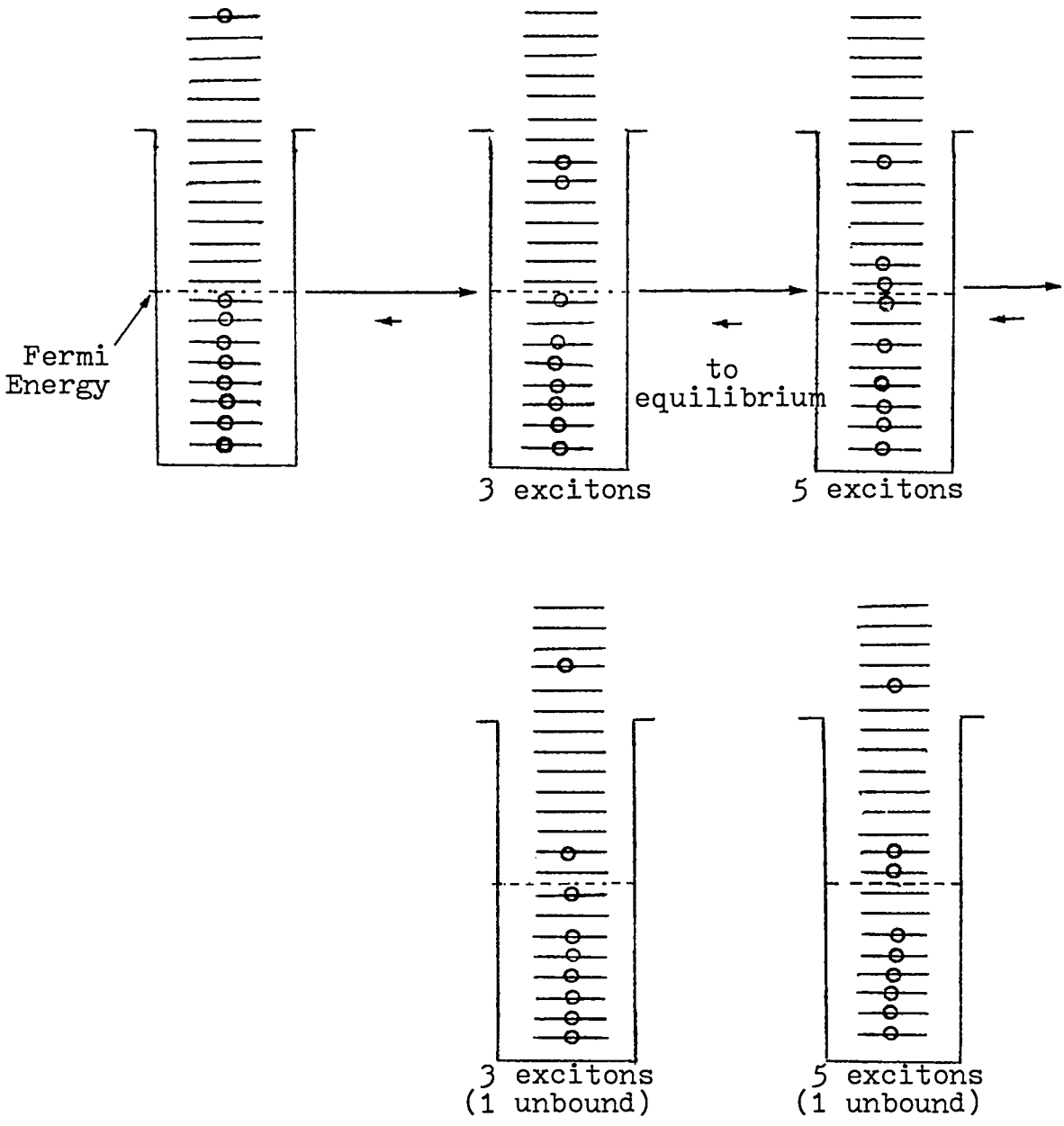

Figure 7. The first few stages of a reaction in the pre-equilibrium model. The particles are shown as circles and the horizontal lines are equally spaced single particle states in the potential well.

at each intermediate state is calculated, depending only on the available phase space and the branching ratio to more complex states with higher exciton number. The transition rate for internal transitions (from n-exciton state to the n + 2 state) was determined from calculations by Kikuchi and Kawai[24] of the average mean free path of excited nucleons in matter. These values were obtained from nucleon-nucleon scattering cross sections.

Since intermediate state densities as in the exciton model and transition times based on nucleon-nucleon scattering data are used for calculation of reaction cross sections, this is called the hybrid model.

The computer program ANREAC[25] was used to calculate the theoretical excitation functions by determining the possibilities of particle and multi-particle emission both for pre-equilibrium emission and for emission from equilibrated systems. An intensity of the emitted particles is calculated for each reaction and divided by the intensity for all reactions. The total reaction cross section gotten from an optical model calculation is multiplied by this fraction to obtain the residual product reaction cross section for each incident particle energy desired.

IV. Results and Discussion

A. Gamma Emitters Produced

After the Van de Graaff irradiations, the target foils were gamma counted as previously described. Representative gamma ray spectra are shown in Figures 8 and 9 of deuteron (E_{MP} = 24.3 MeV) and triton (E_{MP} = 24.5 MeV) irradiated gold foils. All statistically significant peaks in these spectra were identified with respect to the gamma emitters produced during the bombardments. Cross sections were determined for all identified nuclides over the energy range studied.

The gamma ray energies and abundances and the half-lives for the various product nuclei are shown in Table III. The references for the decay data in this table are shown in parentheses.

B. Excitation Functions for the $^{197}Au(d,x)$ and $^{197}Au(t,x)$ Reactions

1. $^{197}Au(t,d)^{198m}Au$, $^{197}Au(t,d)^{198g}Au$ and $^{197}Au(t,p)^{199}Au$

The values of the experimental cross sections and incident particle energies are given in Table IV for these reactions. Experimental and theoretical excitation functions are compared in Figure 10. The theoretical excitation function includes both metastable and ground state products formed by compound-nucleus reactions. These experimental reactions are shown as (t,d) reactions; however, (t,pn) and (t,np) reactions also occur and are the main reaction channels

Table III

Decay Data of the Residual Nuclei
from Triton and Deuteron Irradiations on ^{197}Au

Residual Nucleus	Half-life	E_γ (KeV)	Abundance (Photons per decay)
^{195m}Hg	40.0h (26)	180.1 (27) 261.8 (27) 387.9 (27) 560.2 (27)	0.341 (27)
^{195g}Hg	9.5h (28)	200.4 (29) 207.1 (29)	0.0175 (29)
^{196m}Au	9.7h (30)	147.8 (30) 168.3 (30) 285.5 (30) 316.2 (30)	0.446 (30)
^{196g}Au	6.183d(31)	333.0 (32) 355.7 (32) 426.0 (32)	0.876 (32)
^{197m}Hg	23.8h (33)	134.0 (33) 165.0 (33) 278.9 (33)	0.0424 (34)
^{197g}Hg	64.1h (35)	191.5 (35)	0.00803(36)
^{198m}Au	2.32d (37)	180.0 (37) 204.1 (37) 215.0 (37) 333.5 (37)	0.771 (38)
^{198g}Au	2.698d(39)	411.8 (40)	0.954 (40)
^{199}Au	3.139d(41)	158.4 (41) 208.2 (41)	0.396 (41)
^{199m}Hg	42.6M (42)	158.4 (42) 374.1 (42)	0.493 (42)
^{28}Mg	21.07h(43)	400.6 (44)	0.361 (44)

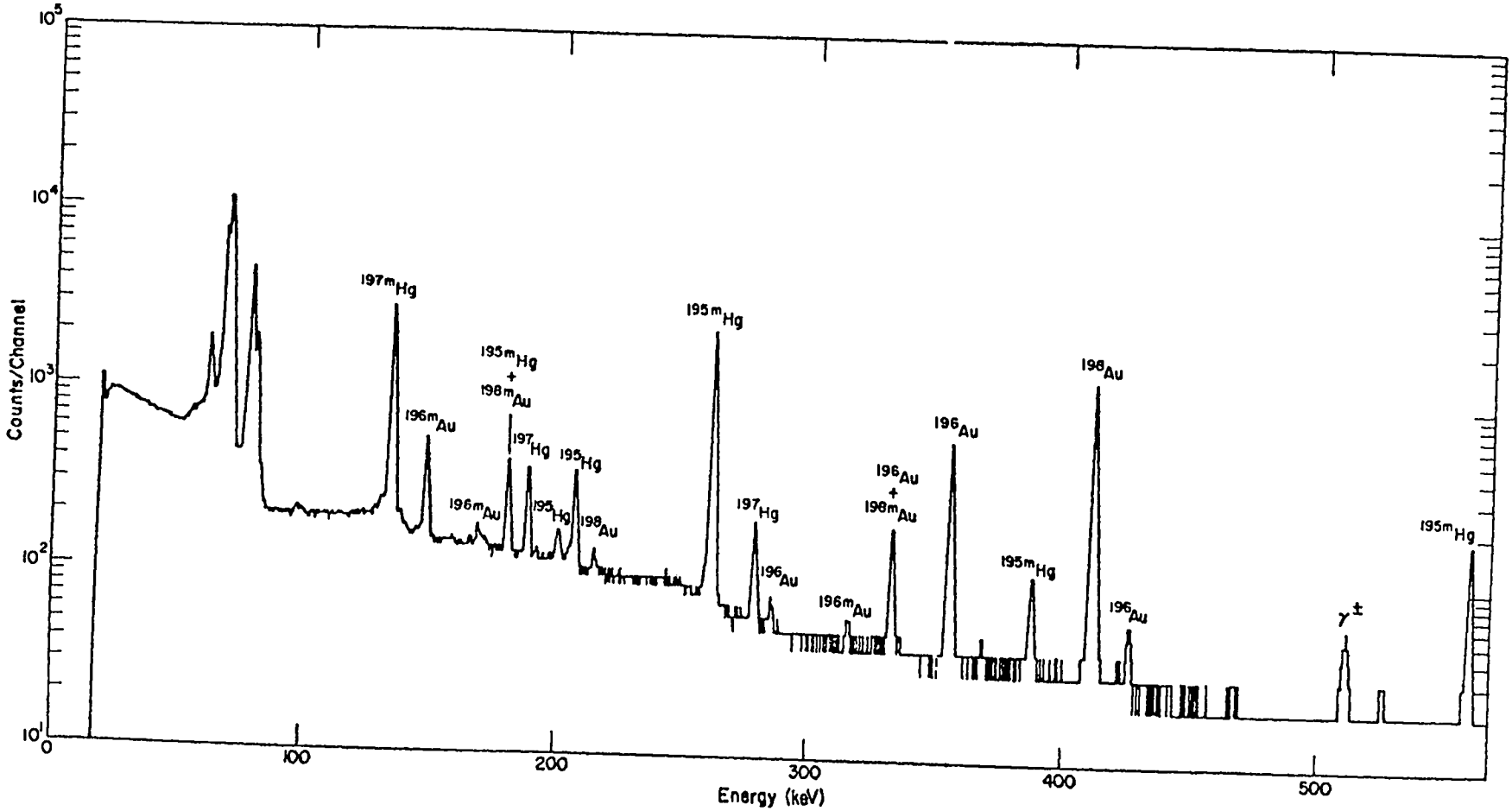

Figure 8. γ-Ray Spectrum of Au Irradiated with 24.29 MeV Deuterons taken 27 Minutes after Bombardment.

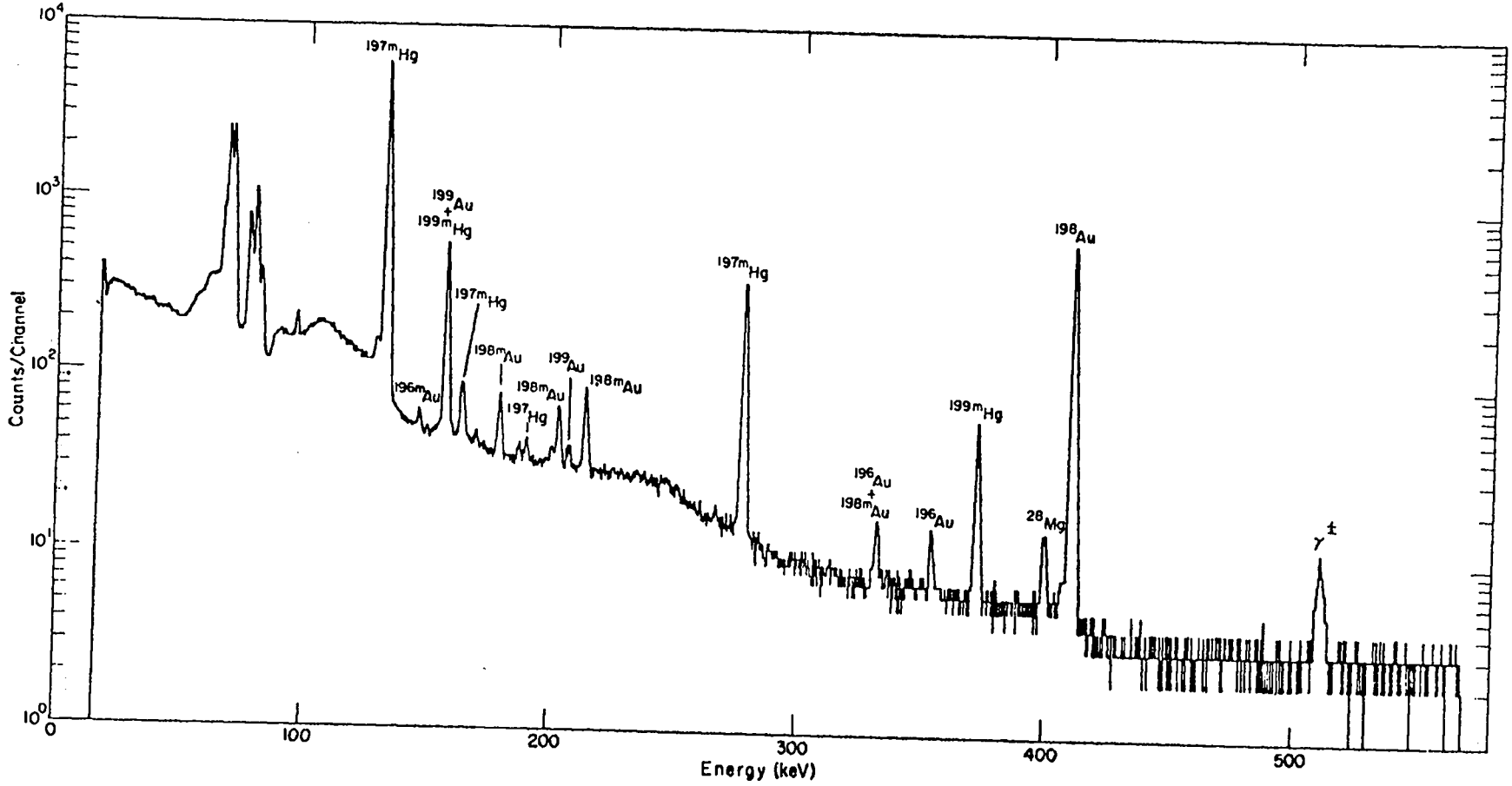

Figure 9. γ-Ray Spectrum of Au Irradiated with 24.45 MeV Tritons, taken 32 Minutes after Bombardment.

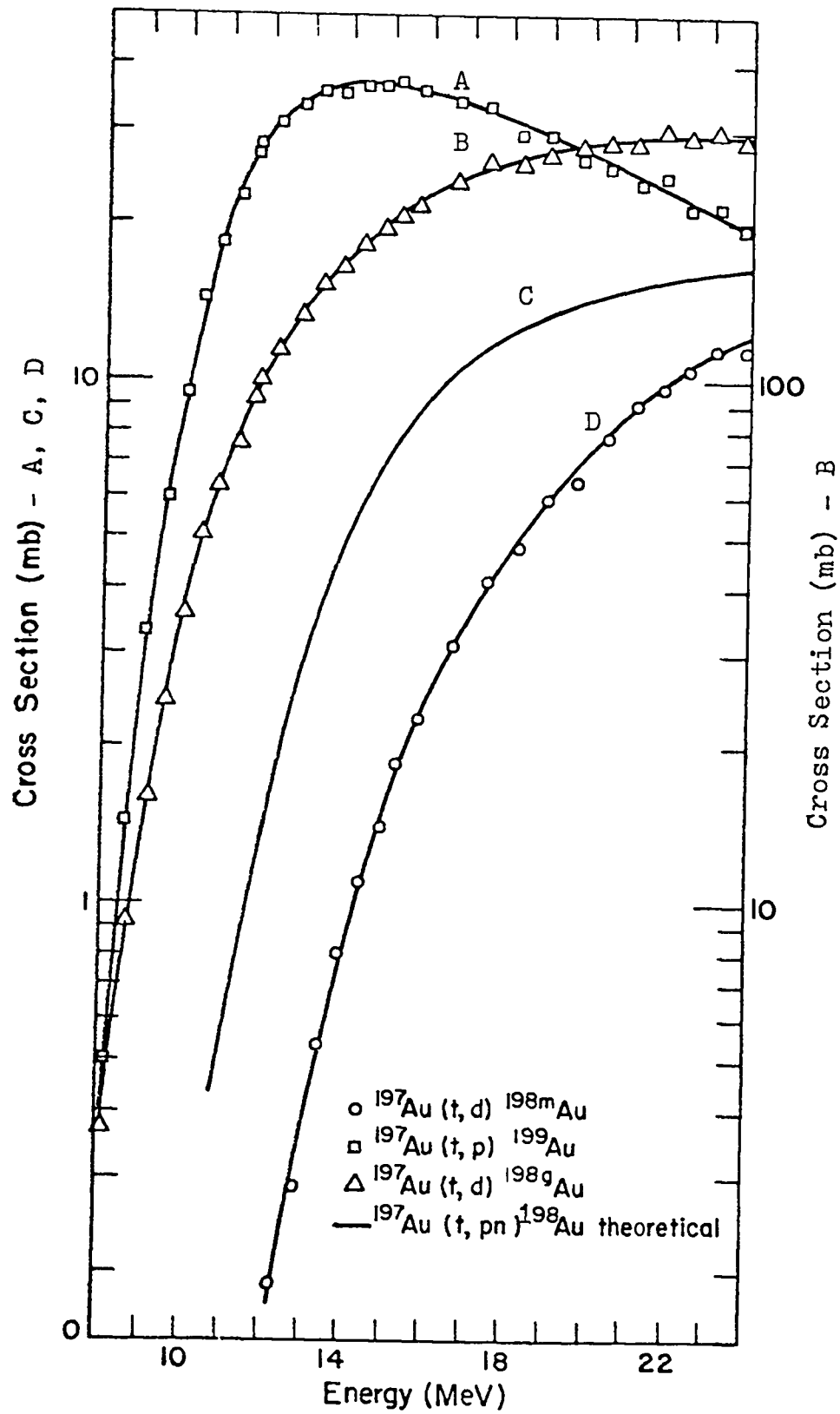

Figure 10. Experimental and Theoretical Excitation Functions for ^{197}Au + t Producing ^{198}Au and ^{199}Au.

Table IV

Experimental Cross Sections and Incident Particle Midpoint Energies for the Reactions $^{197}Au(t,d)^{198m}Au$, $^{197}Au(t,d)^{198g}Au$ and $^{197}Au(t,p)^{199}Au$

E_t(MeV)	σ(mb) ^{198m}Au	σ(mb) ^{198g}Au	σ(mb) ^{199}Au
23.83	11.47	284.3	18.9
23.18	11.64	299.2	20.8
22.53	10.46	288.9	18.8
21.86	9.68	297.1	22.0
21.17	8.95	279.9	22.2
20.47	7.82	284.1	25.1
19.78	6.46	266.5	23.7
19.04	5.96	275.1	27.8
18.27	4.79	254.3	29.5
17.49	4.13	263.5	34.5
16.67	3.10	239.6	32.8
15.77	2.24	218.1	31.3
15.32	1.83	208.1	31.8
14.87	1.41	197.0	36.5
14.39	1.10	182.2	37.2
13.90	0.793	162.8	33.8
13.39	0.544	152.7	34.3
12.87	0.291	133.9	32.5
12.33	0.189	114.5	29.4
11.78		99.9	28.3
11.28		76.5	23.1
11.70		93.2	26.5
11.28		76.6	21.7
10.87		63.0	18.5
10.43		50.8	14.6
10.00		35.6	9.75
9.55		24.6	6.04
9.09		16.1	3.43
8.60		8.15	1.47
8.09		3.71	0.500
7.28		0.975	0.083
6.11		0.182	

for compound-nucleus reactions. The reactions were shown in this way only as a matter of accounting convenience.

A better understanding of how these reactions took place can be obtained from a consideration of the simple shell model configurations of ^{197}Au, ^{198g}Au and ^{198m}Au. In any nucleus of odd A, such as ^{197}Au, all but one of the nucleons are considered to have their angular momentum paired off. The single odd nucleon is thought to move essentially independently, and the net angular momentum of the entire nucleus is determined by the quantum state of this nucleon. The 3/2+ ground state of the target nucleus must be attributed to the odd proton (Z=79), and the shell model configuration for ^{197}Au(g.s.) therefore may be considered to have an odd $d_{3/2}$ proton (and an even number of $h_{11/2}$ protons). The ground state of ^{198}Au is a 2- state (Figure 11) and can be formed from ^{197}Au(g.s.) by stripping a neutron from the incident particle into the target nucleus. This neutron can couple with the $d_{3/2}$ proton state to produce a 2- state; for example, a $d_{3/2}$ proton and a $p_{3/2}$ neutron can produce states 0-, 1-, 2-, or 3-, and a $d_{3/2}$ proton and a $f_{5/2}$ neutron can produce states 1-, 2-, 3-, and 4-.

The isomeric state of ^{198}Au consists of pairing a $h_{11/2}$ proton and an $i_{13/2}$ neutron. Since the ground state of ^{197}Au has an even number of protons in the $h_{11/2}$ state, and it would be very difficult to produce an $h_{11/2}$ protons by a direct interaction, essentially all the metastable state of

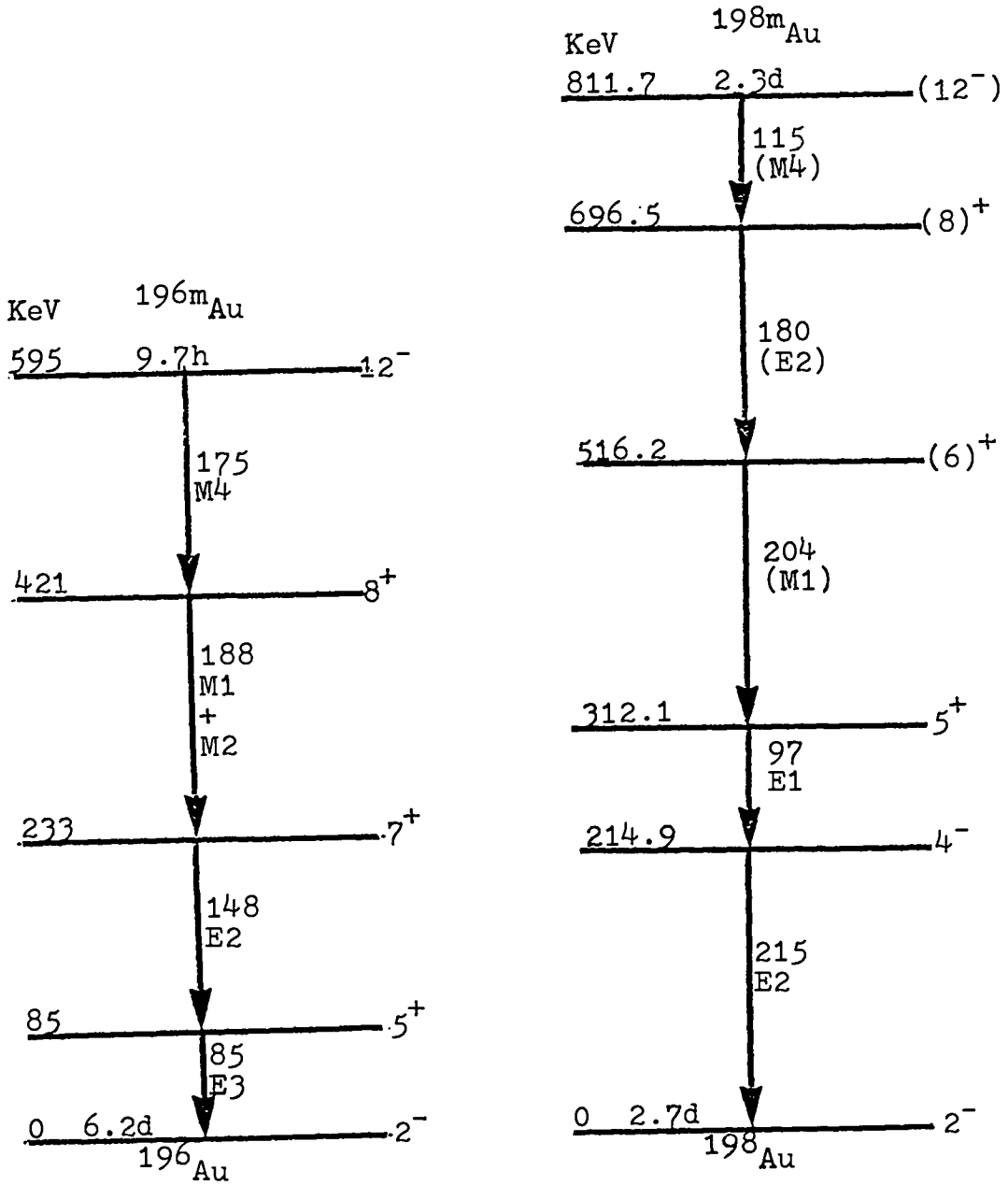

Figure 11. The Decay Scheme for ^{196m}Au and the Proposed Decay Scheme of ^{198m}Au (see Ref. 1)

^{198}Au has to be produced by a compound nucleus reaction.

The excitation function producing ^{198g}Au has much larger cross sections than is predicted by the theoretical compound-nucleus calculations, because both stripping and compound-nucleus reactions are occurring. The production of ^{198m}Au is predominantly by compound-nucleus reactions, and the excitation function has a similar shape as the theoretical excitation function but has lower cross section values. This is expected since the theoretical curve predicts formation of both ^{198m}Au and ^{198g}Au by compound-nucleus reactions. Since an incident triton can produce a large angular momentum change in the target nucleus, a relatively large amount of metastable state is produced.

The ^{197}Au(t,p)^{199}Au reaction is also shown in Figure 10 This excitation function is the sum of both compound-nucleus and direct interaction reactions taking place. A fairly large cross section is observed for this reaction over the incident energy range studied. At energies above 16 MeV, the cross section values for this reaction decrease because at higher energies other "reaction channels" open and proportionally less (t,p) reaction takes place.

2. ^{197}Au(d,p)^{198m}Au and ^{197}Au(d,p)^{198g}Au

The values of the experimental cross sections and incident particle energies are given in Table V for these reactions. The experimental and theoretical excitation

functions are shown in Figure 12. Since the counting statistics for the isomer were poor and the gamma ray peak was not completely resolved in many cases, there is a great deal of scattering of the experimental points in the excitation function for production of ^{198m}Au.

Shell-model considerations for these reactions are essentially the same as those stated for the analogous triton reactions, and many of the same conclusions can be made. The large cross sections observed for production of ^{198g}Au can be attributed to both stripping and compound-nucleus reactions. The shape of the excitation function for production of ^{198m}Au is similar to what is theoretically predicted, but the cross section for this reaction is much lower than predicted. The amount of angular momentum transferred to the target nucleus for deuterons is less than for tritons; therefore, lower ^{198m}Au cross sections are observed for the deuteron reaction. The tritons are seen to be much more effective in producing the high-spin ^{198m}Ag than are the deuterons. There is no obvious single reaction mode responsible for this effect. Rather, it appears to be the consequence of the greater number of favorable reaction channels available for de-excitation of $^{200}Hg^*$ to give a high-angular-momentum form of ^{198}Au.

The last point of the ^{198g}Au excitation function was taken from Jahn, et. al.[9] and agrees very well with the measured excitation function of this work. The results are also in agreement with those of Chevarier, et. al.[8]

Table V

Experimental Cross Sections and Incident Particle Midpoint Energies for the Reactions $^{197}Au(d,p)^{198m}Au$ and $^{197}Au(d,p)^{198g}Au$

E_d(MeV)	σ(mb) ^{198m}Au	σ(mb) ^{198g}Au
24.29		93.5
23.64		106.3
22.97	0.76	115.7
22.28	0.66	115.6
21.59	0.67	129.1
20.87	0.64	133.2
20.14	0.61	147.0
19.38	0.49	163.2
18.60	0.60	167.0
17.79	0.67	186.0
16.95	0.71	200.3
16.08	0.57	200.7
15.83		204.7
15.41	0.58	211.2
14.98	0.56	211.2
14.53		222.3
14.08	0.43	220.1
13.60	0.49	238.2
13.11		237.8
12.61	0.28	246.5
12.11		240.4
11.60		224.0
10.90		209.3
10.38		178.7
10.05		172.0
9.70		151.6
9.32		131.3
8.93		105.3
8.54		82.7
8.14		59.2
7.48		29.8
6.54		9.79

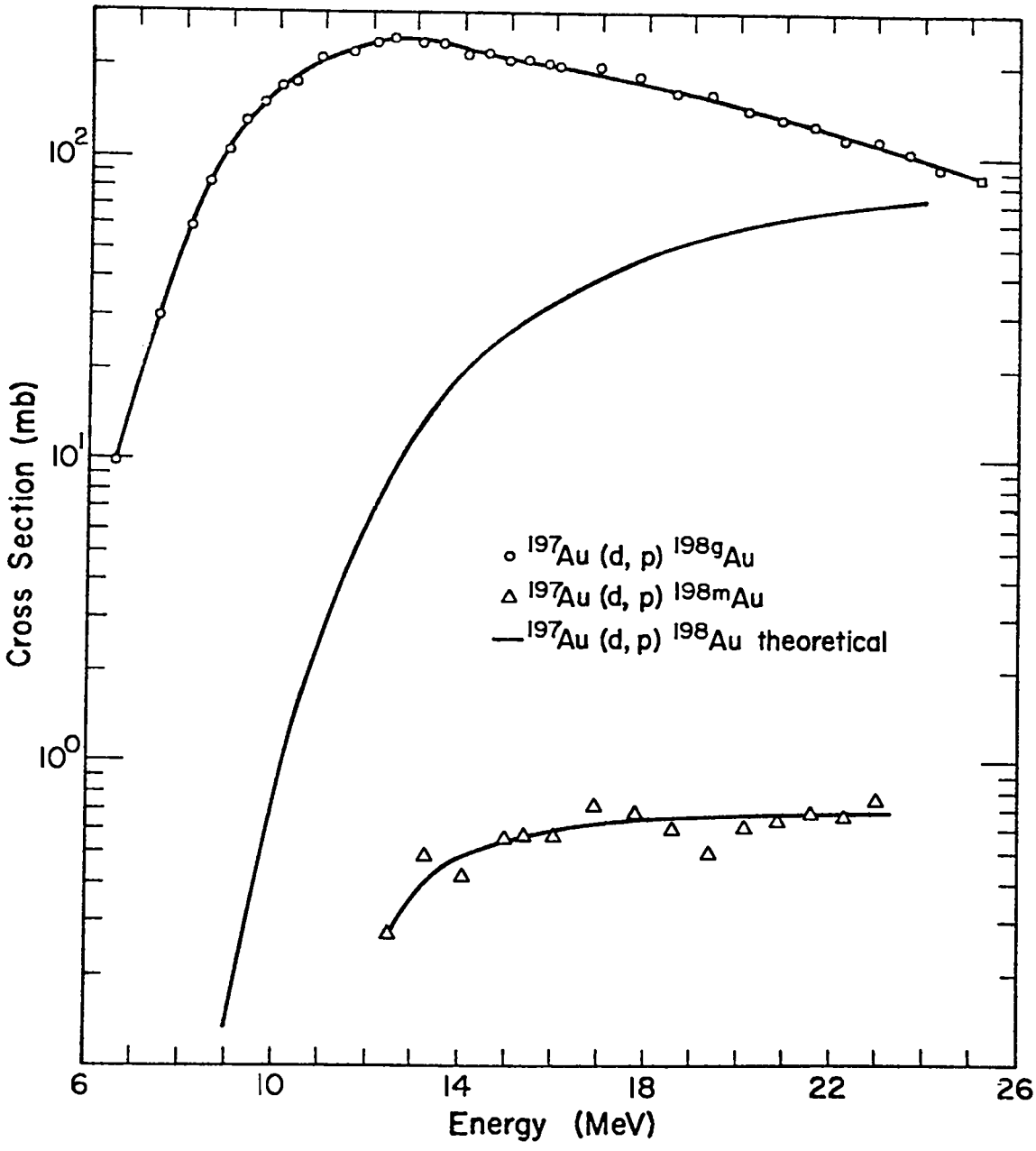

Figure 12. Experimental and Theoretical Excitation Functions for ^{197}Au + d Reactions Producing ^{198}Au.

3. $^{197}Au(t,3n)^{197m}Hg$ and $^{197}Au(t,3n)^{197g}Hg$

The values of the experimental cross section and incident particle energies are given in Table VI for these reactions. The experimental and theoretical excitation functions are shown in Figure 13.

For these reactions to occur, the number of protons in the target nucleus must increase by one, and the number of neutrons in the original target nucleus must decrease by one. This can only occur by formation of the compound-nucleus $(^{200}Hg)^*$, which emits three neutrons forming the products ^{197m}Hg and ^{197g}Hg. The shape and magnitude of the theoretical curve agree fairly well with the experimental (^{197m}Hg + ^{197g}Hg) curve. The theoretical curve predicts lower cross sections than are observed; this behavior is probably because the optical model parameters used to calculate the total reaction cross section with respect to incident particle energy do not describe this function accurately. The ratio of isomer to ground state produced increases as the triton energy increases. This can be explained by the increase in angular momentum transferred to the target nucleus by both the incoming and outgoing particles.

4. $^{197}Au(d,2n)^{197m}Hg$ and $^{197}Au(d,2n)^{197g}Hg$

The value of the experimental cross sections and incident particle energies are given in Table VII for these reactions. The experimental and theoretical excitation functions are shown in Figure 14.

Table VI

Experimental Cross Sections and Incident Particle Midpoint Energies for the Reactions $^{197}Au(t,3n)^{197m}Hg$ and $^{197}Au(t,3n)^{197g}Hg$

E_t(MeV)	σ(mb) ^{197g}Hg	σ(mb) ^{197m}Hg
23.83	245.4	879.8
23.18	265.1	990.9
22.53	241.3	1003.3
21.86	308.7	1020.5
21.17	329.9	947.0
20.47	360.1	932.7
19.78	396.8	848.6
19.04	346.9	758.3
18.27	341.1	708.2
17.49	345.0	685.3
16.67	318.3	556.5
15.77	441.9	237.2
15.32	389.9	219.6
14.87	322.9	202.1
14.39	258.3	166.1
13.90	188.7	129.9
13.39	134.8	101.3
12.87	80.7	68.8
12.33	40.1	
11.78	14.9	

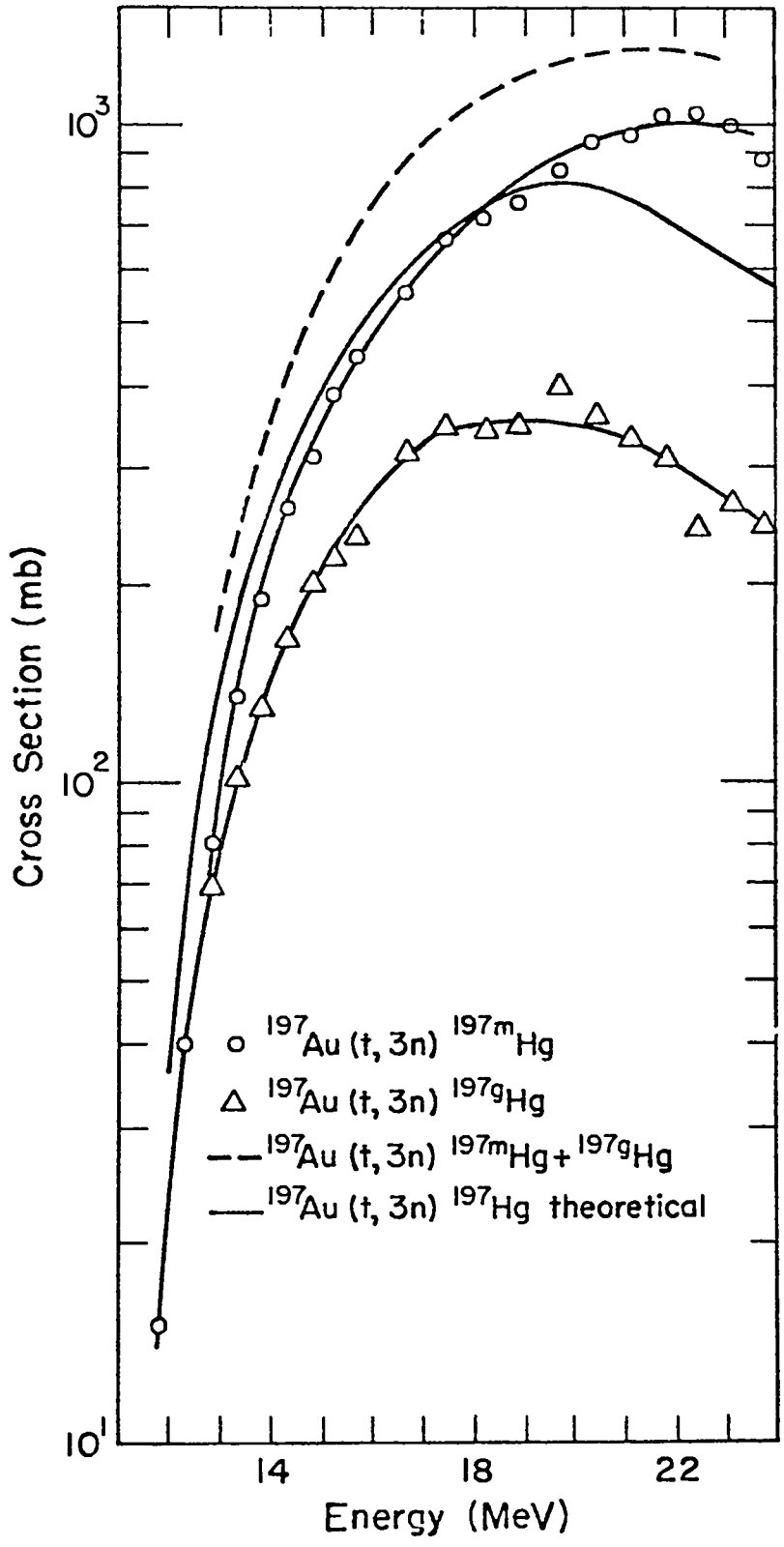

Figure 13. Experimental and Theoretical Excitation Functions for ^{197}Au + t Reactions Producing ^{197}Hg.

These reactions occur by the compound-nucleus process and are analogous to the (t,3n) reactions previously described. Upon bombardment, the compound-nucleus (^{199}Hg)* is formed, which decays by emitting two neutrons to produce ^{197m}Hg and ^{197g}Hg. The shape of the theoretically predicted excitation function agrees fairly well with the measured (^{197g}Hg + ^{197m}Hg) excitation function, but the magnitude of the theoretical cross sections are low; this discrepancy may be attributed to the optical model parameters used. The ratio of isomer to ground state increases for energies up to about 16 MeV, and then decreases. The increase is probably caused by an increase in the transfer of angular momentum for energies below 16 MeV, but for energies above 16 MeV the pre-equilibrium emission seems to occur more readily in the ground state causing the metastable to ground state ratio to decrease. The metastable/ground state ratio is much higher for the triton reaction, where more angular momentum is transferred to the target nucleus.

The shapes of these excitation functions agree very well with the determination of Chevarier, et. al.[8]; however their measured cross section values are higher than the cross sections measured in this work. Since they used different gamma ray peaks (77 KeV and 134 KeV), than were used for this work (191 KeV and 279 KeV), it is difficult to compare decay scheme data. But they used a conversion coefficient of 2.1 for the 134 KeV transition from Nuclear Data Sheets,

Table VII

Experimental Cross Sections and Incident Particle Midpoint Energies for the Reactions $^{197}Au(d,2n)^{197m}Hg$ and $^{197}Au(d,2n)^{197g}Hg$

E_d(MeV)	σ(mb) ^{197m}Hg	σ(mb) ^{197g}Hg
23.64	61.6	
22.97	66.7	90.6
22.28	70.2	98.8
21.59	70.8	99.5
20.87	84.2	97.1
20.14	96.3	108.6
19.38	112.4	120.0
18.60	131.8	140.9
17.79	166.7	158.3
16.95	199.4	166.2
16.08	226.1	
15.83	235.3	157.7
15.41	250.4	185.0
14.98	251.0	169.5
14.53	261.3	210.7
14.08	248.0	215.6
13.60	249.0	242.8
13.11	226.7	220.6
12.61	205.5	245.3
12.11	176.4	244.9
11.60	152.7	
10.38	66.5	199.7
10.05	67.8	130.8
9.70	40.7	117.5
9.32	27.9	89.4
8.93	17.9	54.1
8.54	10.8	40.2
8.14	6.23	

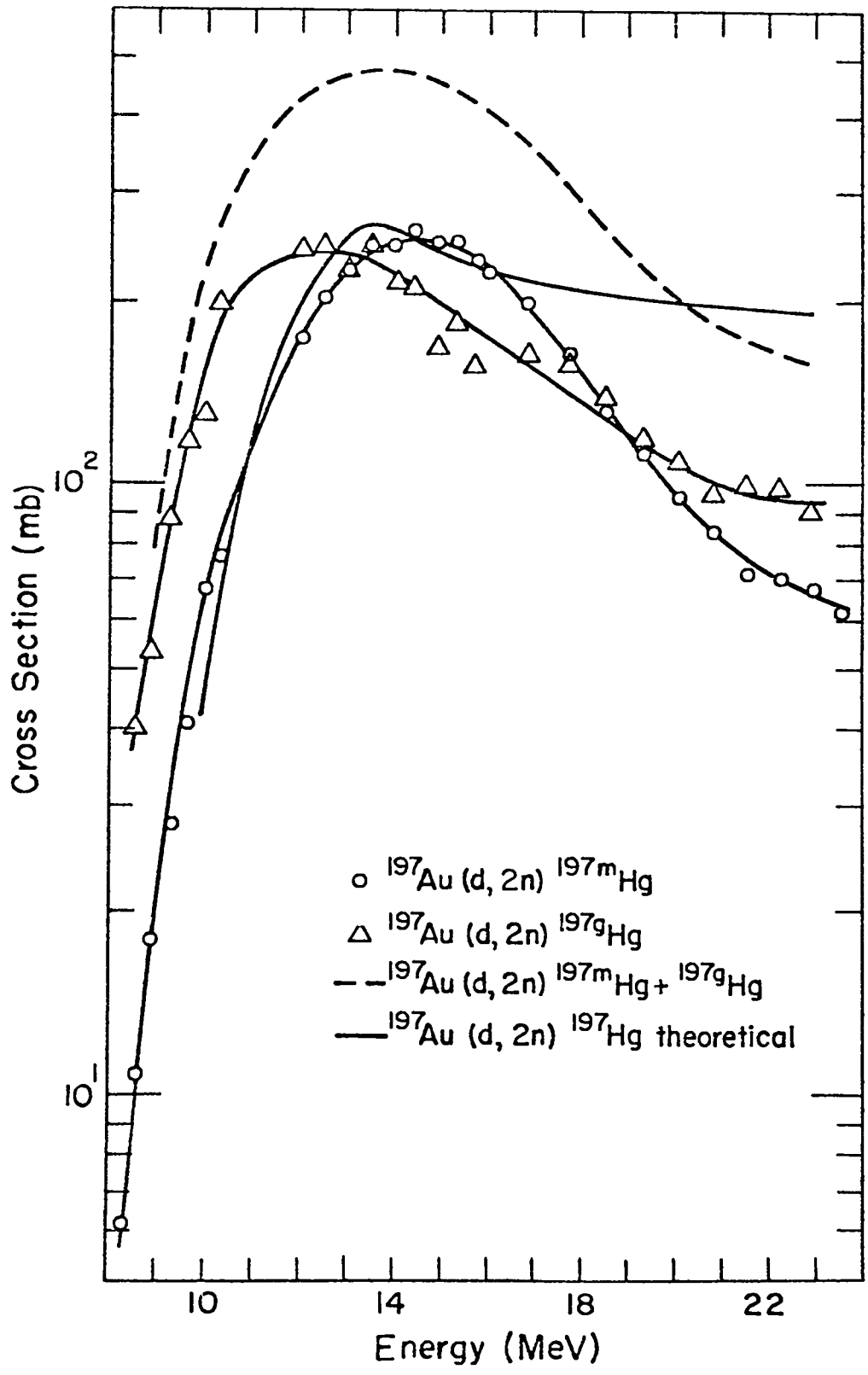

Figure 14. Experimental and Theoretical Excitation Functions for ^{197}Au + d Reactions Producing ^{197}Hg.

1959-1965; a recent value in Nuclear Data Sheets 1972 is 1.73. They also used the intensity ratio for the ground state calculation resulting in a similar error. If one uses the most recent value for this conversion coefficient, their cross section values are decreased by 17.7%, and very good agreement is seen between our work and their work. Since the abundances for the transitions measured in our work were determined by absolute gamma counting, our cross section determinations should be more accurate.

5. $^{197}Au(d,t)^{196m}Au$ and $^{197}Au(d,t)^{196g}Au$

The values of the experimental cross sections and incident particle energies are given in Table VIII for these reactions. The experimental and theoretical excitation functions are shown in Figure 15. For accounting convenience, these reactions are shown as (d,t) reactions; however, these reactions can also occur by other paths, such as (d,p2n), (d,npn), etc.

The excitation function producing ^{196g}Au has a very steep slope to about 13 MeV; then there is a leveling off of the excitation function for energies up to 20 MeV, and another moderately steep slope is seen above 20 MeV. These results can be explained by considering the types of reactions taking place. At energies up to 20 MeV direct reactions are the primary way in which the ^{196g}Au is produced, but above this energy the contribution to the reaction cross section

Table VIII

Experimental Cross Sections and Incident Particle Midpoint Energies for the Reactions $^{197}Au(d,t)^{196m}Au$ and $^{197}Au(d,t)^{196g}Au$

E_d(MeV)	σ(mb) ^{196m}Au	σ(mb) ^{196g}Au
23.64	2.40	80.0
22.97	1.80	71.7
22.28	1.24	60.1
21.59	0.63	56.7
20.87	0.40	49.3
20.14		47.9
19.38		46.7
18.60		42.4
17.79		42.4
16.95		40.4
16.08		36.6
15.83		35.6
15.41		34.6
14.98		32.3
14.53		31.0
14.08		28.6
13.60		27.8
13.11		23.7
12.61		21.1
12.11		16.6
11.60		11.6
10.90		6.85
10.38		3.65
10.05		2.52
9.70		1.60
9.32		0.843
8.93		0.440
8.54		0.286
8.14		0.118
7.48		0.094
6.54		0.075

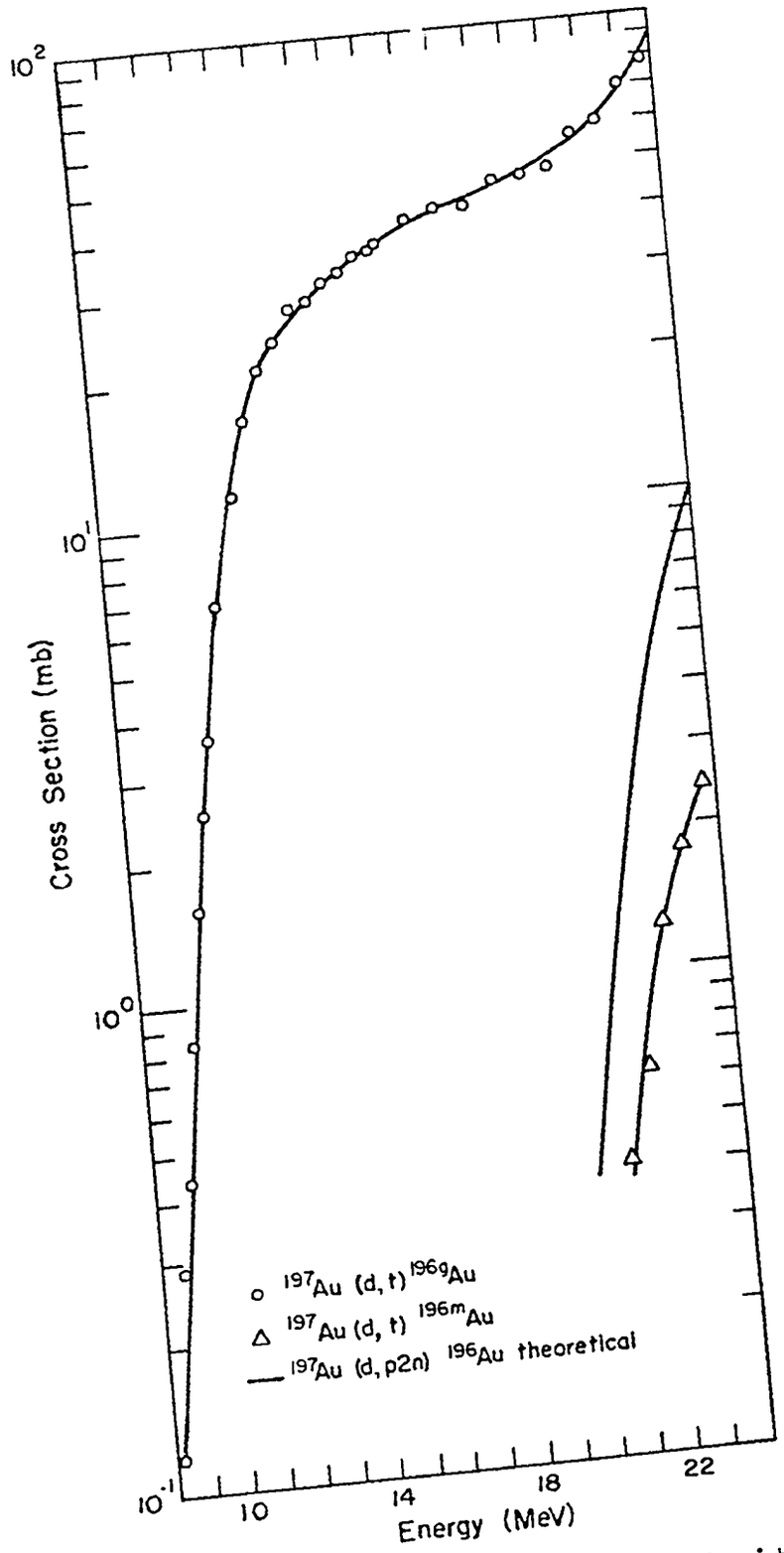

Figure 15. Experimental and Theoretical Excitation Functions for ^{197}Au + d Reactions Producing ^{196}Au.

from compound-nucleus reactions becomes very significant. This explanation is supported by the theoretical calculation which predicts that the compound-nucleus reaction should become significant at about 20 MeV and by the detection of ^{196m}Au above 21 MeV. The production of ^{196m}Au should be predominantly by compound-nucleus reactions, since the excited state (12-) and the ground state (2-) of this isomer have essentially the same simple shell-model configurations as ^{198m}Au and ^{198g}Au, and the same shell-model arguments can be applied (Figure 11).

Jahn, et. al.[9] have measured the $^{197}Au(d,p2n)^{196g}Au$ cross section for incident deuteron energies from 35 to 80 MeV. The excitation function measured by Jahn, et. al. together with the excitation function determined in the present work are shown as one plot in Figure 16. This excitation function from 8 to 80 MeV indicates one reaction process (direct reaction) to 20 MeV and a large increase in cross section above 20 MeV attributed to an additional reaction process (both direct reaction and compound-nucleus reactions). Excitation functions for these reactions were also measured by Chevarier, et. al.[8] above 20 MeV, but the results of this work includes the incident particle energy range from 8-24 MeV.

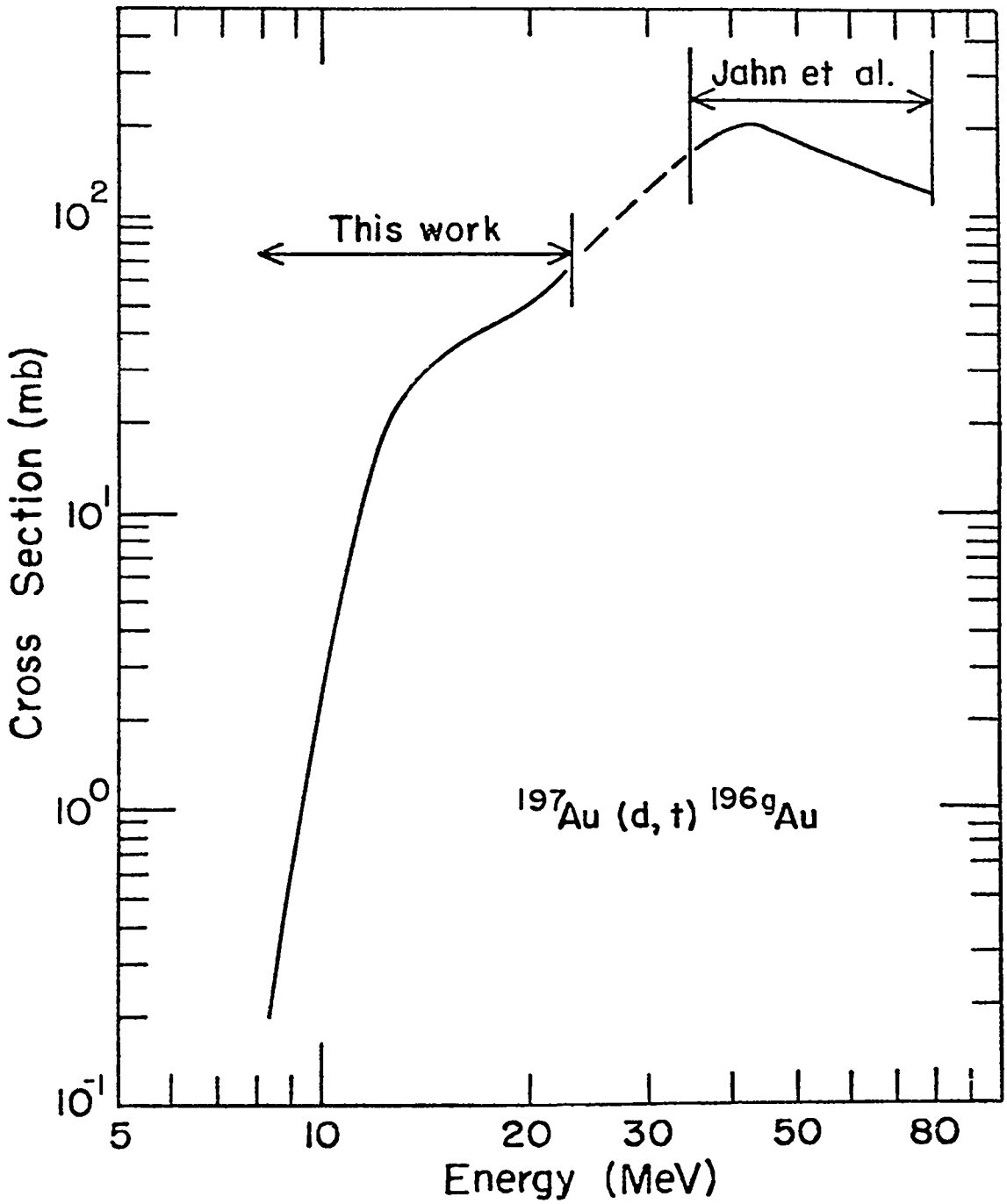

Figure 16. Comparison of the Experimentally Determined Excitation Function of this work to 24 MeV and the Excitation Function of Jahn et. al. Determined from 35 MeV to 80 MeV.

6. $^{197}Au(d,4n)^{195m}Hg$ and $^{197}Au(d,4n)^{195g}Hg$

The values of the experimental cross sections and incident particle energies are given in Table IX for these reactions. The experimental and theoretical excitation functions are shown in Figure 17.

The reactions proceed by forming the compound-nucleus $^{199}Hg^*$, which decays by emitting 4 neutrons to ^{195m}Hg and ^{195g}Hg. The shape of the theoretical curve agrees fairly well with the experimental excitation function (^{195g}Hg + ^{195m}Hg), but the cross section values for the theoretical curve are larger. The ratio of isomer to ground state increases with deuteron energy as expected.

These excitation functions were determined for deuteron energies from 25 to 60 MeV by Chevarier, et. al.,[8] and in this work the excitation functions were measured up to 24 MeV. The results from these two measurements match very well.

7. $^{197}Au(t,t'n)^{196m}Au$, $^{197}Au(t,t'n)^{196g}Au$ and $^{27}Al(t,2p)^{28}Mg$

The values of the experimental cross sections and incident particle energies are given in Table X for these reactions. The experimental excitation functions are shown in Figure 18. For accounting convenience, the reactions of gold are shown as (t,t'n) reactions; however, these reactions may also occur by other paths, such as (t,p3n).

Production of ^{196m}Au and ^{196g}Au are detected only for the relatively high energies and have very low cross sections

Table IX

Experimental Cross Sections and Incident Particle Midpoint Energies for the Reactions $^{197}Au(d,4n)^{195m}Hg$ and $^{197}Au(d,4n)^{195g}Hg$

E_d(MeV)	σ(mb) ^{195m}Hg	σ(mb) ^{195g}Hg
24.29	157.4	49.9
23.64	105.2	35.7
22.97	57.2	17.1
21.59	21.7	2.7
20.87	6.5	

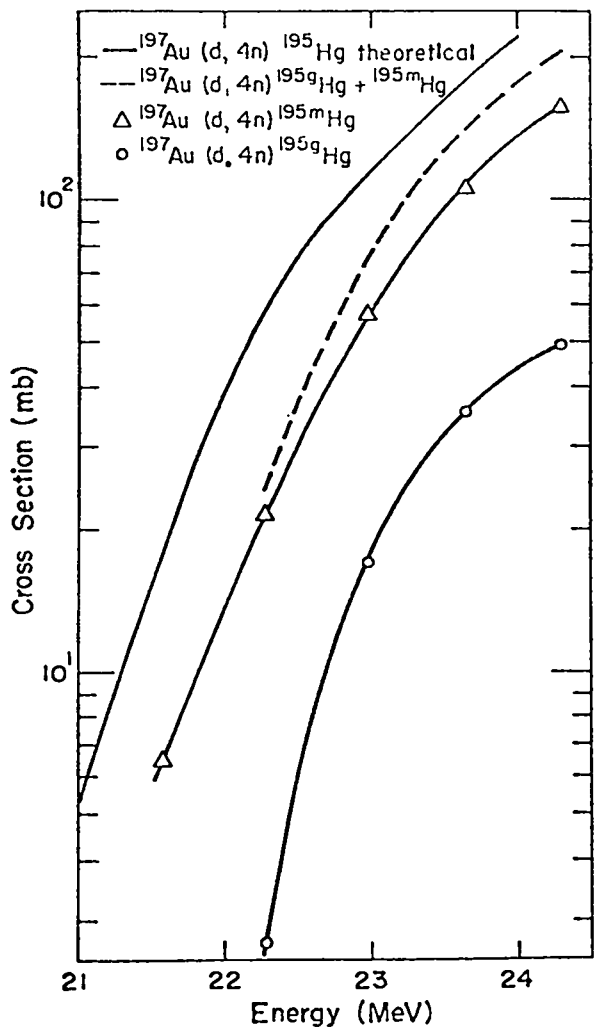

Figure 17. Experimental and Theoretical Excitation Functions for ^{197}Au + d Reactions Producing ^{195}Hg.

Table X

Experimental Cross Sections and Incident Particle Midpoint Energies for the Reactions $^{197}Au(t,t'n)^{196m}Au$, $^{197}Au(t,t'n)^{196g}Au$ and $^{27}Al(t,2p)^{28}Mg$

E_t(MeV)	σ(mb) ^{196m}Au	σ(mb) ^{196g}Au	E_t(MeV)	σ(mb) ^{28}Mg
23.64	0.043	6.38	24.14	4.49
22.97	0.041	5.41	23.51	4.64
22.28	0.036	4.69	22.85	4.69
21.59		3.99	22.19	4.73
20.87		3.44	21.52	4.98
20.14		3.04	20.82	4.84
19.38		2.50	20.12	4.67
			19.41	4.54
			18.66	4.36
			17.88	3.95
			17.08	3.57
			16.25	3.10
			15.55	2.42
			15.09	2.18
			14.63	1.97
			14.15	1.82
			13.65	1.65
			13.13	1.50
			12.60	1.34
			12.06	1.17
			11.53	1.04
			11.03	0.930
			11.92	1.13
			11.49	1.02
			11.08	0.932
			10.65	0.813
			10.21	0.706
			9.32	0.565
			8.84	0.440
			8.35	0.436
			7.84	0.249
			6.71	0.099
			5.49	0.024

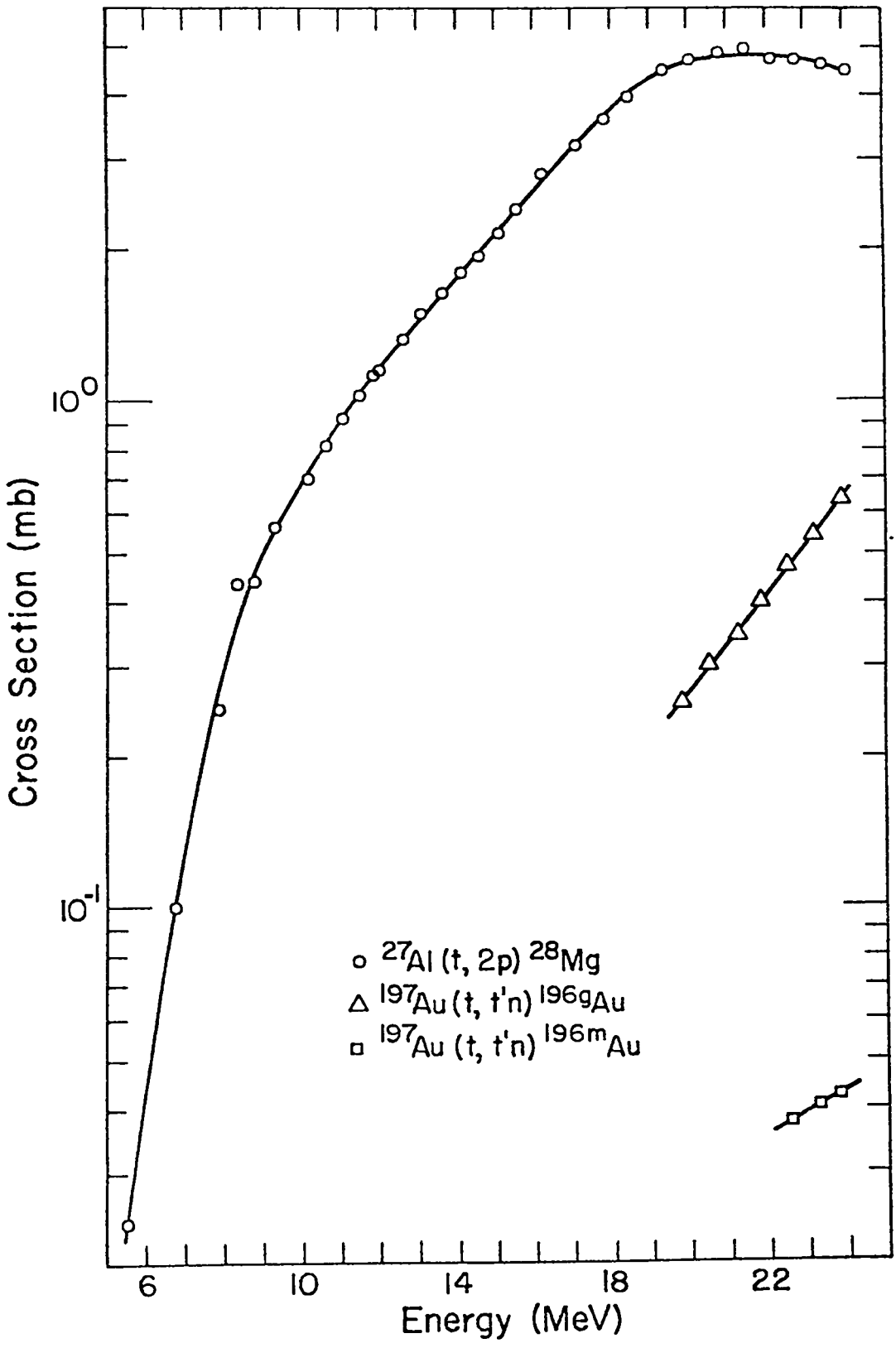

Figure 18. Experimental Excitation Functions for ^{197}Au + t Reactions Producing ^{196}Au and for the $^{27}Al(t,2p)^{28}Mg$ Reaction.

for the energy range studied. These products may be obtained by the direct-interaction process, if a triton collides with a neutron in the target nucleus causing this neutron to be ejected. Compound-nucleus formation and subsequent ejection of a proton and 3 neutrons is another path these reactions may follow. A compound-nucleus process would be expected to produce more isomer than the direct-interaction process.

The $^{27}Al(t,2p)^{28}Mg$ cross section was measured from the activity produced in the aluminum catcher foils. This reaction proceeds mainly by compound-nucleus formation and subsequent ejection of two protons. An accurate measurement of this excitation function is valuable, because this information allows one to use aluminum as an energy monitor for other reactions over the energy range studied.

8. $^{197}Au(t,n)^{199m}Hg$

The values of the experimental cross sections and incident particle energies are shown in Table XI for this reaction. Since ^{199m}Hg has a relatively short half-life of 42.6 minutes, this activity was not detected for many of the foils measured, because the gold foils were usually counted several hours after bombardment. Cross sections for this reaction over the energy range of 12-24 MeV appear to be fairly constant (3.5-4.6 mb.).

Table XI

Experimental Cross Sections and Incident Particle Midpoint Energies for the Reaction $^{197}Au(t,n)^{199m}Hg$

E_t(MeV)	σ(mb) ^{199m}Hg
23.64	3.67
22.97	4.12
22.28	3.98
15.77	4.47
15.32	4.40
14.87	4.56
14.39	4.49
13.90	4.42
13.39	4.51
12.87	4.34
11.78	4.13

V. Conclusions

The excitation functions measured in this work were discussed in terms of compound-nucleus and direct-interaction reactions. In general, the reactions producing ^{198m}Au, ^{197m}Hg, ^{197g}Hg, ^{196m}Au, ^{195m}Hg, ^{195g}Hg and ^{28}Mg were believed to take place predominantly by compound-nucleus (hybrid) reactions. However, the production of ^{198g}Au, ^{196g}Au and ^{199}Au was believed to occur by both direct-interaction and compound-nucleus reactions.

The shapes of the theoretically predicted excitation functions for production of ^{198m}Au, ^{197}Hg and ^{195}Hg agreed fairly well with the experimental excitation functions, but the measured cross section values showed fairly large deviations from the predicted values. These deviations were attributed to a poor knowledge of the optical model parameters.

Isomer to ground state ratios usually increased with an increase in incident particle energy and were usually larger for triton reactions when compared to corresponding deuteron reactions. This behavior was attributed to an increase in the amount of angular momentum transferred to the target nucleus, and in some cases, to an increase in the number of reaction channels available for de-excitation of a compound-nucleus to give the isomer.

Previous measurements of the $^{197}Au(d,p)^{198}Au$ and $^{197}Au(d,2n)^{197}Hg$ excitation functions are in very good

agreement with the work presented here. When the excitation function for the reaction $^{197}Au(d,t)^{196g}Au$ to 24 MeV measured in this work is compared to a previous measurement from 35 to 80 MeV, it is obvious that at incident particle energies below 20 MeV, the ^{196g}Au is formed primarily by direct-interaction reactions, while at higher incident particle energies compound-nucleus reactions also make a large contribution to product formation.

PART II

Discovery and Half-Lives of Isomeric States of ^{93}Y and ^{101}Ag.

I. Introduction

As pointed out in Part I, nuclear isomerism exists when there is a large angular momentum difference between an upper and lower state which hinders electromagnetic decay of the former to the point where its half-life becomes appreciable. All excited states of nuclei are subject to decay to lower states by emission of electromagnetic radiation (γ-rays), although other modes of decay may also occur. Purely electromagnetic effects produce the gamma radiation, and these effects may be thought of as changes in charge and current distributions in nuclei. Electric moments are associated with charge distributions, and magnetic moments are associated with current distributions; therefore, γ-transitions are classified as electric (E) and magnetic (M). The gamma radiation is classified according to the angular momentum (in units of $\hbar$) carried off by the gamma ray. The accepted nomenclature is to refer to radiations carrying off $l = 1, 2, 3, 4, 5$ units of $\hbar$ as dipole, quadrupole, octupole, 2^4-pole and 2^5-pole radiations, and the 2^l-pole transitions are written as El or Ml.

A system has odd parity if the wave function for the system changes sign when the signs of all the space coordinates are changed, and a system has even parity if the wave function does not change sign under these conditions. The parity properties of electric and magnetic multipole transitions are shown up to 2^4-pole in Table XII.

Table XII

Nomenclature of γ-Ray Processes

Type	Name	Units h Carried Away	Parity Change
E1	Electric Dipole	1	Yes
M1	Magnetic Dipole	1	No
E2	Electric Quadrupole	2	No
M2	Magnetic Quadropole	2	Yes
E3	Electric Octupole	3	Yes
M3	Magnetic Octupole	3	No
E4	Electric 2^4-pole	4	No
M4	Magnetic 2^4-pole	4	Yes

Instead of γ-ray emission, an excited state can decay to a lower state by ejection of an electron from an atomic orbit. This process is known as internal conversion, and the ratio of internal conversion events to γ-emission events is called the internal conversion coefficient for that type of transition. Internal conversion coefficients can be calculated very accurately when the energy of the corresponding γ-ray, the multipolarity of the transition, the particular atomic orbit, and the wave functions of the electrons involved are known.[45] Multipolarities of γ-ray transitions can be deduced from comparisons of experimental and theoretical conversion coefficients.

The shell model[46] has been very successful in accounting for the existence of the "islands of isomerism", the occurrence of many long-lived isomers in nuclei that have an odd proton or odd neutron in an orbital just below one of the closed shells. However, in many cases the shell-model alone cannot completely describe the nuclear states involved in transitions.

Many nuclear properties cannot be explained by the shell-model, for instance, the appearance of very large electric quadrupole moments in nuclei far from closed shells. This phenomenon was explained with the advent of the collective-model by the motion of nucleons outside a closed shell producing core deformation. Many nuclei are strongly deformed into an oblate or prolate spheroidal shape, and the vast

majority of deformed nuclei have shapes close to that of a prolate spheroid. The quantity β gives the extent of deformation as:

$$\beta = \frac{\text{(major semi-axis)-(minor semi-axis)}}{\text{average of minor and major semi-axes}}$$

Bohr and Mottelson[47] postulated that low-lying energy levels can arise from the rotation of the deformed nucleus. These rotational bands have been observed, and collective motions of a vibrational type are also observed.

The motion of a single nucleon in a deformed potential well was studied by S. G. Nilsson.[48] The projection of the nucleon's angular momentum on the nuclear symmetry axis defines the Ω quantum number. A nucleon of total angular momentum j may have Ω values of 1/2, 3/2, 5/2, ..., j. The nucleon is independent of Ω if the nucleus is undeformed. For a deformed nucleus, each shell model level of angular momentum j breaks up into $(j + \frac{1}{2})$ "Nilsson levels", each of which may contain up to two protons or neutrons. Figure 19 illustrates how the energies of the Nilsson levels vary as a function of the deformation β (of the potential well) for up to 20 nucleons. Positive values of β correspond to prolate deformation and negative values to oblate, and the number and sign at the end of each line give the value of Ω and the parity.

Blatt and Weisskopf[49] have derived expressions to estimate partial half-lives (considering γ-emission only) for

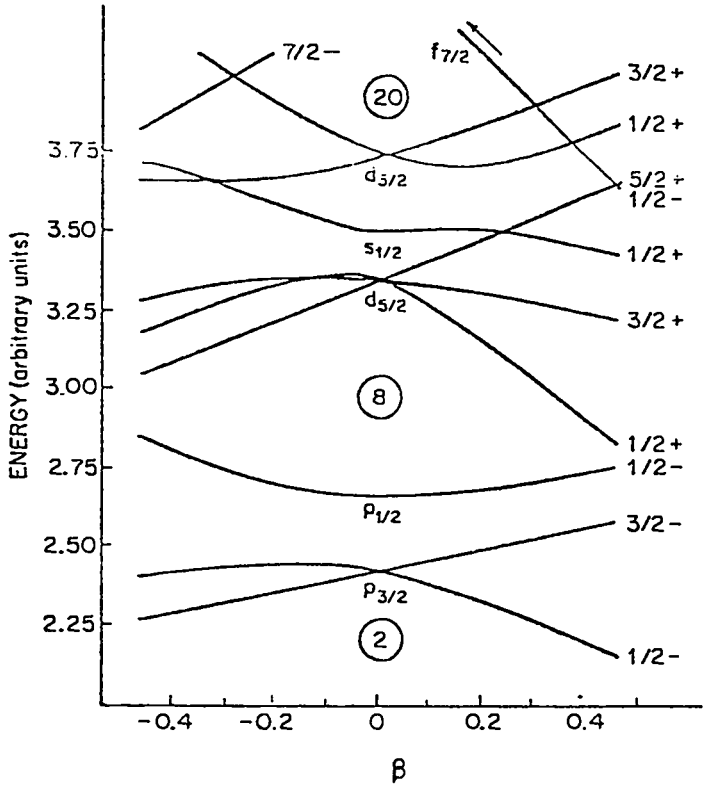

Figure 19. Energy of a single nucleon in a potential well of deformation β for $8 < Z < 20$ or $8 < N < 20$.

gamma transitions. For these derivations, many assumptions were made. They considered emission of radiation by a single non-relativistic proton which is moving in a potential due to the other particles in the nucleus. This potential is central, independent of the proton velocity and independent of time. Of course, these estimates are crude and are not expected to represent accurately transitions in actual nuclei.

The half-lives obtained using the Weisskopf formula are usually considered as lower limits, because transitions between states whose spins and parities cannot be ascribed completely to the properties of the individual nucleons, but involve also interaction of several nucleons outside a closed shell, are normally expected to be slower. Observed lifetimes which are longer than the Weisskopf lifetime are frequently explained in terms of multiple-particle configurations, although still in the spirit of the single-particle model.

Moszkowski[50] derived essentially the same single-particle expressions as Weisskopf, except that he included a "statistical factor" S, which is dependent upon the spins of the initial and final states of the transition.

The quantum mechanical transition probability for any given process is given by the equation:

$$T_{i\rightarrow f} = \frac{2\pi}{\hbar} \left| \langle f | H' | i \rangle \right|^2 \frac{dN}{dE} ,$$

where $T_{i\rightarrow f}$ is the transition probability for the process, $\hbar$ is Plank's constant divided by 2π, $\frac{dN}{dE}$ is the number of possible final states per unit energy interval and $\langle f | H' | i \rangle$ is the

first order matrix element, $\int \psi_f^* |H'| \psi_i d\tau$.

The matrix element is a very important quantity, since its square is proportional to the probability that the state described by ψ_i will transform into the state described by ψ_f. Since the matrix element contains the wave functions of the states between which decay occurs, it is the quantity that determines the effect of the spins, parities and detailed structures of the two states on the transition probability.

There were two primary objectives for this work. First, to prove the existence of the nuclear isomers by observing the characteristic gamma radiations and measuring the half-lives of the isomeric decay. Second, to compare the measured nuclear properties to those predicted by the models previously discussed, and from these comparisons to obtain information about nuclear states between which the transitions occur.

II. Experimental System

A. On-Line Apparatus

A diagram of the system used for the half-life measurements is shown in Figure 20. The reaction chamber consisted of a 12" brass tube with two removable Lucite windows, inserted in one of the Van de Graaff beam lines. An aluminum target holder was positioned inside the chamber and perpendicular to the beam axis. The detector was placed near the Lucite window to observe γ-radiation given off.

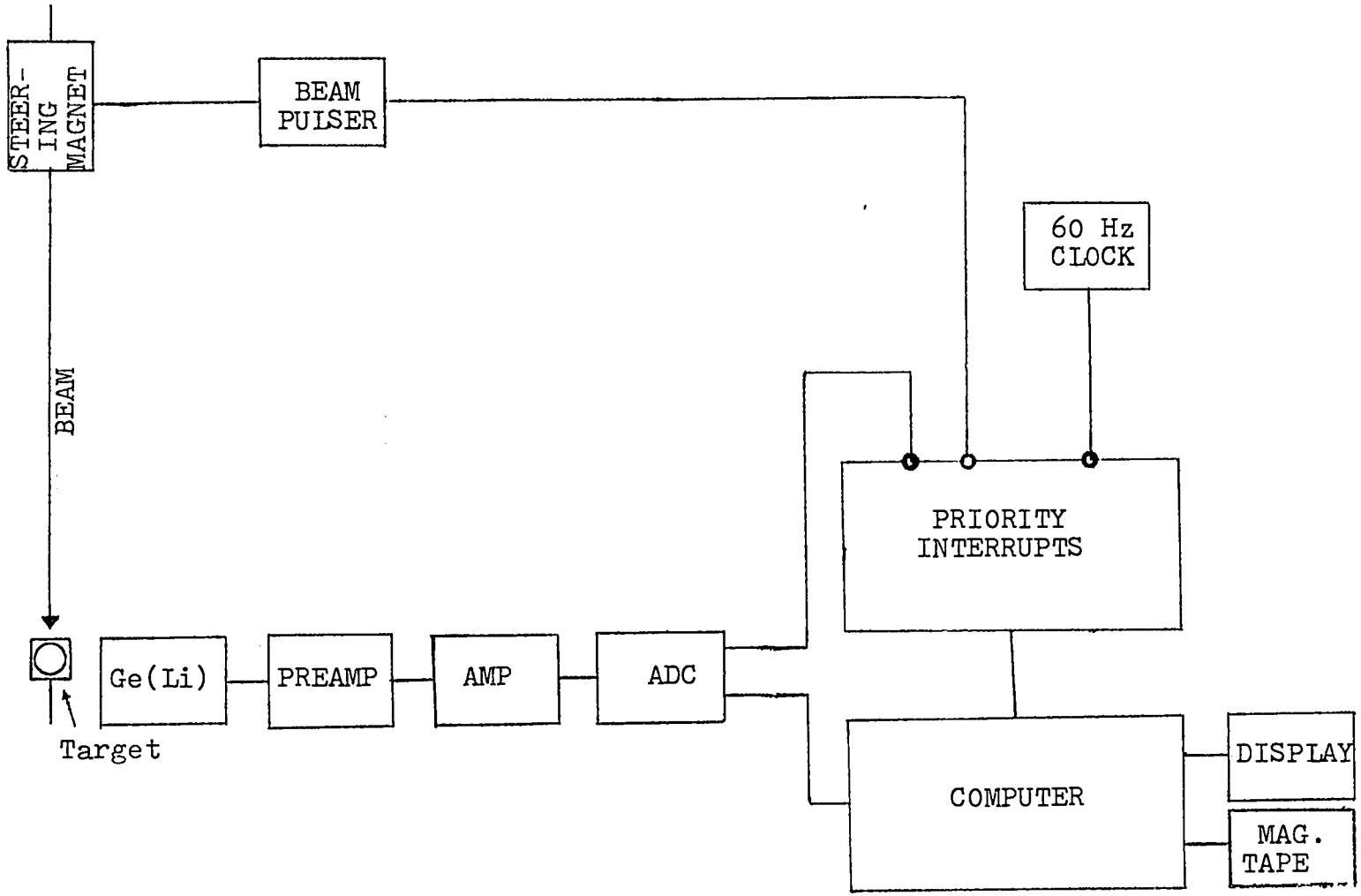

Figure 20. Schematic Representation of the System Used to Measure the Half-Lives of ^{93m}Y and ^{101m}Ag.

The detector system consisted of a Nuclear Diodes Trapezoidal Ge(Li) crystal of 24 cm^3 active volume. At the ^{60}Co 1.3325 MeV photopeak, the detector has a resolution of 3.2 KeV FWHM, a relative efficiency of 2.5% (relative to NaI) and a 11:1 Peak/Compton Ratio. Also included in the spectrometer system were a Tullamore 1CA-4096· Victoreen analog-to-digital converter and an XDS-930 computer incorporating a cathode-ray-tube display.

Since the half lives of the isomers of interest were expected to be short, of the order of seconds, the experiment had to be set up to perform the bombardment-measurement sequence on this time scale. And, since a single bombardment and measurement would not provide enough decay data to be useful, the sequence had to be repeated until enough data were accumulated. These requirements were accomplished by a two-part system: a beam interrupter with adjustable on and off times which cycled automatically with cycle times as short as 0.5 sec., and a computer-controlled data-storage arrangement which recorded a series of γ-spectrum data during each measurement period. At each turn-off, a signal from the beam interrupter caused the computer to initiate the counting sequence; in practice, a variable signal delay was included, so that the signal from the interrupter to the ADC could be delayed by a desired amount (usually 1 msec).

B. Program for Computer Control

A program[51] was devised at the Los Alamos Van de Graaff Facility which stored the series of successive spectra (taken during a measurement period) on the XDS-930 computer fixed head drum and added subsequent cycles of spectra to the stored spectra. The computer software allowed the experimenter to vary the number of successive spectra taken per run and the length of counting time for each spectrum to a lower limit of 100 msec.

Computer interrupts were used for measuring the counting time and correcting for ADC dead time. A 60-Hz clock was used for counting time measurements, and the gates-lost signal from the ADC was used to correct for dead time counting losses. The program corrected for dead time errors by multiplying the observed counts in each channel of the spectrum by the ratio

$$\frac{\text{total counts in spectrum + gates lost}}{\text{total counts in spectrum}}$$

The computer program allowed one to print out the spectra, and store the spectra on magnetic tape for subsequent analysis.

III. Isomeric State of ^{93}Y

A. Experimental

The isomer was produced by the $^{94}Zr(t,\alpha)^{93}Y$ reaction in enriched (>95%) ^{94}Zr with 10 MeV tritons. A triton energy of 10 MeV was selected, because additional Van de Graaff

bombardments at three triton energies from 8 to 16 MeV, showed that this energy would produce nearly as much ^{93}Y as the higher energies, while the background was kept at a minimum. A low background was very desirable because this decreased the dead time correction of the analog-to-digital converter.

Before each bombardment, a quartz disc was placed in the foil holder as a tuning indicator. Upon irradiation from the incident beam the quartz glowed, and a camera-TV remote vision system was used to determine the beam location.

The beam interrupter was set so that a beam on-target time of 0.75 seconds and a beam off-target time of 3.25 seconds was provided for each cycle. During each off-target time of cycle, the on-line computer was programmed to record 10 successive γ-ray spectra at 0.20-second intervals, and the sum of the corresponding spectra for each cycle were stored by the computer. Two runs of 2.5 and 5 hours were completed, and the spectra for these runs were dumped on magnetic tape. Typical incident particle currents were of the order of 0.4 μA.

B. Results

The tape-recorded gamma spectra were analyzed on a CDC 6600 computer with the computer program BRUTAL,[10] which provided energy and activity information on all statistically significant gamma-ray peaks. A list of peak energies above 100 KeV with corresponding radioactive nuclides are shown in Table XIII. The ^{207m}Pb peak observed was due to shielding

Table XIII

γ-Ray Energies and Residual Nuclei for 10 MeV Triton Bombardments for ^{94}Zr

Gamma-Ray Energy(KeV)	Nuclide
122	^{57}Fe
137	^{57}Fe
162	^{116m}In
169	^{93m}Y
219	^{96}Nb
236	^{95m}Nb
241	^{96}Nb
266	^{93}Y
372	^{96}Nb
412	^{198}Au
416	^{116}In
460	^{96}Nb
478	^{93}Y
511	e^+-e^- annihilation
570	^{207m}Pb
590	^{93m}Y
658	^{97}Nb
719	^{96}Nb
724	^{95}Zr
743	^{97m}Nb
758	^{95}Zr
766	^{95}Nb
778	^{96}Nb
810	^{96}Nb
850	^{96}Nb

around the detector; the indium peaks were believed to be due to indium found at the cold finger of the detector apparatus, and the gold peak was also believed to be of a spurious nature. A separate bombardment with just an empty target holder produced peaks at 122 KeV, 137 KeV, 162 KeV, 416 KeV, 511 KeV and 570 KeV, which were proved to be from the experimental apparatus.

In the partial decay scheme[52] of ^{93m}Y, shown in Figure 21, the 169 KeV and 590 KeV γ-rays are seen to be characteristic of the decay of the isomeric state. Spectra for the counting intervals 0-0.2 seconds, 1.0-1.2 seconds and 1.8-2.0 seconds are shown in Figure 22; the decay of the 169-KeV and 590-KeV peaks is easily recognized. From the areas of these characteristic gamma-ray peaks for two separate runs, the half-life of ^{93m}Y was determined using the computer code SKITZO.[11] The isomeric half-life determined from the weighted average of these data is 0.82 seconds, with a standard deviation of 0.019 seconds. With systematic errors also taken into account, the half-life may be cited as 0.82 ± 0.04 sec.

C. Discussion

There is a great deal of proof that the gamma-transitions measured in this work were, in fact, from ^{93m}Y. Both the 169 KeV and the 590 KeV gamma-rays have been observed[53] in the β decay of ^{93}Sr to levels of ^{93}Y. Separate bombardments

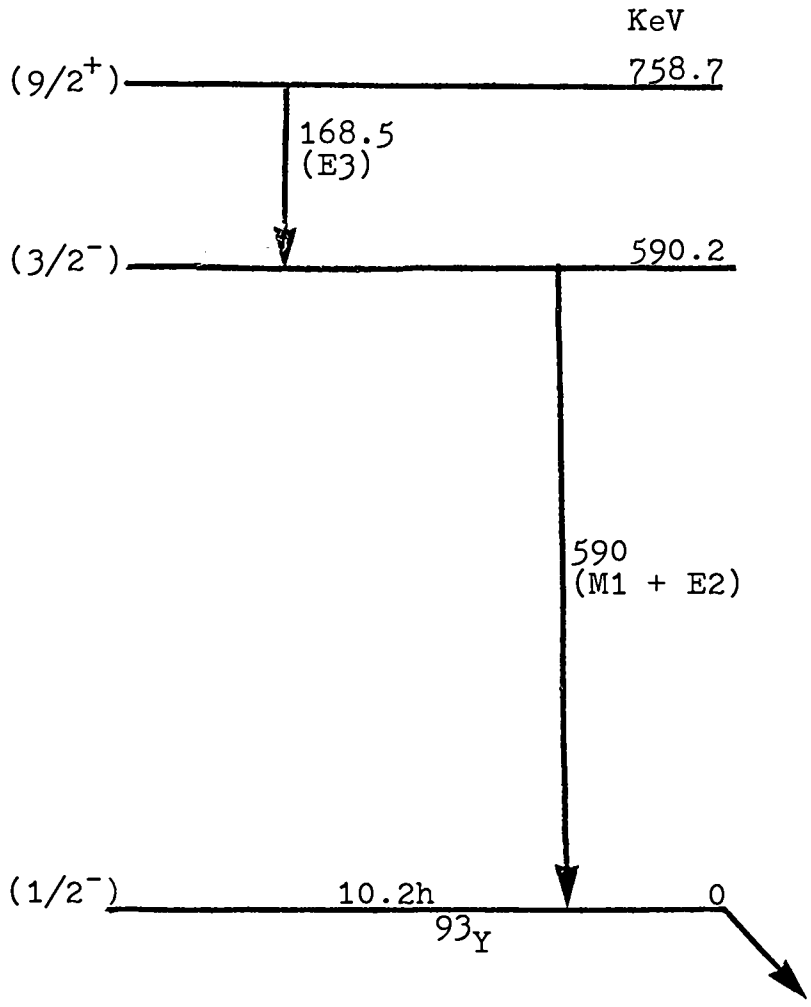

Figure 21. Decay Scheme of ^{93m}Y

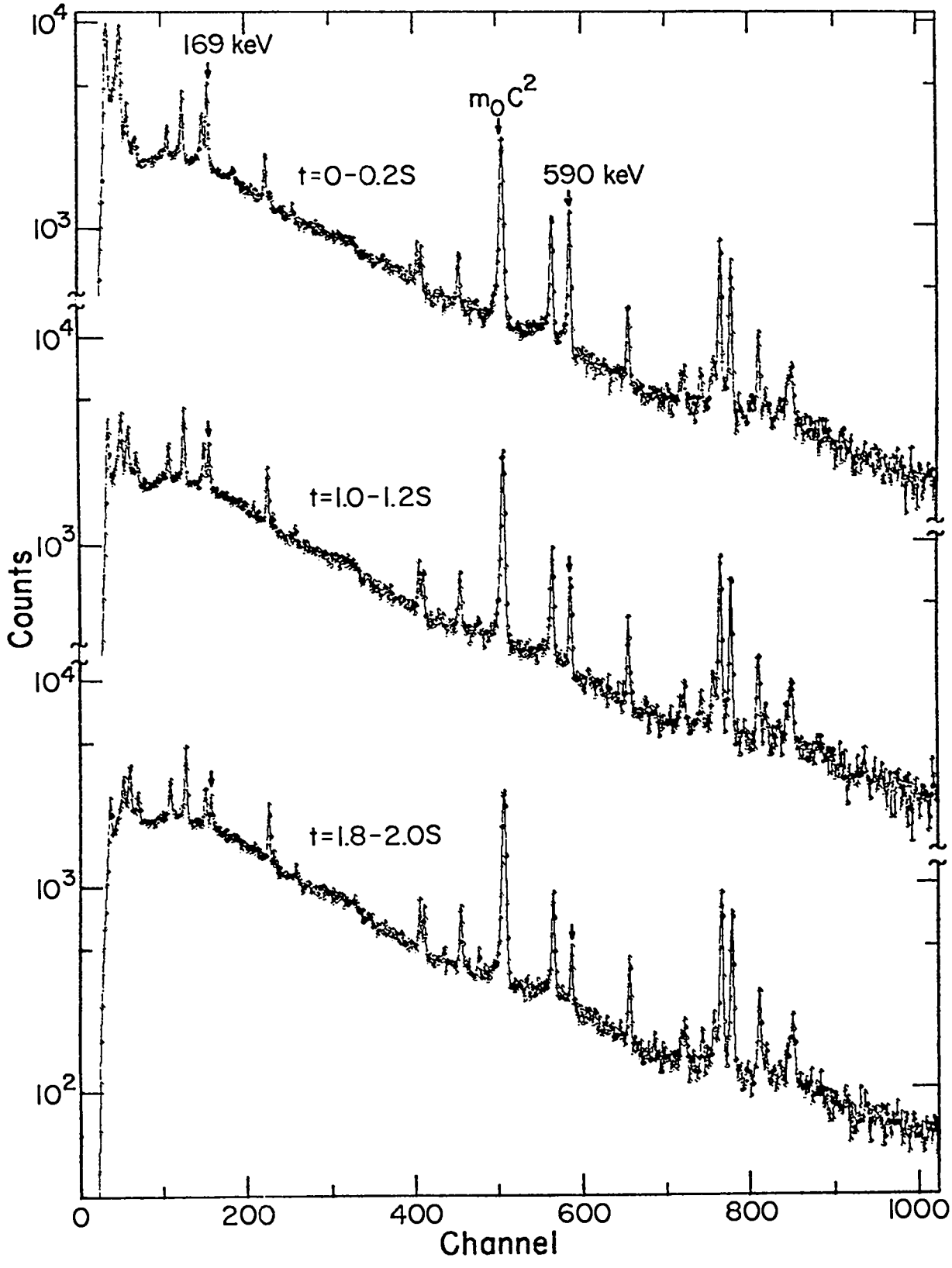

Figure 22. Representative Delayed γ-Spectra Showing Decay of ^{93m}Y Peaks.

of the enriched ^{94}Zr foil with 10 MeV deuterons and protons did not produce the 169 KeV and 590 KeV peaks, and the ^{93}Y (g.s.) peak was also not observed. After correcting for internal conversion, assuming M1 and E3 conversion coefficients, the relative intensities of the 169 KeV and 590 KeV transitions agreed within experimental error. Since the isomer has never been directly observed previously, the half-life would be expected to be very short, which was found to be the case (less than one second).

The isomeric de-excitation in ^{93}Y was expected to be $J^{\pi} = 9/2^{+}(758\ \text{KeV}) \xrightarrow{E3} 3/2^{-}(590\ \text{KeV}) \xrightarrow{M1+E2} 1/2^{-}(\text{g.s})$ on the basis of reported level information.[54] The only previous information on its decay rate gave the half-life as <30 seconds or >3 hours,[55] which is consistent with the measured half-life of 0.82 ± 0.04 seconds.

The radiative transition half-life is obtained by multiplying the measured half-life by $(1 + \alpha)$, where α is the total internal conversion coefficient. With correction for internal conversion (with $\alpha_{tot}(E3) = 0.945$)[56] the radiative transition half-life comes out to be $t_{\frac{1}{2}}(\gamma) = 1.60 \pm 0.08$ seconds. (β decay of the isomeric state was assumed to be negligible). The corresponding single-particle Moszkowski[50] estimate can be calculated using the formula for E3 transitions:

$$E3: \quad t_{\frac{1}{2}}(\gamma) = 2.04 \times 10^{-2} A^{-2} E_{\gamma}^{-7} S^{-1},$$

where A is the atomic weight (93), E_{γ} is the gamma-ray

energy (.590 MeV) and S is a "statistical factor" (4/3). The transition probability of a single proton from this estimate is calculated to be $t_{\frac{1}{2}}$(s.p.) = 0.46 seconds, indicating an apparent hindrance factor of (1.60/0.46) = 3.5. There exists some other experimental data, however, which allows a calculation of the hindrance factor. Preedom et. al.,[57] in a study of the d,^{3}He (proton pick up) reaction on ^{94}Zr, observed of the total ℓ_p = 1 spectroscopic strength for transformation of ^{94}Zr to excited states in ^{93}Y that 25 ± 7% represented population of the 590 KeV level. The 758-KeV level was the only one seen to be populated with l_p = 4. If one makes the following assumptions from shell model considerations with regard to ^{93}Y, (a) the $g_{\frac{1}{2}}^1$ configuration is contained only in the 758-KeV level; (b) all of the observed ℓ_p = 1 produced states have $J^\pi = 3/2^-$ and are populated in proportion to their $p_{3/2}$- (hole state) content; and (c) only $g_{9/2}^1 \longrightarrow p_{3/2}^{-1}$ transformations can contribute to the E3 transition, then the calculated single-particle half-life must be lengthened by the factor 1/0.25, i.e., $t_{\frac{1}{2}}$ (s.p.) should be adjusted to ~1.8 seconds, which is in satisfactory agreement with the observed value of 1.6 seconds.

IV. Isomeric State of ^{101}Ag

A. Experimental

Production of this isomer was accomplished by the $^{102}Pd(p,2n)^{101}Ag$ reaction with 24-MeV protons on enriched ^{102}Pd. Detailed isotopic and spectrographic analysis of the target material was done at Oak Ridge National Laboratory, and the results are shown in Table XIV. After tuning, a proton current of about 0.2 μA was used for the experimental bombardments. A beam-on-target time of 1 second and beam-off time of 11 seconds was used, giving a total cycle time of 12 seconds. During the beam-off time period of each cycle, 10 successive one-second spectra were recorded and added to the corresponding previous spectra. Four runs of 15 to 50 minutes were completed, and the spectra for these runs were dumped on magnetic tape for later analysis.

B. Results

The experimental γ-spectra were analyzed with a CDC 6600 computer using the program BRUTAL,[10] which determined the areas and energies for the statistically significant peaks. A list of the energies of the predominant gamma ray peaks with corresponding nuclides is shown in Table XV.

The partial decay scheme of ^{101m}Ag is shown in Figure 23; the 97.7 KeV and 175.5 KeV peaks are seen to be characteristic of the isomeric state. Spectra for the counting intervals 0-1 second, 4-5 seconds and 9-10 seconds after

Table XIV

Analyses of ^{102}Pd Target

Isotopic Analysis			Spectrographic Analysis			
Isotope	Atomic Percent	Precision	Element	Percent	Element	Percent
102	75.45	±0.10	Ag	0.02	Hg	<0.05
			Ca	0.02	In	<0.05
104	12.13	±0.10	Cu	0.02	Ir	<0.05
			Fe	0.03	Li	<0.005
105	6.46	±0.05	K	0.05	Mn	<0.02
			Mg	0.01	Mo	<0.02
106	3.81	±0.05	Na	0.05	Ni	<0.05
			Si	0.07	Pb	<0.02
108	1.62	±0.05	Al	<0.05	Pt	<0.05
			Au	<0.01	Rb	<0.02
110	0.52	±0.05	B	<0.01	Rh	<0.05
			Ba	<0.01	Ru	<0.05
			Be	<0.001	Sb	<0.05
			Bi	<0.02	Sn	<0.02
			Cb	<0.05	Sr	<0.01
			Cd	<0.05	Ta	<0.05
			Co	<0.05	Ti	<0.01
			Cr	<0.05	V	<0.02
			Cs	<0.05	W	<0.05
			Ge	<0.05	Zr	<0.05
			Hf	<0.05		

Table XV

γ-Ray Energies and Residual Nuclei for 24 MeV Proton Bombardments of ^{102}Pd

Gamma-Ray Energies(KeV)	Nuclide
98	^{101m}Ag
176	^{101m}Ag
263	^{101g}Ag
511	e^+-e^- annihilation
557	^{102}Ag
585	^{101g}Ag
650	^{101g}Ag
668	^{101g}Ag

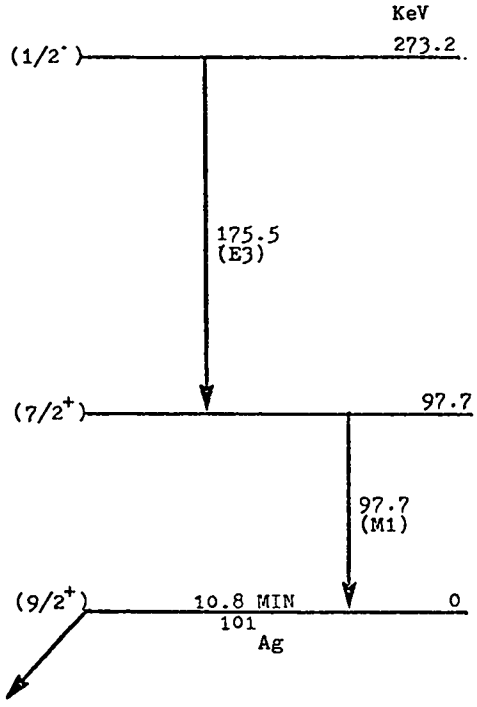

Figure 23. Decay Scheme of ^{101m}Ag

bombardment are shown in Figure 24. Decay of the isomeric transitions is easily observed.

A small amount of long-lived background was also found to contribute to the peak areas at 176 KeV; therefore, the half-life was determined only using the 97.7 KeV peak. Half-life determinations for each run were calculated using the computer code SKITZO.[12] A weighted average of the four separate runs gave an isomeric half-life of 3.12 seconds, with a standard deviation of 0.060 seconds. With systematic errors also taken into account, the half-life may be cited as 3.12 ± 0.12 seconds.

C. Discussion

The following proof contributed to isomer identification. (a) The 98-KeV and 176-KeV gamma-rays were detected by Hnatowich et. al.[58] in the β decay of ^{101}Cd to levels of ^{101}Ag, and these gamma-rays were shown to be in coincidence. Since their experimental system could not measure half-lives of less than 4 seconds, they concluded that this value was a higher limit for the isomeric half-life. (b) A preliminary bombardment at a proton energy of 16-MeV, produced only very small γ-ray peaks at 98-KeV and 176-KeV, and only a trace of ^{101g}Ag may have been detected. The cross section for the ^{102}Pd(p,2n)^{101m}Ag reaction should be very small at this energy, because this reaction has a Q value of -16.0 MeV.

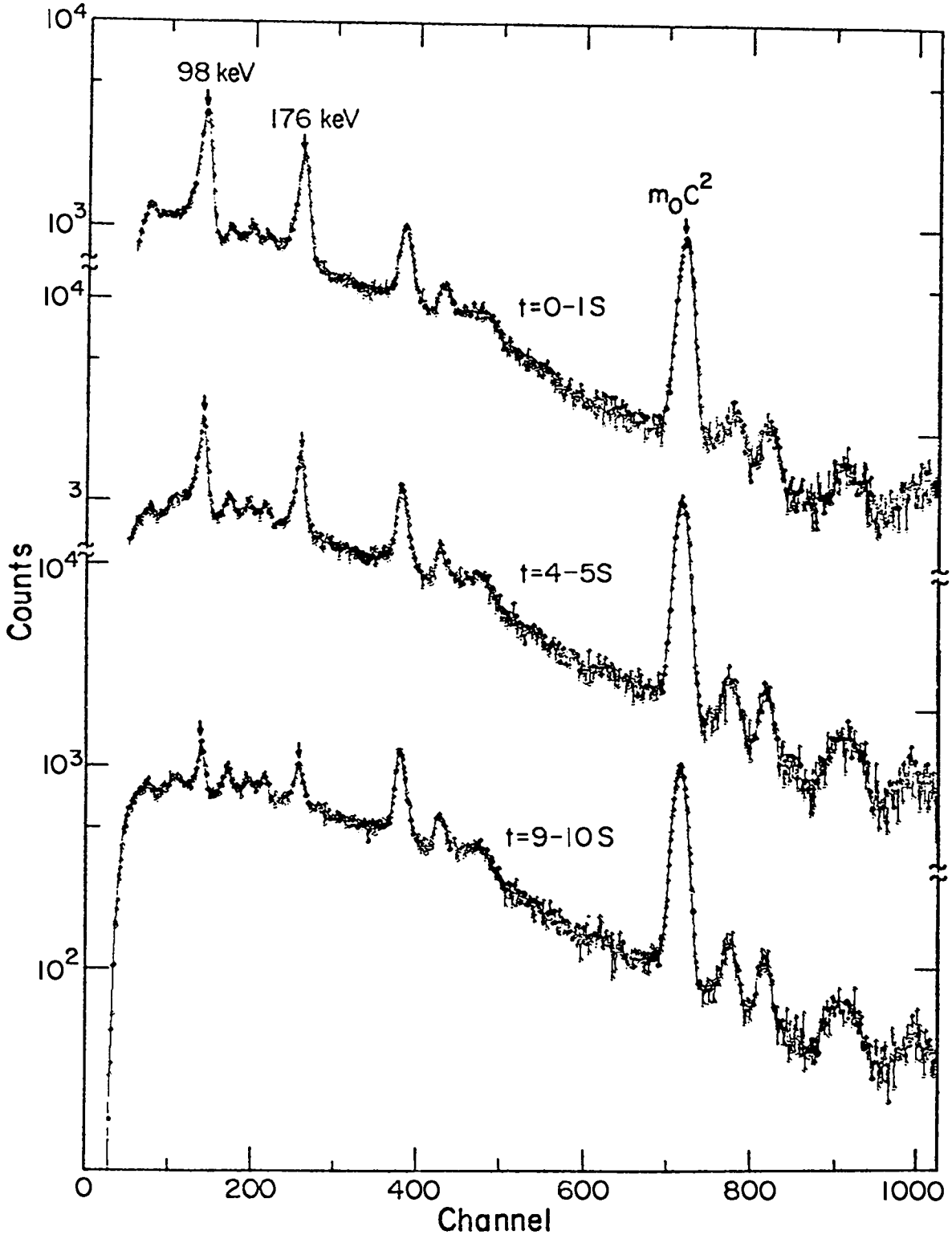

Figure 24. Representative Delayed γ-Spectra Showing Decay of ^{101m}Ag Peaks.

(c) After correcting for internal conversion, assuming M1 and E3 conversion coefficients, the relative intensities of the two transitions were found to be identical within experimental error.

The previous data, together with the measured ground state spin,[59] indicate that the de-excitation sequence is

$$J^{\pi} = 1/2- \ (274 \text{ KeV}) \xrightarrow{E3} 7/2+ \ (98 \text{ KeV}) \xrightarrow{M1} 9/2+ \ (\text{g.s}).$$

Correcting for internal conversion[56] (with $\alpha_{tot}(E3) = 1.12$) the radiative transition is found to be $t_{\frac{1}{2}}(\gamma) = 6.6 \pm 0.3$ sec. The reduced radiative half-life,[60] $t_{\frac{1}{2}}(\gamma) \cdot A^2E^7S$, is shown in Table XVI, along with the corresponding values for the odd silver isomers; the smooth trend of increasing transition probability with increasing neutron number is apparent. A plot of log E_{γ} vs. log $(T_{\frac{1}{2}})_{rad}$ is shown in Figure 25 for a comparison of the energy dependence of the six E3 radiative processes for the odd silver isomers. If the wave functions of the initial states and of the final states were the same for all the odd-mass Ag isomers, the radiative half-lives would be proportional to E^{-7}. The line in Figure 25 is drawn to show a seventh power energy dependence; the consistency is quite good even though the six E3 radiative lifetimes span an interval of six orders of magnitude.

The Moskowski single-particle estimate for the radiative half-life of a 176-KeV transition at mass number 101, using the same formula as for the ^{93m}Y case, is $9.7 \cdot x \ 10^{-2}$ seconds. Comparison with the measured 6.6 second value

Table XVI

Reduced Radiative Half-Lives of the Odd Silver Isomers

A	E (MeV)	S	$t_{\frac{1}{2}}(\gamma)$ (sec)	$t_{\frac{1}{2}}(\gamma) \cdot A^2E^7S$ (amu^2MeV^7 sec)
101	0.176	4	6.6_1	1.38
103	0.138	4	24.3	0.98
105	0.0255	1	9.37×10^6	0.73
107	0.0931	1	9.48×10^2	0.71
109	0.0877	1	1.13×10^3	0.54
111	0.065	1	8.81×10^3	0.52

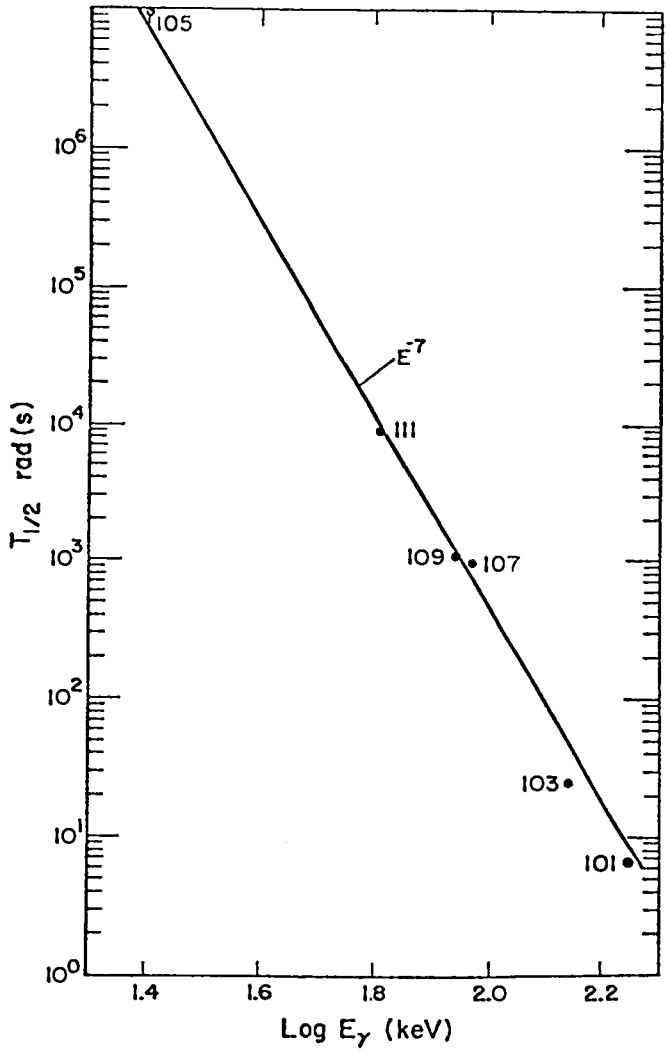

Figure 25. Plot of log E_γ vs log ($T_{\frac{1}{2}}$) rad for the Odd Silver Isotopes ^{101}Ag through ^{111}Ag.

indicates a hindrance factor of 68. There are no other experimental data available, such as a proton-pick up reaction on ^{102}Pd, which could be used to calculate the hindrance factor.

Another approach to the problem of predicting the amount of 7/2+ state available for decay can be obtained by considering nuclear deformation. If only $p_{\frac{1}{2}}$ and $g_{9/2}$ proton single-particle orbitals are involved in the 1/2- and 7/2+ states, the connecting E3 transition is forbidden; an admixture of the $g_{7/2}$ orbital into the 7/2+ state would permit this process. The theoretical reduced E3 matrix element can be calculated using the formula derived by Bohr and Mottelson[61] and including the statistical factor S as follows:

$$B_{Th}(E3) = \frac{(1.2)^{2l}}{4\pi}\left(\frac{3}{l+3}\right)^2 A^{2l/3} S\ e^2(fm)^{2l}$$

where l is the multipolarity of the transition (3), S is the statistical factor (4), A is the atomic weight (101), and the radius is assumed to be $R = 1.2A^{1/3}$ fm. The theoretical single-particle matrix element is calculated to be 2.4×10^3 e^2fm^6. The corresponding experimental value can be calculated from the following formula:[61]

$$B_{exp}(E3) = (.693/6.6)(1.764 \times 10^{-3})(E^{-7}),$$

and for an energy of 0.1755 MeV, $B_{exp}(E3) = 36.1e^2fm^6$. From a comparison of the experimental and theoretical matrix elements the effective amplitude of the $g_{7/2}$ proton state to the 7/2+ state of the silver isotope can be estimated to be of order 10^{-1}.

We note that nuclear deformation can introduce just such an admixture. Eigenvalues and eigenfunctions for Shell 4, Nilsson orbital 21, nuclear deformation N=4 and $\Omega=7/2$ are given by Nilsson.[48] The eigenvalue contributing to the $g_{9/2}$ state is -13.351, while the eigenvalues contributing to the $g_{7/2}$ state are 0.972 and 0.235. Since the effective amplitude of the state is proportional to the square of the eigenvalue one can calculate $g_{9/2}$ and $g_{7/2}$ contributions as follows:

$$\text{for } g_{9/2} \quad \frac{(-13.351)^2}{(-13.351)^2 + (0.972)^2 + (0.235)^2} = 0.994$$

$$\text{for } g_{7/2} \quad (1 - (0.994)^2)^{\frac{1}{2}} = 0.106$$

Therefore, at nuclear deformation N=4 ($\beta=0.2$) the single-particle Nilsson orbital 21, correlating with the $1g_{9/2}$ shell-model orbital, can be expanded as:

$$|K = 7/2\rangle = 0.994\,|g_{9/2},\ 7/2\rangle + 0.106\,|g_{7/2},\ 7/2\rangle.$$

Thus, moderate static or dynamic nuclear deformation can provide the necessary amplitude. It is also important to note that the 2^+ first excited states of the even palladium isotopesdecrease uniformly in energy from mass number 102 to mass number 112 (556 to 349 KeV), indicating an increasing tendency for static or dynamic deformation which mirrors the increasing transition probabilities of the E3 processes found in the adjacent odd silver isotopes.

V. Preliminary Search for ^{92m}Y and ^{94m}Y

A. Experimental

The experimental parameters were exactly the same as those used for production of ^{93m}Y; that is, beam-on-target time of 0.75 second, beam-off-target time of 3.25 seconds, and 10 successive 0.20 second spectra.

Foils enriched in ^{94}Zr (>95%) and ^{96}Zr (Table XVII) were bombarded with 10 MeV deuterons in an attempt to produce ^{92m}Y and ^{94m}Y by (d,α) reactions. One 2.5 hour run was performed with the foil enriched in ^{96}Zr, while 2.5 hour and 4.5 hour runs were performed with the foil enriched in ^{94}Zr. Typical incident particle currents were of the order of 0.5 μA.

B. Results

The γ-spectra were analyzed using the computer code BRUTAL,[10] and a list of the peak energies observed and assigned nuclides for the deuteron bombardment of ^{96}Zr is given in Table XVIII. The only gamma-ray peaks having areas greater than 200 counts for the deuteron irradiation of ^{94}Zr were from the experimental apparatus or background peaks, and therefore, these results are not listed. No peaks in these irradiations could be attributed to ^{94m}Y or ^{92m}Y.

C. Discussion

No isomeric state of ^{92}Y could be identified, and no ground state ^{92}Y was observed. Since no ground state was observed, very little (d,α) reaction took place. It is

Table XVII

Analyses of ^{96}Zr Target

(done at Oak Ridge National Laboratory)

Isotopic Analysis			Spectrographic Analysis			
Isotope	Atomic Percent	Precision	Element	Percent	Element	Percent
90	7.25	±0.10	Ag	<.01	Mg	<.01
91	1.41	±0.05	Al	<.05	Mn	<.02
92	2.24	±0.05	B	<.01	Mo	<.02
94	3.85	±0.05	Ba	<.01	Na	<.01
96	85.25	±0.10	Be	<.001	Ni	<.05
			Bi	<.02	Pb	<.02
			Ca	.02	Pt	<.05
			Cd	<.05	Rb	<.02
			Co	<.05	Sb	<.05
			Cr	<.05	Si	.01
			Cs	<.05	Sn	<.02
			Cu	.01	Sr	<.01
			Fe	.02	Ta	<.05
			Ge	<.05	Ti	<.01
			Hg	<.05	V	<.02
			K	<.01	W	<.05
			Li	<.005	Zr	<.2

Table XVIII

γ-Ray Energies and Residual Nuclei
for Deuteron Bombardment of ^{96}Zr

Gamma-Ray Energies(KeV)	Nuclide
122	^{57}Fe
138	^{57}Fe
162	^{116m}In
219	^{96}Nb
241	^{96}Nb
372	^{96}Nb
416	^{116}In
460	^{96}Nb
481	^{96}Nb
511	e^+-e^- annihilation
570	^{96}Nb+ ^{207m}Pb
658	^{97}Nb
719	^{96}Nb
743	^{97m}Nb
778	^{96}Nb
810	^{96}Nb
850	^{96}Nb
917	^{94}Y

obvious that the experimental conditions were not appropriate for producing the desired (d,α) reaction, and another irradiation with higher incident particle energy should be done.

An isomeric state of ^{94}Y was not observed; however, some ground state of ^{94}Y was observed. This implies that if any ^{94m}Y was produced, it had already decayed to the ground state during the first 0.2 second counting interval. If one assumes that some isomeric state was produced during this irradiation, a higher limit of the half-life of ^{94m}Y can be estimated to be <0.2 seconds.

These results represent only a preliminary search for these isomers, and a much more detailed study is necessary.

VI. Conclusions

The experimental matrix elements for radiative E3 transitions vary widely and irregularly from predictions based on the single-particle model.[56] For the odd-mass nuclei, the observed transition probabilities usually fall between one and four orders of magnitude below the Weisskopf prescription. This behavior is in marked contrast to the relative constancy of the M4 matrix elements, and is generally assumed to indicate that the E3 transitions proceed via relatively minor components in the wave functions of the initial or final states.

Two new E3 odd-proton isomers near the beginning and the end of the Z=39 and Z=49 region are reported here. Half-lives

for the E3 isomers of ^{93}Y and ^{101}Ag have been measured to be 0.82 ± 0.04 seconds and 3.12 ± 0.12 seconds, respectively, and the single-particle hindrance factors were also determined.

A single-particle hindrance factor of 3.5 was determined for ^{93m}Y. This hindrance was explained in terms of other experimental data, which inferred that the $p_{3/2}^{-1}$ state contribution to the 590 KeV, ℓ_p=1 level was only about 25%. Other $p_{3/2}$ configurations which could not produce the E3 transition accounted for the observed hindrance, and the single-particle concept could still be invoked.

A different approach was used to explain the measured hindrance factor of 68 in ^{101m}Ag. If only $p_{\frac{1}{2}}$ and $g_{9/2}$ proton single-particle orbitals are involved in the $\frac{1}{2}$- and 7/2+ states, the connecting E3 transition is forbidden; however, an admixture of the $g_{7/2}$ orbital into the 7/2+ state would allow this transition. Just such an admixture was shown to exist, if one considers nuclear deformation.

Enriched foils of ^{94}Zr and ^{96}Zr were bombarded in a preliminary search for ^{92m}Y and ^{94m}Y by (d,α) reactions. It was concluded that the experimental conditions for the ^{94}Zr irradiation were not appropriate, and higher deuteron (>10 MeV) energies should probably be used. The (d,α) reaction on ^{96}Zr produced some ^{94}Y (g.s), and if the isomeric state was formed its half-life is less than ~0.2 seconds.

PART III

Radiochemical Isolation of Spallation-Produced ^{88}Y and ^{43}K.

I. Production of Radioisotopes at LAMPF

The Clinton P. Anderson Los Alamos Meson Physics Facility (LAMPF) linear accelerator will produce a one-milliampere current of 800-MeV protons to be used primarily for producing secondary meson beams. The main accelerator characteristics are shown in Table XVIV. Approximately one-half of this beam, with an energy of about 700 MeV, is expected to ultimately reach the main beam stop, and this residual beam of protons will be used to produce substantial amounts of radioisotopes of potential use in biomedicine, Safeguards, and other fields of research.

Figure 26 shows the LAMPF experimental areas, and the Isotope Production Facility is located at the far east end of the accelerator, in front of the primary accelerator beam stop. This facility will have several independently-operable stringers to position selected targets to intercept the proton beam. These stringers, along with the beam stop and water-cooling lines, are shown schematically in Figure 27. The configuration of one of the target chambers coupled to the end of a stringer and positioned ahead of the beam stop is shown in Figure 28. The six-inch diameter target chamber will accommodate targets up to 1.5 inches thick.

At the Isotope Production Facility, desired nuclides are produced primarily by spallation reactions in which several particles are emitted from the target nuclei after bombardment with the energetic protons. A broad

Table XVIV

LAMPF ACCELERATOR CHARACTERISTICS

BEAM ENERGY = 800 MeV, CONTINUOUSLY VARIABLE

BEAM INTENSITY

AVERAGE CURRENT = 1 mA

EXTRACTION EFFICIENCY = 100%

PULSE LENGTH = 500-1000 μSEC

REPETITION RATE = 120 CPS

BEAM QUALITY

ENERGY SPREAD = ± 0.4%

BEAM AREA IN TRANSVERSE PHASE SPACE = π MRAD-CM.

MACRO DUTY FACTOR = 6-12%

RF MICROSTRUCTURE = 0.25 NS PULSES SEPARATED BY 5 NS

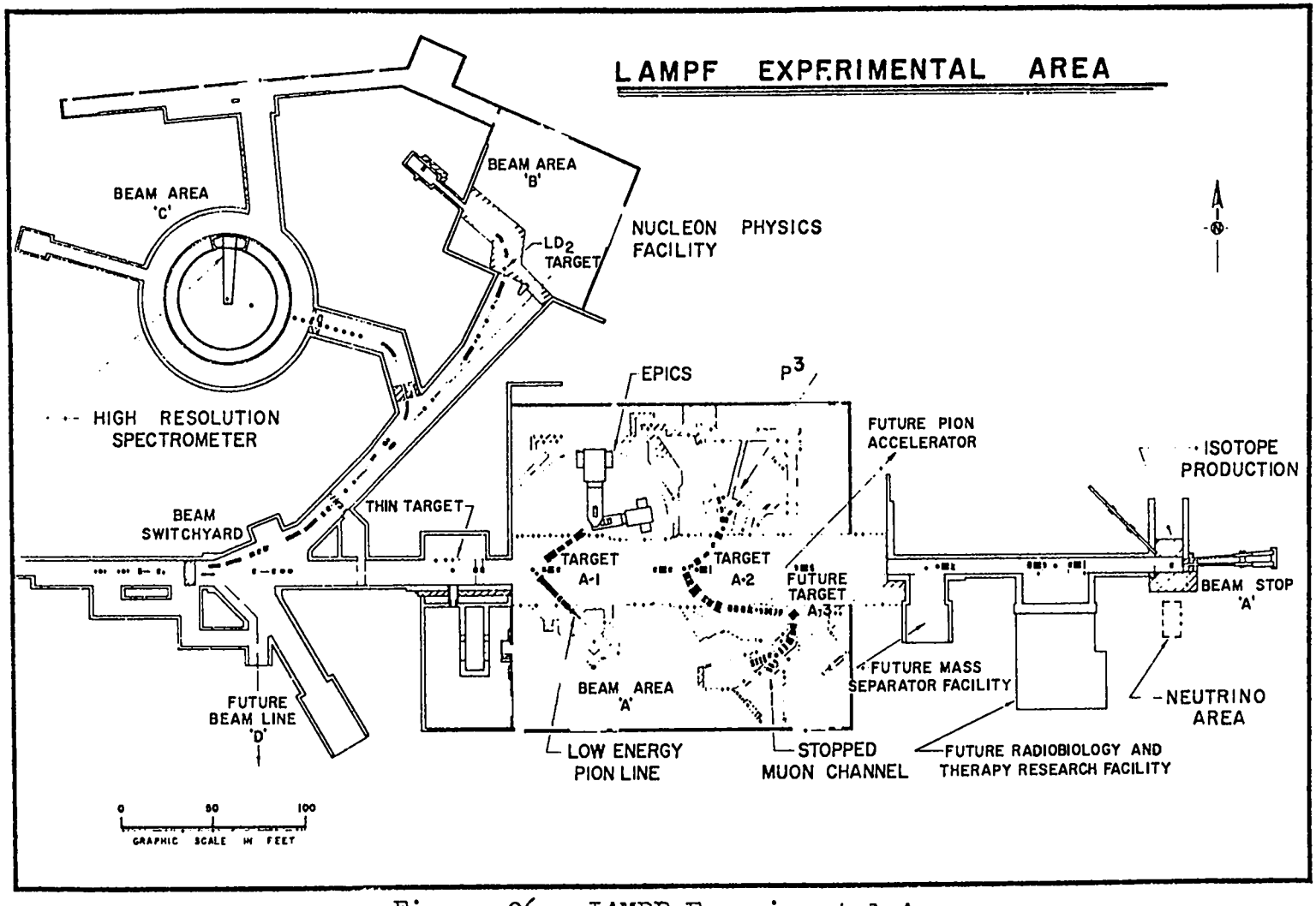

Figure 26. LAMPF Experimental Area

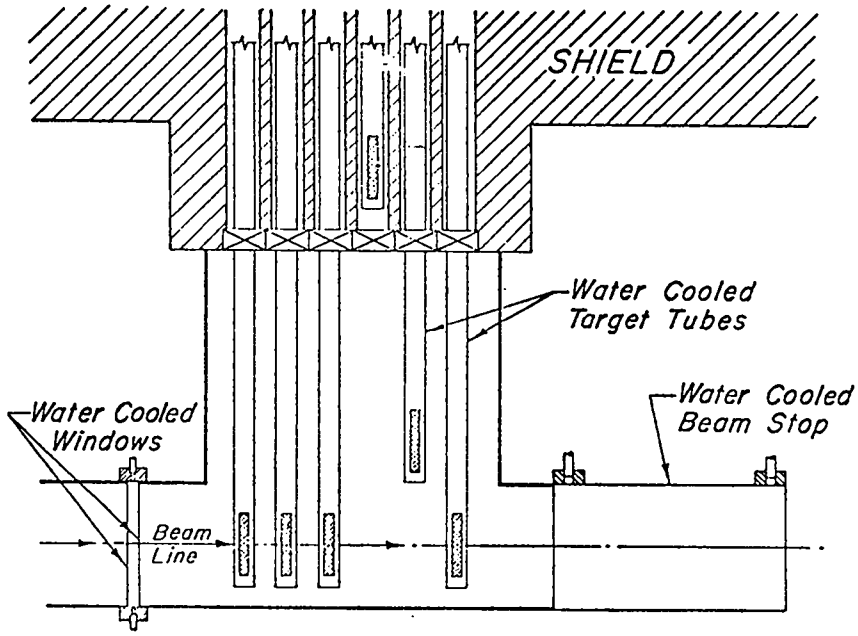

Figure 27. PROPOSED ISOTOPE PRODUCTION TARGET ASSEMBLY

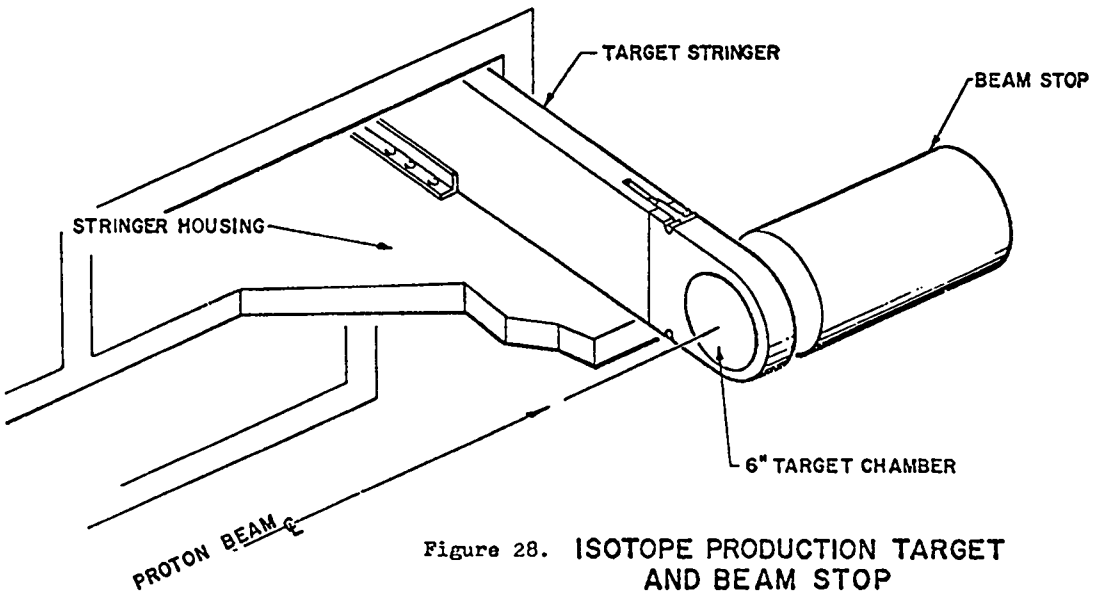

Figure 28. ISOTOPE PRODUCTION TARGET AND BEAM STOP

spectrum of mainly neutron-deficient species is generated during the course of an irradiation, and the activity of interest must then be isolated from a number of radiocontaminants. Laboratory-scale chemical separation procedures using microcurie amounts of radioactivities are currently being developed for the isolation of selected radioisotopes. The techniques developed at this level will eventually be scaled up and implemented in a hot-cell operation to process multi-curie quantities of the radionuclides of interest.

II. Isolation of ^{88}Y from Molybdenum Targets

A. Introduction

Several radionuclides possess nuclear properties that would be useful for making photoneutron sources of various neutron energies. Such sources would have diverse applications in remote activation analysis systems, including oil well logging and the Nuclear Safeguards Program.[62] A discussion of how LAMPF can be utilized for production of selected radionuclides for use as the active component in low-energy (<1 MeV) photoneutron sources has been published by O'Brien and Schillaci.[63] Two primary criteria which determine whether a nuclide can be useful in photoneutron sources are: (a) the half-life of the nuclide must be at least a few days, and (b) a gamma ray of energy greater than the threshold for ^{9}Be neutron evaporation (1.666 MeV) must be emitted by the nuclide. At present, the source most commonly used to

produce low energy (24 KeV) photoneutrons when combined with beryllium is 60.2-d ^{124}Sb.

Because the isotope ^{88}Y has a half-life of 107 days and emits a 1.8361 MeV gamma ray,[64] it is a likely candidate for use in photoneutron sources. A comparison of the proposed ^{88}Y-Be source with the ^{124}Sb-Be source by O'Brien and Schillaci[63] pointed out that the yttrium source has almost a factor-of-2 advantage in half-life, can be made smaller than the ^{124}Sb source (because of the high specific activity), has about the same total neutron intensity on a per-curie basis as the ^{124}Sb source, and would produce the more-penetrating 150-KeV neutrons as opposed to the 24-KeV neutrons of ^{124}Sb-based sources. In general, a ^{88}Y-Be source should be able to compete favorably with the ^{124}Sb-Be source.

A radiochemical procedure has been developed by Grant, et. al.,[65] for the quantitative recovery and purification of strontium activities from proton-irradiated molybdenum targets (^{82}Sr is of use in diagnostic nuclear medicine). Since a great deal of ^{88}Y is also obtained from irradiated Mo targets (primarily from the decay of spallation-produced ^{88}Zr), it was decided to branch-off from and extend the Mo-^{82}Sr procedure to isolate a pure radioyttrium fraction. Consequently, some knowledge of the analytical work done by Grant et. al.[65] is necessary for an understanding of the present work, and a summary of their experimental technique follows.

A target packet containing very pure molybdenum (99.95%) was irradiated with medium-energy protons at LAMPF for 1 to 10 μA-hrs. of integrated intensity. Following several days decay, the molybdenum target was dissolved in 30% H_2O_2, after which the excess peroxide was driven off by gentle heating. The solution was then made basic with NH_4OH, causing a yellow-brown solid (probably one or more hydrous molybdenum oxides) to precipitate. Most of the yttrium activity (~90%) was carried by this precipitate. After separation of the solid from the alkaline solution, Pb^{+2} was added to the liquid to form lead molybdate, which coprecipitated the strontium and the remainder of the yttrium activity. The lead precipitate was then subjected to solvent extraction with 0.12M HCl and a 50% bis-(2-ethylhexyl) phosphoric acid (HDEHP) in toluene solution. The radiostrontium remained in the aqueous phase, while the yttrium was quantitatively extracted into the organic phase.

Subsequent sulfide precipitation and ion exchange steps resulted in the final isolation of pure radiostrontium. The chemical procedures used by Grant, et. al.[65] are depicted schematically in Figure 29 , and the overall chemical yields for each of the various steps are reproduced in Table XX.

B. Experimental

In the radiostrontium separation procedure previously discussed, most of the radioyttrium was found with the hydrous molybdenum oxide (molybdenum hydroxide) precipitate,

1. DISSOLUTION

$$\text{Mo Target} \xrightarrow{30\%\ H_2O_2} H_2MoO_4 \cdot H_2O$$

2. MOLYBDENUM HYDROXIDE PRECIPITATION

$$H_2MoO_4 \cdot H_2O \xrightarrow{NH_4OH} MoO(OH)_x\downarrow$$

3. LEAD MOLYBDATE PRECIPITATION

$$H_2MoO_4 \cdot H_2O \xrightarrow[Pb^{2+}]{\text{basic}} PbMoO_4\downarrow$$

4. SOLVENT EXTRACTION

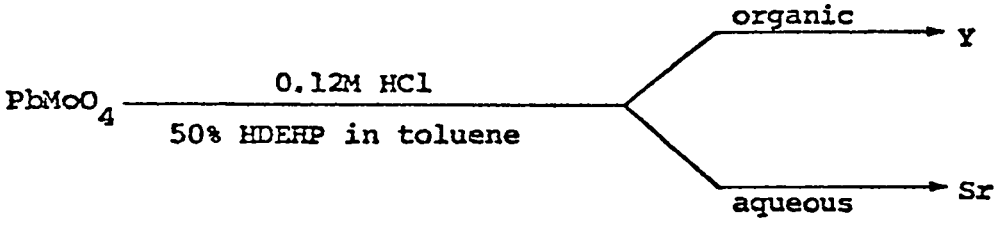

5. SULFIDE PRECIPITATION

$$\text{Aqueous Solution} \xrightarrow[H_2S]{\text{basic}} PbS\downarrow + MoS_4^{=} \xrightarrow{\text{acidic}} MoS_3\downarrow$$

6. ION EXCHANGE

$$\text{Sulfide Filtrate (+ Sr carrier)} \xrightarrow[pH = 6]{HZO} Sr$$

Figure 29. Radiochemical procedure for the separation of ^{82}Sr from proton-irradiated Mo targets.

Table XX

Radiochemical Isolation of ^{82}Sr from Proton-irradiated Mo Metal

Analytical Step	Chemical Fraction	Overall Chemical Yield (%)									
		Tc	Nb	Zr	Y	Sr	Rb	Se	As	Zn	Co
Original Solution	---	100	100	100	100	100	100	100	100	100	100
$MoO(OH)_x$ ↓	precipitate	0	0	89 ± 5	88 ± 6	0.9 ± 2	0	0	0	0	0
	filtrate	100	100	11 ± 5	12 ± 6	99 ± 2	100	100	100	100	100
$PbMoO_4$ ↓	filtrate	95 ± 5	66 ± 20	0.9 ± 1	0.3 ± 0.4	0.6 ± 0.5	99 ± 1	98 ± 2	94 ± 6	92 ± 10	97 ± 2
	precipitate	4.8 ± 5	34 ± 20	10 ± 1	12 ± 0.4	98 ± 0.5	0.8 ± 1	2.4 ± 2	6.2 ± 6	8.0 ± 10	2.8 ± 2
HDEHP	organic	0	28 ± 20	9.9 ± 1	12 ± 0.4	0.8 ± 1	0	0	0	0	0
	aqueous	4.8 ± 5	5.8 ± 10	0.2 ± 0.3	0.02±0.05	98 ± 1	0.8 ± 1	2.4 ± 2	6.2 ± 6	8.0±10	2.8 ± 2
Sulfide ↓	precipitate	4.8 ± 5	5.8 ± 10	0.2 ± 0.3	0.02±0.05	3.0 ± 3	0	0	5.0 ± 4	1.0 ± 2	2.2 ± 3
	filtrate	0	0	0	0	95 ± 2	0.8 ± 1	2.4 ± 2	1.2 ± 2	7.0±10	0.5 ± 1
HZO	exchanger	0	0	0	0	1.0 ± 1	0.4±0.5	2.4 ± 2	1.2 ± 2	7.0±10	0.5 ± 1
	eluent	0	0	0	0	94 ± 2	0.4±0.5	0	0	0	0

while the remainder was found in the organic phase of the HDEHP extraction. The only other elements associated with the yttrium at these points were Nb, Zr, Mo, and a small amount of Sr.

After dissolution of the molybdenum hydroxide precipitate in 10 ml. of 0.1N HCl, this solution was equilibrated with 10 ml. of a 50% HDEHP in toluene mixture on a Burrell wrist-action shaker for 50 minutes. The organic phase of this extraction contained the yttrium activity and was added to the organic phase from the prior Mo-^{82}Sr HDEHP extraction. All of the ^{88}Y present was therefore combined into one experimental fraction here for further chemical processing.

An independent investigation[66] showed that solvent extraction with 8M HCl will strip 95% of the yttrium from the organic HDEHP phase; however, less-concentrated HCl or much-more concentrated HCl is not as effective. Therefore, the combined HDEHP experimental solution was stripped twice successively with equal volumes of 8M HCl, to insure quantitative yttrium removal from the organic phase. Each acid-strip was performed on the Burrell shaker for 50 minutes. These stripping steps resulted in an excellent separation of Y from Nb and Zr, both of which remained in the organic phase while Y and Mo migrated into the aqueous layer.

Previous work by Kraus and Nelson[67] indicated that the separation of Y from Mo could be accomplished by anion exchange at high hydrochloric acid concentration. Although

Nb and Zr were effectively separated from Y during the previous 8M HCl solvent extraction, performing the anion exchange step in a 12M HCl medium would insure removal of any remaining minute quantities of these radioelements (along with the Mo) from solution. This consideration becomes increasingly important in scaling the procedure to a hot-cell operation.

Therefore, the aqueous solution from the 8M HCl stripping procedure was evaporated to near-dryness on a steam bath and redissolved in 10 ml. of 12M HCL. This solution was then passed through an anion exchange column composed of Bio-Rad AG1-X10 resin in the chloride form. The 100-200 mesh resin was previously conditioned with 12M HCl. Dimensions of the column were 0.8 cm in diameter and approximately 9 cm in length, and representative flow rates were of the order of 0.1 ml./min. The resin under these conditions absorbed Mo, Nb, and Zr, but allowed Y to pass through with essentially no chemical interaction. A representation of the supplementary chemical steps used in the ^{88}Y isolation is shown in Figure 30.

During the analytical separations, one to five-milliliter aliquots were removed from the experimental solutions and mounted in a constant geometry for radioactivity counting by γ-ray spectrometry. The spectrometer system consisted of a closed-end coaxial, cylindrical Ge(Li) crystal of 57 cm^3 active volume, a Canberra Model 8060 analog-to-digital

1. SOLVENT EXTRACTION

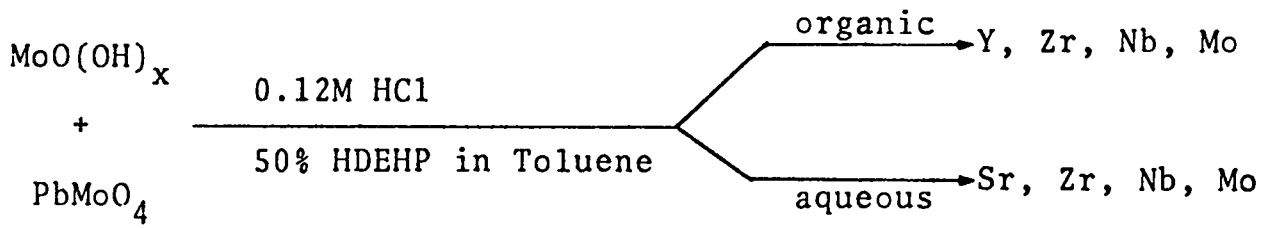

2. ACID STRIP

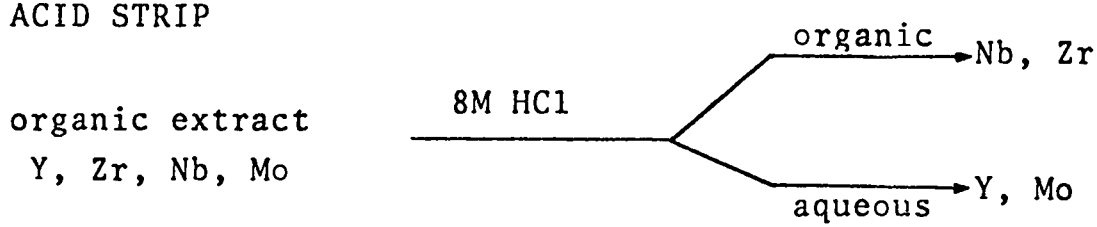

3. ION EXCHANGE

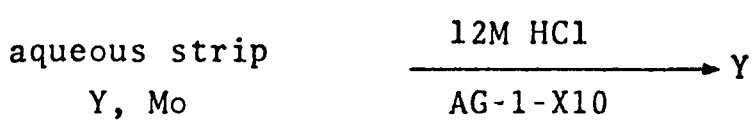

Figure 30. Partial Radiochemical Procedure for the Isolation of ^{88}Y from Proton-irradiated Mo Targets.

converter, a Canberra Model 8700 processor and memory unit, and a Pertec fast magnetic-tape transport.

Magnetic tape containing stored γ-spectra were analyzed with the computer code GAMANAL[68] on a CDC 7600 computer. Chemical yields were determined from the calculated activities of well-characterized gamma energies found by this code. Nuclidic assignments of individual gamma rays were based upon literature values of gamma energies and half-lives.[69]

Prohibitively-short half-lives precluded the tracing of Mo behavior through any of its isotopes. Concentrations of this element were consequently measured with a Perkin-Elmer 403 Atomic Absorption Spectrophotometer.

C. Results and Discussion

Three independent experiments were performed to determine the overall chemical yields and their errors (1 σ), and the results are shown in Table XXI. A zero in this table means that the element was not detected in any of the three analysis, and all values of the quantities of radioelements initially present for this study were obtained from the work of Grant et. al.[65]

The addition of three steps to the radiostrontium procedure was sufficient for the complete isolation of Y. As expected, the extraction with HDEHP provided an excellent Sr-Y separation, and the subsequent HCl back-extraction quantitatively separated the Y from both Nb and Zr. Some Mo

Table XXI

Radiochemical Separation of ^{88}Y from Proton-irradiated Mo Targets

ANALYTICAL STEP	CHEMICAL FRACTION	OVERALL CHEMICAL YIELD (%)			
		Nb	Zr	Y	Sr
Original Soln ($MoO(OH)_x$ PPT. + HDEHP Organic From Mo - ^{82}Sr Procedure		28 ± 20	99 ± 6	100 ± 6	1.7 ± 3
HDEHP	aqueous	1.4 ± 2	6.5 ± 5	0.06 ± 0.1	1.7 ± 3
	organic	27 ± 20	93 ± 6	100 ± 6	0
8M HCl Strip (twice)	organic	27 ± 20	93 ± 6	0.5 ± 0.3	0
	aqueous	0	0	100 ± 6	0
AG1 · X10	resin	0	0	3.8 ± 4	0
	eluent	0	0	96 ± 4	0

target material was also present in the 8M HCl solution, and it was completely separated from the Y through adsorption on the anion exchange column.

Molybdenum distribution coefficients (equal volume) for the HDEHP and the 8M HCl solvent extractions were determined by atomic absorption spectroscopy to be:

$$K_D = [Mo]_{HDEHP}/[Mo]_{.12M\ HCl} = 15.2 \pm 0.15 \text{ and}$$

$$K_D = [Mo]_{8M\ HCl}/[Mo]_{HDEHP} = 0.166 \pm .005.$$

Additional atomic absorption analysis showed that essentially all of the Mo initially present was removed after the anion exchange procedure. (Greater than 0.1% would have been detected, but none was).

Since much of the Y (~90%) was carried by the hydrous molybdenum oxide precipitate in the Mo-^{82}Sr procedure, recovery of only this Y fraction might prove to be more cost-effective in the eventual large-scale hot-cell operation, even though it would mean sacrificing 10% of the chemical yield. A one-step separation was therefore developed, in which this precipitate was dissolved in 12M HCl and passed directly through the AG1-X10 anion exchange column. Gamma-spectral analysis of the eluents from two independent experiments determined that 99 ± 5% of the Y and 1.5 ± 0.5% of the Zr initially charged onto the column were not retained by it. No Mo was detected in either eluent.

To illustrate the performance of the total Mo-^{88}Y separation procedure, a spectrum of an original target solution

acquired approximately one month after irradiation is shown in Figure 31 , with a detailed listing of all long-lived radioactivities observed in Mo targets given in Table XXII. These can be compared to the gamma-spectrum of the final AG1-X10 eluent shown in Figure 32. The spectral illustration of the original solution depicts about 25 identified gamma-ray transitions, while the spectrum of the final chemical process solution contains but five discernible peaks. All of these have been attributed to the decay of ^{88}Y: 511 KeV annihilation radiation, 898 and 1836 KeV gamma transitions, and single- and double-escape peaks from the 1836 KeV gamma ray.

D. Conclusions

A supplement to the radiochemical procedure for the isolation of ^{82}Sr from molybdenum targets bombarded with medium-energy protons has been developed. With an additional three chemical steps, a quantitative recovery (96 ± 4%) of carrier-free ^{88}Y decontaminated from at least ten other elements has been accomplished.

Spallation yields from 600-MeV proton-induced reactions in molybdenum[70] infer that approximately three times as much ^{88}Zr ($t_{1/2}$=85D) is produced as ^{88}Y. Since ^{88}Y is the daughter of ^{88}Zr, much more radioyttrium can be obtained if there is a waiting period after the irradiation to allow for ^{88}Zr decay. The maximum ^{88}Y activity resulting from ^{88}Zr decay

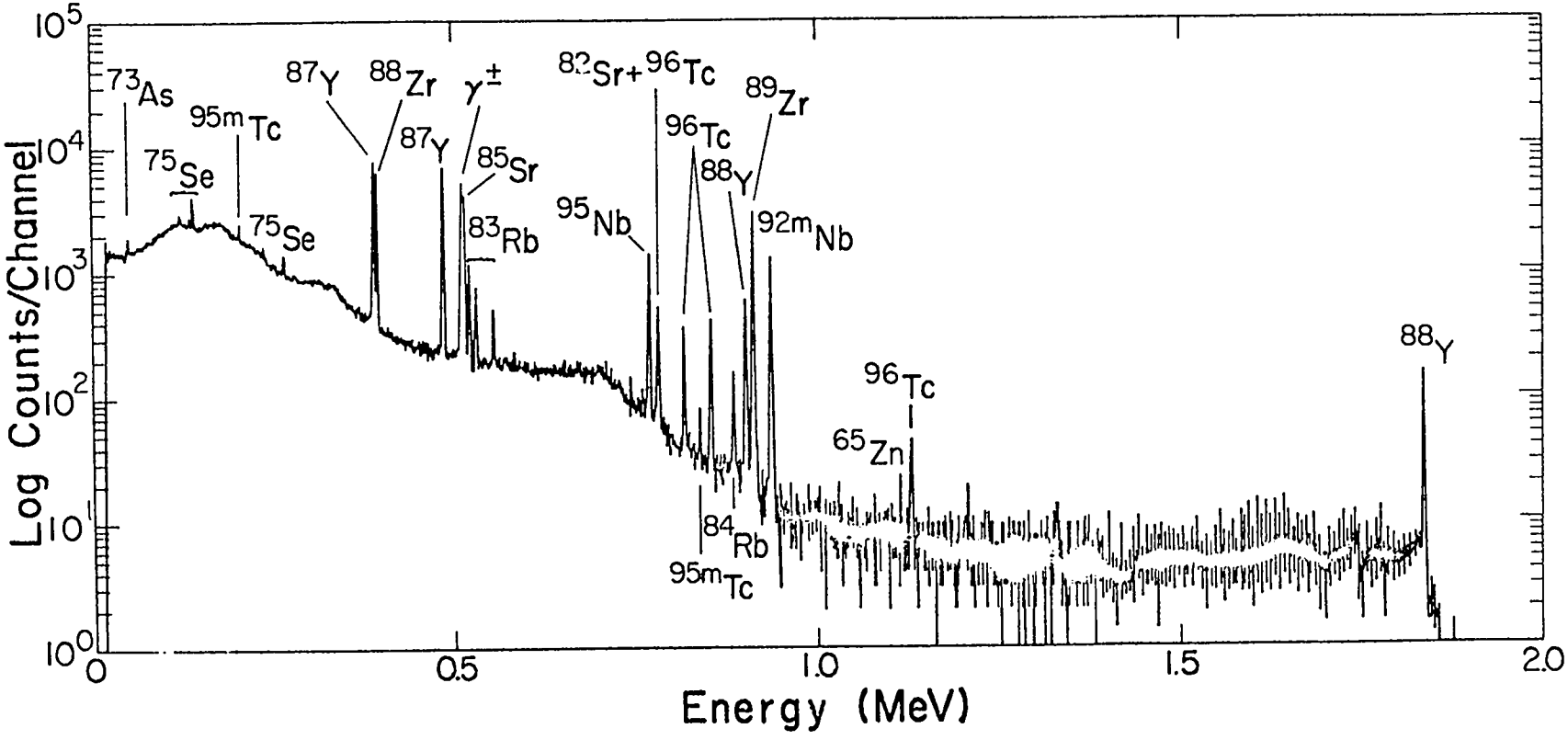

Figure 31. γ-Spectrum of the Original Mo Target Solution before Radiochemical Separation.

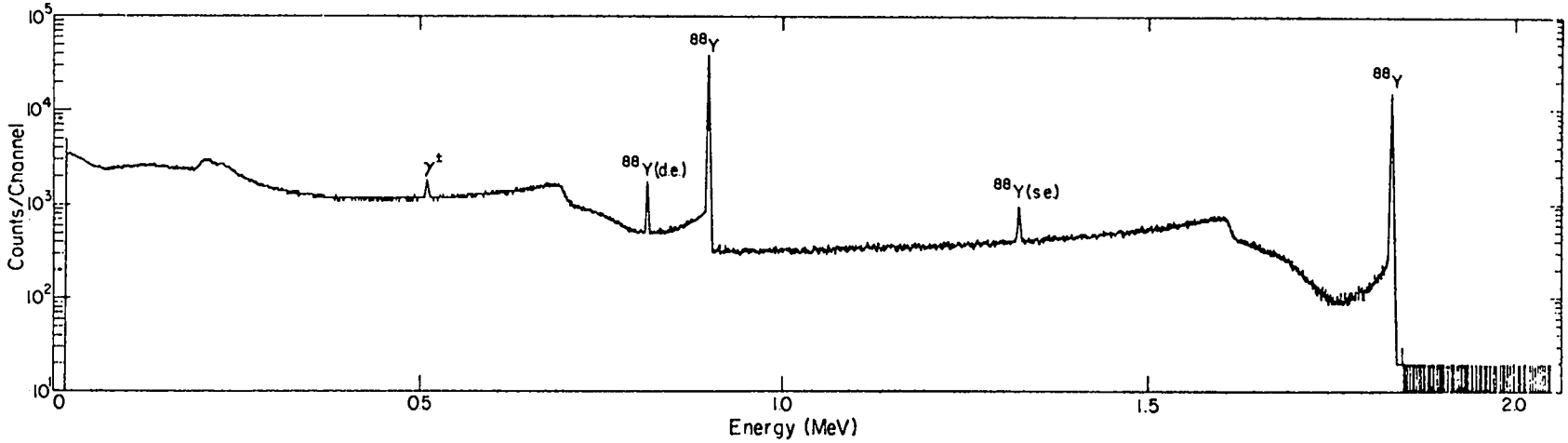

Figure 32. γ-Spectrum of the Final Radioyttrium Solution

Table XXII

Long-lived Radioactivities Observed in 500 MeV Proton-irradiated Mo Targets

Z	A	Half-life (Days)	E_γ(KeV); Intensity
Tc	96	4.3	780(100%), 814(82%), 851(99%), 1126(15%)
	95m	61	203.9(100%), 582.2(55%), 786.2(6%), 820.6(8%), 835.1(45%)
Nb	95m	3.8	235.7(100)
	95	35	765.8(99%)
	92m	10	934.5(98%)
	91m	62	104.5(0.5%), 1205.9(3%)
Zr	95	65	724.2(43%), 756.7(55%)
	89	3.2	909.2(100%)
	88	85	392.8(97%)
Y	88	108	898.0(92%), 1836.1(100%)
	87	3.3	388.3D(80%), 484.8(92%)
Sr	85	64	514.0(100%)
	82	25	698.4D(0.1%), 776.8D(13%) 1395.2D(0.5%)
Rb	84	33	881.5(73%)
	83	83	520.4(47%), 529.6(30%), 552.6(17%) 790.1(0.7%), 801(0.3%)
Se	75	120	66.0(1%), 96.7(3%),121.1(17%) 136.0(58%), 198.6(1%), 264.6(61%) 279.6(25%), 304.0(1%), 400.7(12%)
As	74	18	596.0(60%), 608.3(0.6%), 634.9(15%) 1204.3(0.2%)
	73	76	53.4(10%)
Zn	65	245	1115.4(49%)
Co	58	71	810.6(99%)
	56	77	846.8(100%), 1037.8(13%), 1238.3(67%)
Be	7	53	477.4(10%)

can be calculated from the following formula:[71]

$$t_m = \left(\frac{1}{\lambda_2 - \lambda_1}\right) \ln\left(\lambda_2/\lambda_1\right).$$

Substituting $\lambda_2(^{88}Y) = 6.48 \times 10^{-3} d^{-1}$ and $\lambda_1(^{88}Zr) = 8.2 \times 10^{-3} d^{-1}$, the maximum ^{88}Y activity is calculated to occur approximately 140 days after the end of bombardment. As a result, the hot-cell operation should be delayed about 5 months after the irradiation in order to obtain the maximum yield of ^{88}Y. This, in effect, would require storing the HDEHP organic phase and hydrous molybdenum oxide precipitate from the Mo-^{82}Sr procedure for the necessary time period before implementing the supplemental ^{88}Y chemical techniques described above.

After the 8M HCl back-extraction of the ^{88}Y, most (93 ± 6%) of the zirconium was observed to be present in the HDEHP organic phase (along with some niobium, molybdenum, and a small amount of yttrium). If the ^{88}Zr could be recovered in the carrier-free state, it might also be incorporated into the photoneutron source without adding any additional bulk. A photoneutron source prepared with the philosophy of a combined ^{88}Zr-^{88}Y component could allow fabrication without a required ^{88}Zr decay period, perhaps facilitate hot-cell handling by reducing the quantity of very-penetrating 1836-KeV gamma rays, and probably increase the useful half-life of the source by having a ^{88}Y-generator to partially replenish some of the ^{88}Y lost through decay.

III. Isolation of ^{43}K from Vanadium Targets

A. Introduction

Radioactive isotopes have become a very valuable tool in diagnostic medicine. Since heart disease is the leading cause of death in the U.S., there is a great deal of interest in finding suitable radioisotope agents for a variety of diagnostic tests of cardiac abnormality. There has been considerable interest generated in the last five years for production and isolation of ^{43}K for medical uses;[72,73] particularly in myocardial studies, because potassium ions rapidly migrate from blood to myocardial tissue.

The cells of the myocardium (heart muscle) receive blood by way of two small vessels, the right and left coronary arteries. Since millions of people suffer from coronary disease each year, non-traumatic and non-invasive techniques to provide knowledge about the distribution of coronary artery branches has the utmost practical importance.

A fact, of life-and-death importance is that only a few detours exist between the larger branches of the coronary arteries, through which arterial blood can travel if the main route becomes obstructed. If, for example, a blood clot closes one of the larger coronary artery branches, either the blood supply is diminished (an area of myocardial tissue becomes ischemic) or it is cut off completely. In the latter case, cells deprived of oxygen and nutrients carried by the blood rapidly die (necrose), with the affected area being

termed an infarction. However, another anatomical fact brightens this picture somewhat-many blood detours do exist between very small arterial vessels in the heart, and given time, new ones develop and provide collateral circulation to ischemic areas. Several surgical procedures have been devised to aid this process, one of which is the aortocoronary by-pass graft.

At this time there are at least four immediate uses for ^{43}K in myocardial studies.[74] (1) Myocardial infarction can be detected using ^{43}K, which shows a decreased concentration in the infarcted area. (2) The myocardium may receive sufficient blood at rest; however under stress ischemia or angina pectoris (sudden attack of chest pain with feeling of suffocation) occurs. Potassium-43 scans taken both at rest and following exercise to angina can distinguish the extent of the condition. (3) Major vessels containing aneurysms (blood-filled saclike dilatations of the wall of an artery) contain only about 10% of the normal activity and can readily be detected using ^{43}K. (4) Surgical aortocoronary by-pass grafts are performed for severe cases of arterial obstruction. Potassium-43 can be used for evaluation of the operation of a bypass graft soon after placement is completed, while the most commonly used technique used to evaluate a graft, contrast angiography, cannot be used until two months after surgery. Contrast angiography involves injection of a dense radio-opaque dye into the coronary

arteries and x-ray detection, and therefore, this technique would have a traumatic effect on the graft.

Of the several radioactive isotopes of potassium only ^{42}K(12.4h) and ^{43}K(22.3h) have sufficiently long half-lives for use in clinical investigations. Potassium-42 can be readily produced from a reactor irradiation and has been used extensively in nuclear medicine, but the very energetic principal γ-ray energy (1.524 MeV) and β^- end-point energy (3.52 MeV) make it unsuitable for many diagnostic applications because of the excessive radiation dose to the patient and the difficulty of organ visualization using conventional medical scanners. Potassium-43 has abundant γ-ray energies of 373 KeV and 618 KeV and β^- end-point energies of 830 KeV and 460 KeV, making this isotope more suitable for medical use.

Potassium-43 is currently prepared either with a low energy cyclotron by the $^{40}Ar(\alpha,p)^{43}K$ reaction, with the High Flux Isotope Reactor at Oak Ridge National Laboratory by the $^{43}Ca(n,p)^{43}K$ reaction (the natural abundance of ^{43}Ca is only 0.145%), or by the $^{44}Ca(\gamma,p)^{43}K$ reaction. The current price for ^{43}K ($100 per mCi) is a deterrent to widespread utilization. Production of this isotope can be accomplished at LAMPF by 600- to 800-MeV proton bombardments of vanadium targets and subsequent chemical separation. Because of the high beam intensity of this accelerator, ^{43}K yields are substantially larger so that greater economics

can be realized.

The two main objectives of this work were: (1) to measure the thin-target cross sections for formation of ^{43}K and ^{42}K in 800-MeV proton-irradiated vanadium targets, and (2) to develop a radiochemical procedure for isolation of the radiopotassium (^{43}K) produced in these targets.

B. Cross Section Measurements of ^{43}K and ^{42}K from 800-MeV Protons on Vanadium

The thin-target cross sections for production of ^{43}K and ^{42}K with 800-MeV protons have not been previously reported. This information is of value in determining whether vanadium is a suitable target for production of ^{43}K at LAMPF, and the extent of isotopic contamination by ^{42}K.

1. Experimental Procedures

A packet consisting of thin foils arranged in order - Al,Al,Al,Al,V,Al - was used for the irradiation. The first three aluminum foils served as monitors to determine the number of protons impinging on the target array, and the aluminum foils before and after the vanadium foil served as catcher foils for recoiling vanadium reaction products. Thicknesses of the aluminum and vanadium foils were about 7 mg/cm^2 and 27 mg/cm^2, respectively, and a spectrochemical analysis done by Group CMB-1 of LASL of the vanadium used is given in Table XXIII. The packet was bombarded at LAMPF Experimental Beam Area "B" with 800-MeV protons for about 3 μA-hr. of integrated intensity.

Table XXIII

Analysis of Vanadium Target

Element	ppm	Element	ppm
Li	<6	Sr	<60
Be	<2	Cu	<6
B	<20	Zn	<600
Na	<60	Ga	<60
Mg	2	Ge	<20
Al	900	Zr	<200
Si	250	Mo	<200
K	<200	Ag	<6
Ca	<6	Cd	<60
Ti	<60	In	<200
Cr	<60	Sn	<60
Mn	<6	Sb	<60
Fe	110	Ba	<20
Co	<20	Pb	<60
Ni	<20	Bi	<60

After the end of bombardment, the packet was allowed to decay for 30 minutes and was then disassembled, and the individual foils were radioautographed with Polaroid film. The aluminum monitor and vanadium foils were then centered on aluminum rectangular plates for subsequent counting by γ-ray spectrometry (with the same spectrometer system used in Part I of this thesis).

2. Cross Section Calculations

Cross sections were computed according to the formula:

$$\sigma_x = \sigma_m \frac{A_x^0 f_m g_m W_x}{A_m^0 f_x g_x W_m}$$

In this formula A_x^0 and A_m^0 are disentegration rates of the target and monitor nuclides, g is the corresponding foil thickness in mg/cm^2, W is the atomic weight of the respective elements, and f is the saturation factor, $1 - e^{-\lambda t}$, where t is the length of irradiation and λ is the appropriate decay constant. The value of the calculated cross section, σ_x, is dependent upon a previously measured monitor cross section, σ_m, of aluminum reaction products (^{24}Na, ^{22}Na, ^{7}Be) with 800-MeV protons.

The EOB disintegration rates were calculated using the data[75] listed in Table XXIV, and the experimental cross sections were determined from the monitor cross sections[76] given in Table XXV.

Table XXIV

Nuclear Data Used to Calculate ^{43}K and ^{42}K Cross Sections for 800-MeV Protons on Vanadium

Nuclide	Half-Life	Gamma-Ray Energy (KeV)	Photons/Decay
^{42}K	12.36h	1524.2	0.18
^{43}K	22.3h	372.8	0.85
^{24}Na	15.02h	1368.6	1.00
^{22}Na	2.602Y	1274.6	1.00
^{7}Be	53.28d	477.6	0.103

Table XXV

Measured ^{43}K and ^{42}K Cross Sections for Different Monitors

Monitor	σ(mb) for 800-MeV protons on Al	σ(mb) ^{43}K	σ(mb) ^{42}K
^{24}Na	10.75	5.6	10.0
^{22}Na	16.3	6.5	11.5
^{7}Be	6.4	6.3	11.2

3. Results and Discussion

Cross section values of ^{43}K and ^{42}K are also shown in Table XXV based upon ^{24}Na, ^{22}Na and ^{7}Be monitor cross sections with 800-MeV protons; the calculated cross sections agreed to within 15% for the three monitor cross sections used. It was determined that the cross sections for 800-MeV protons on vanadium are 6 mb and 11 mb for ^{43}K and ^{42}K, respectively.

The major sources of error in these measurements were: (1) the uncertainty in determining the number of target atoms per unit area in the beam, (2) the effect of secondary reactions on product yields, (3) the uncertainties in determining detector γ-ray peak efficiency curves, (4) statistical errors, (5) variations in beam intensity during irradiation, (6) the uncertainties of beam monitor cross sections, and (7) the uncertainties in nuclear decay scheme data.

The reported cross sections have been corrected for recoiling potassium activities in the aluminum catcher foils. Experimental errors were estimated to be about ±15%, without regard to secondary reactions which took place or to errors in monitor cross sections.

C. Chemical Isolation of ^{43}K from Vanadium Targets

1. Experimental Procedures

The potassium activity was produced by irradiating two 0.01 inch V foils (spectrochemical analysis shown in Table XXIII) with 800-MeV protons at LAMPF for about 3 μA-hrs. of integrated intensity. About one hour after bombardment, the vanadium foils were dissolved in 8M HNO_3, resulting in a deep blue solution. This dissolution was slow at first, but as the exothermic reaction heated the test tube, the reaction became vigorous and gave off a brown gas (NO_2). Aliquots of this solution were used in the chemical procedures that follow.

Of primary concern for ^{43}K isolation was the separation of the bulk vanadium target from the radionuclides produced, and the separation of radiosodium from the radiopotassium. Previous work[77] had shown that sodium is quantitatively retained on the inorganic separator hydrated antimony pentoxide (HAP) with an excellent selectivity from concentrated hydrochloric acid solution. In dilute HCl solutions both potassium and sodium would be retained on the HAP; however, the behavior of vanadium under this condition was not known.

The HAP used was previously backwashed with distilled water to remove very fine particles, and the columns used were made by pouring the HAP into a shortened 50 ml. burrett which contained 5 mls. of 4M HNO_3. This HAP was either purchased from C. Erba, Milano, Italy or prepared using the

procedure of Girardi and Sabbioni.[78] Typical column dimensions were 0.8 cm in diameter and 2 cm in length, while representative flow rates were of the order of 0.2 ml/min.

After dilution of the original solution to a concentration of 4M in nitric acid and addition of Sc(150 μg) and K(150 μg) carriers, the resulting solution was then passed through a column of hydrated antimony pentoxide. An additional 15 ml. 4M HNO_3 wash was also eluted through the column, and, since the nitrate ion is a biological poison, the column was then washed with 1M HCl until a negative carbozole test[79] for nitrate ion was observed (about 15 mls. 1M HCl).

Of the radioelements detected, essentially all of the K, Na and Ca and most of the Sc and Be remained on the HAP column at this point, while all detectable vanadium had been eluted. As stated earlier, published work showed that sodium is quantitatively retained on HAP in concentrated HCl solutions. Therefore, about 40 mls. of 12M HCl were passed through the column; in some instances, fine particles of the column were found in the eluent, requiring centrifugation or filtration for removal. This eluent contained only K, Sc and Ca radioactivities, but a light yellow color indicated the presence of another contaminant. The presence of antimony (obviously from a breakdown of the HAP) was confirmed by atomic absorption spectroscopy.

Ion exchange studies by Kraus and Nelson[67] had shown that antimony could be effectively removed from solution at

fairly strong acid strength (8M HCl) using an anion exchange resin, and that Sb(V) was adsorbed to the resin more readily than Sb(III) under these conditions. To oxidize the antimony to the higher oxidation state, two mls. of 30% H_2O_2 were added to the 12M HCl eluent and low heat was applied until bubbling of the peroxide ceased. The heat applied was increased, and the solution was evaporated to a volume of 0.5-1.0 ml. Subsequently, 8M HCl was added to this solution until a volume of 15 ml. was attained, and this resulting solution was passed through the anion exchange resin Bio-Rad Ag 1-X8 in the chloride form. The 50-100 mesh resin was previously conditioned with 8M HCl. Typical column dimensions were 0.8 cm in diameter and 10 cm in length, while representative flow rates were of the order of 0.3 ml/min. The resin under these conditions adsorbed the antimony but not K, Sc and Ca.

The ion-exchange resin Bio-Rad Chelex 100 has been shown[80] to be selective for elution of alkali metal ions in basic solution; therefore, this resin was chosen for the final purification step. The 8M HCl eluent from the previous anion exchange step was evaporated to 0.5-1.0 ml. on a hotplate, and the pH of the resulting solution was adjusted to 10 with NH_4OH. After addition of about 15 ml. of the buffer solution 0.1N NH_4OH + 0.1N NH_4Cl (pH 9.4), this basic solution was passed through a Bio-Rad Chelex 100 column in the sodium form, and additional buffer solution was passed through the

column to a final volume of about 50-60 mls. The 100-200 mesh resin was previously conditioned with this buffer solution. Typical column dimensions and flow rate were essentially the same as was used for the previous anion exchange step. The potassium was present in the eluent, while the Ca and Sc (except for possibly a trace amount) remained on the column.

The radioactivity analysis was done in exactly the same manner as was described for isolation of ^{88}Y in the previous section. Nuclidic assignments of individual gamma rays were based upon literature values of gamma energies and half-lives. Since very little vanadium radioactivity was detected, concentrations of this element were measured with a Perkin-Elmer 403 Atomic Absorption Spectrophotometer. A representation of the chemical steps used in the ^{43}K isolation is shown in Figure 33.

2. Results and Discussion

Three independent experiments were performed to determine the overall chemical yields and their errors (1σ), and the results are shown in Table XXVI. A zero in this table means that the element was not detected in any of the three analyses. After dissolution of the vanadium target, all radioactivities were assumed to be present in solution in 100% yield. The inorganic exchanger hydrated antimony pentoxide was used to remove the bulk vanadium, sodium and any residue nitrate ion from the dissolution medium. Subsequently, an anion exchange step was used to remove antimony,

1. Dissolution

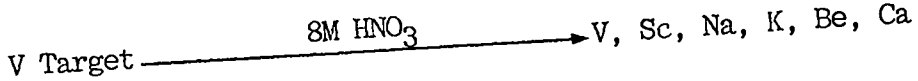

2. Separation Using Hydrated Antimony Pentoxide

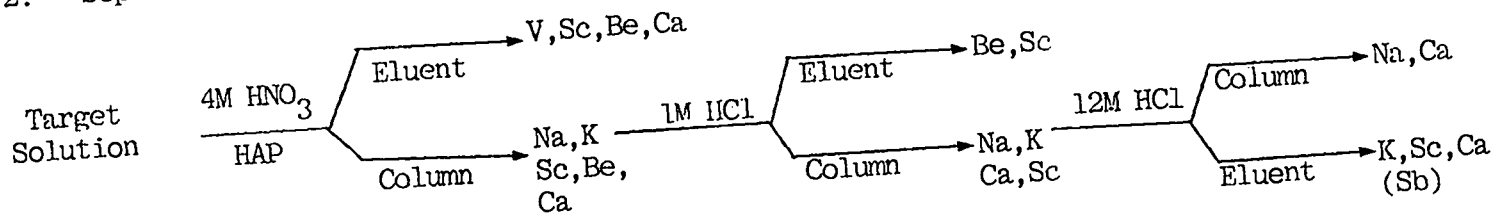

3. Ion Exchange

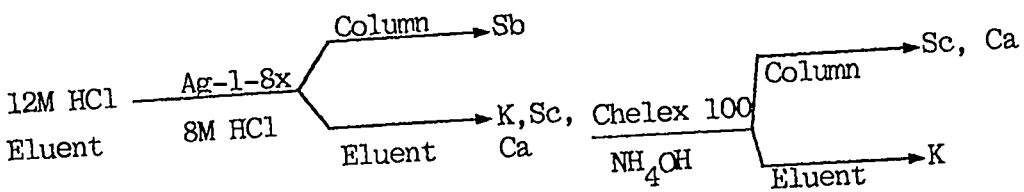

Figure 33. Radiochemical Procedure for the Isolation of ^{43}K from Proton-irradiated V Targets

Table XXVI
Radiochemical Separation of ^{43}K from Proton-Irradiated V Targets

ANALYTICAL STEP	CHEMICAL FRACTION	OVERALL CHEMICAL YIELD (1%)				
		K	Sc	Na	Ca	Be
Original Solution		100	100	100	100	100
HAP	4M HNO_3 Eluent	0	28 ± 30	0	3.2 ± 6	0
	Column	100	72 ± 30	100	97 ± 6	100
HAP	1M HCl Wash	0	6.5 ± 4	0	1.1 ± 1	48 ± 2
	Column	100	66 ± 30	100	96 ± 6	52 ± 2
HAP	Column	9.3 ± 3	4.6 ± 4	100	74 ± 6	52 ± 2
	12M HCl Wash	91 ± 3	61 ± 30	0	22 ± 4	0
AG-1-8X	Column	0	0	0	0	0
	Eluent	91 ± 3	61 ± 30	0	22 ± 4	0
CHELEX 100	Column	0	61 ± 30	0	22 ± 4	0
	Eluent	91 ± 3	0.1 ± 0.1	0	0	0

resulting from dissolution of some HAP column material, and the exchanger Chelex 100 was used to isolate potassium radioactivity from the other radiocontaminants.

Atomic absorption analysis of the 12MHCl hydrated antimony pentoxide eluent did not detect any vanadium present, and AA analysis of the final potassium solution did not detect any Sb or V present. Less than 1 ppm would have been detected. Only very small amounts of Be were detected by γ-ray spectrometry. The Sc and Ca radioactivities remaining in the Chelex 100 column were found to be quantitatively eluted with about 50 mls. of 1.0M HCl.

To illustrate the V-^{43}K separation procedure, a spectrum of an original target solution acquired a few days after irradiation is shown in Figure 34, with a detailed listing of the radioactivities observed given in Table XXVII. These can be compared to the final Chelex-100 eluent shown in Figure 35. The spectral illustration of the original solution depicts about 10 different radioactivities, while the final process solution contains peaks resulting from only potassium activities.

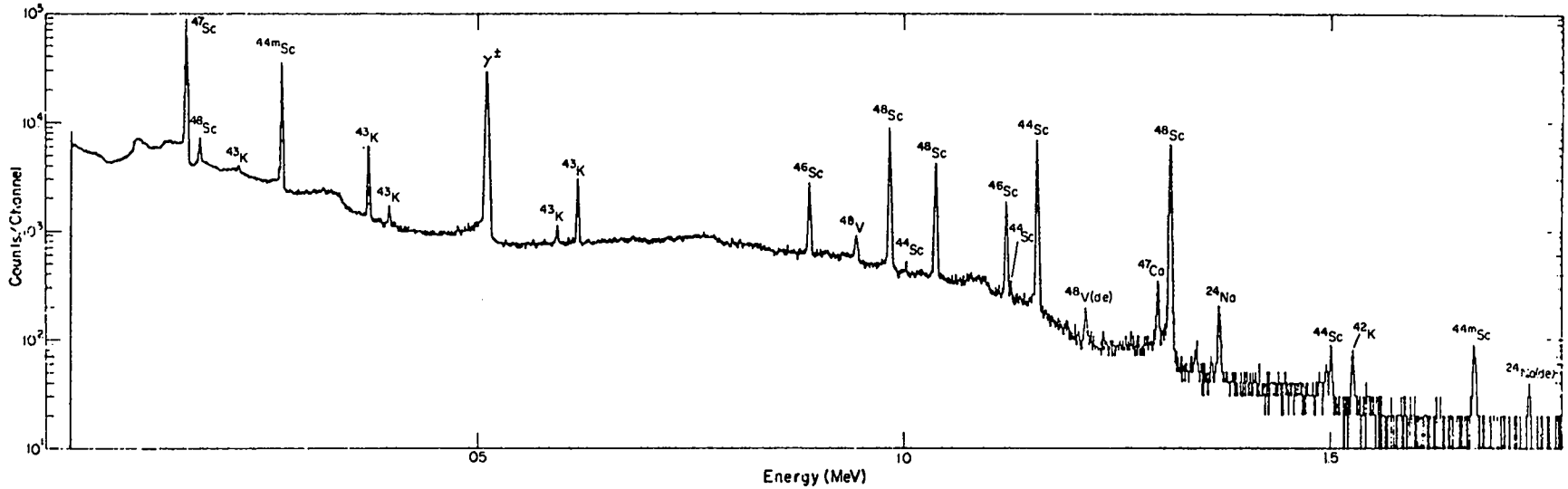

Figure 34. γ-Spectrum of the Original V Target Solution before Radiochemical Separation.

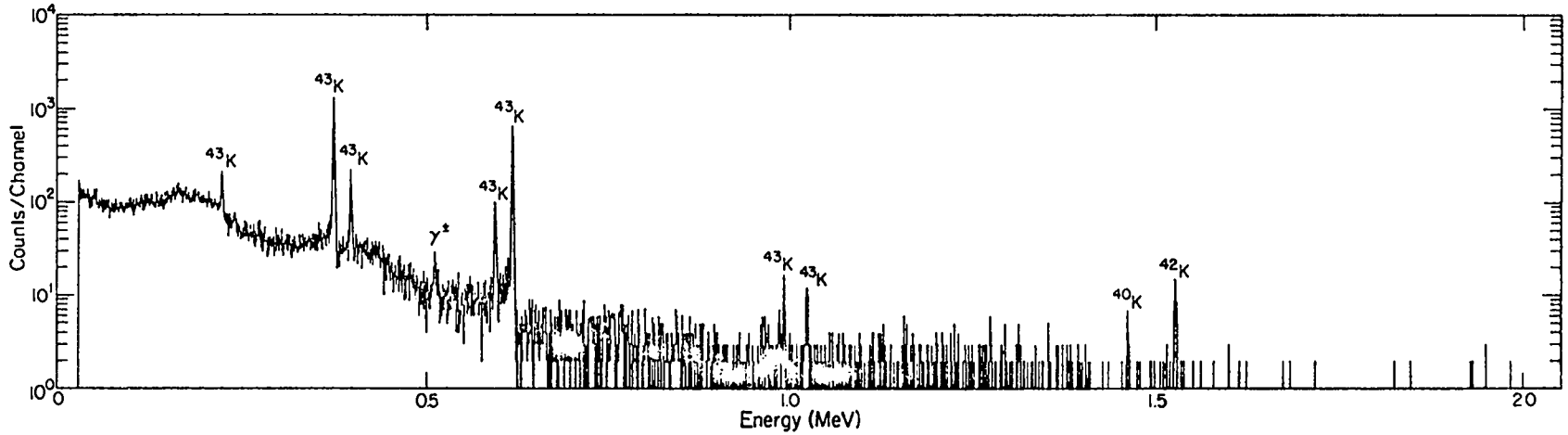

Figure 35. γ-Spectrum of the Final Radiopotassium Solution

Table XXVII

Radioactivities Observed in 800-MeV Proton-Irradiated V Targets

Z	A	Half-life	E_γ(KeV); Intensity(%)
V	48	16.0d	983.5(100%), 1311.9(97%)
Sc	48	1.83d	175.4(6%), 983.4(100%), 1037.5(100%), 1312.1(100%)
	47	3.43d	159.4(73%)
	46	83.9d	889.2(100%), 1120.6(100%)
	44m	2.44d	270.4(86%), 1667(0.2%)
	44	3.92d	1002.0(1.2%), 1126.2(1.2%), 1157.0(100%), 1499.0(0.92%)
Ca	47	4.53d	1297.1(76%)
K	43	22.3h	220.7(4.3%), 372.9(85%), 396.4(11%), 593.6(10%), 617.1(79%), 1022.0(2.3%)
	42	12.36h	312.4(0.18%), 1524.7(17.9%)
Na	24	15.00h	1368.6(100%), 2754.1(99.85%)
	22	2.60y	1274.5(99.95%)
Be	7	53.3d	477.6(10.3%)

3. Conclusion

The thin-target cross sections for producing ^{43}K and ^{42}K with 800-MeV protons were determined to be 6 mb and 11 mb, respectively, and a radiochemical procedure for the isolation of radiopotassium from targets bombarded with medium-energy protons has been developed.

Oak Ridge National Laboratory prepares ^{43}K by the $^{43}Ca(n,p)^{43}K$ reaction in the center-island hydraulic tube of the High Flux Isotope Reactor.[81] Targets consist of 400-600 mg of enriched ^{43}CaO(61% ^{43}Ca), and the irradiation length is usually about 66 hours. The ^{43}K yield at the end of the irradiation is about 0.085 mCi/mg of CaO (total yield ~50 mCi), and approximately four hours of process time are required before shipping. After processing and shipping, about 24 mCi of ^{43}K with a 10 to 12% ^{42}K content can be delivered.

The amount of ^{43}K and ^{42}K produced by a 0.5 mA beam of 800-MeV protons in a one-inch vanadium target for an irradiation time of 66 hours (at LAMPF) is calculated to be 80 curies and 160 curies, respectively, based on the cross sections determined in this work. After a waiting (and processing) period of five days about 2 curies of ^{43}K with ~10% ^{42}K contamination would be ready for immediate use.

The significance of this work is the development and demonstration of an alternative, high-yield method of preparing ^{43}K, which should have a major impact on the widespread utilization of this nuclide in cardiovascular diseases.

ACKNOWLEDGMENTS

The author wishes to express his appreciation to Dr. Jere D. Knight for his expert guidance and counsel during the course of this research. It has been a pleasure to be associated with a man of such high personal as well as scientific standards.

I wish to express my deep appreciation to Dr. Bruce Erdal for his most valuable guidance and aid. He has been an unceasing source of helpful suggestions throughout the course of these investigations.

My sincere appreciation is expressed to Dr. Jerry Wilhelmy for his willingness to provide computer programs for the theoretical excitation function calculations. I have also benefited greatly from the technical discussions and assistances of Jerry.

I would like to thank James Gilmore for being most helpful in decay scheme analysis problems and absolute counting techniques.

The author is greatly indebted to Dr. Patrick Grant and Dr. Harold O'Brien for their advice, guidance and inspiration.

My association with Dr. Robert Naumann and Dr. Milton Kahn has been most enjoyable and enlightening.

Dr. Victor Ryan deserves warm thanks for his guidance and advice throughout the course of this work.

I am very grateful for the help given to me by Dr. Silvio Balestrini, and I have enjoyed his friendship of the last two years.

My sincere thanks are expressed to all the members of Group CNC-11, LASL, in particular Dr. Kurt Wolfsberg, David Clinton, Dr. John Balagna, Dr. Allen Ogard, Dr. George Ford, T. Devon Baker, Alice Staritzky and Lynn Holmes.

I am extremely indebted to Dr. James Sattizahn and Dr. George Cowan for giving me the opportunity to do my dissertation research at LASL.

My appreciation is extended to the members of the Los Alamos Van de Graaff accelerator staff, in particular Mr. T. O. Gibson, Dr. R. V. Poore, Dr. J. W. Sunier and Mr. R. Woods.

The support during the last two years from the Atomic Energy Commission and Associated Western Universities is gratefully acknowledged. The assistance of Dr. G. Victor Beard and Emma Turley is greatly appreciated.

Finally and most important of all, I want to express my deep gratitude to Diane Casella for her essential assistance and her unfailing support throughout the course of this work.

REFERENCES

1. J. C. Cunnane and P. J. Daly, Phys. Rev. C 6, 1407 (1972).
2. A. Pakkanen, P. Puumalainen, H. Helppi and T. Komppa, Nucl. Phys. A206, 164 (1973).
3. M. Blann, Phys. Rev. Letters 21, 1357 (1968).
4. M. Blann and F. M. Lanzafame, Nucl. Phys. A142, 559 (1970).
5. R. Vandenbosch and J. R. Huezenga, Phys. Rev. 120, 1313 (1960).
6. E. Sandoval and E. Paez, Phys. Rev. 136, 415 (1964).
7. S. J. Nassif, E. Quel and J. Testoni, Nucl. Phys. 88, 344 (1966).
8. N. Chevarier, A. Chevarier, A. Demeyer and Tran Minh Duc, J. de Phys. 32, 483 (1971).
9. P. Jahn, H. Probst, A. Djaloeis, W. F. Davidson and C. Mayer-Boricki, Nucl. Phys. A209, 333 (1973).
10. Modification by B. R. Erdal of a program written by R. Gunnink, H. B. Levy and J. B. Niday, Univ. Calif. Lawrence Radiation Lab. Rep. No. UCID-15140(unpublished).
11. R. H. Moore and R. K. Zeigler, Los Alamos Scientific Laboratory Report LA-2367 (1960) (unpublished).
12. Modification by G. P. Ford of Los Alamos Scientific Laboratory Report LA-2367 Addenda (1963) (unpublished).
13. Modification by Silvio Balestrini of Los Alamos Scientific Laboratory Report LA-2367 (1960)(unpublished).
14. Williamson, Boujot and Picard, AEC Report No. CEA-R3042 (1966) (unpublished).

15. G. Friedlander and C. S. Wu, Phys. Rev. 63 228 (1943).

16. J. B. Cumming, U. S. Atomic Energy Commission Rep. No. NAS-NS-3107 (1963) (unpublished).

17. W. Bambynek, B. Crasemann, R. W. Fink, H. Freund, H. Mark, C. D. Swift, R. E. Price and P. V. Rao, Rev. Mod. Phys. 44, 716 (1972).

18. M. B. Lewis, Nuclear Data Sheets B7, 144 (1972).

19. G. Friedlander, J. W. Kennedy and J. M. Miller, Nuclear and Radiochemistry, Second Edition, John Wiley and Sons, Inc., New York, 1964. p 72.

20. H. Enge, Introduction to Nuclear Physics, Addison-Wesley Publishing Company, Inc., Reading, Massachusetts, 1966. p. 410.

21. M. P. Fricke and G. R. Satchler, Phys. Rev. 139, B567 (1965).

22. E. H. Auerback and S. O. Moore, Phys. Rev. 135, B895 (1964).

23. J. J. Griffin, Phys. Rev. Letters 17, 478 (1966).

24. K. Kikuchi and M. Kawai, Nuclear Matter and Nuclear Reactions, North-Holland Publishing Co., Amsterdam, 1968.

25. Computer Program written by Jerry Wilhemy, CNC-11, Los Alamos Scientific Laboratory (unpublished).

26. M. J. Martin, Nucl. Data Sheets B8, 432 (1972).

27. O. Huber, J. Halter, R. Joly, D. Maeder, and J. Brunner, Helv. Phys. Acta 26, 591A (1953).

28. O. Huber, R. Joly, P. Scherrer, and N. F. Verster, Helv. Phys. Acta 25, 621 (1952).

29. M. J. Martin, Nucl. Data Sheets B8, 462 (1972).

30. M. R. Schmorak, Nucl. Data Sheets B7, 409 (1972).

31. H. Ikegami, K. Sugiyama, T. Yamazaki, and M. Sakai, Nucl. Phys. 41, 130 (1963).

32. M. R. Schmorak, Nucl. Data Sheets B7, 408 (1972).

33. M. B. Lewis, Nucl. Data Sheets B7, 146 (1972).

34. Determined in this work by "4π" scintillation counting.

35. M. B. Lewis, Nucl. Data Sheets 137, 145 (1972).

36. Determined in this work by "4π" scintillation counting.

37. A. Pakkanen, P. Puumalainen, H. Helppi and T. Komppa, Nucl. Phys. A206, 165 (1973).

38. R. S. Hager and E. C. Seltzer, Nucl. Data A4, 161 (1968).

39. W. J. Keeler and R. D. Conner, Nucl. Phys. 61, 513 (1965).

40. R. L. Auble, Nucl. Data Sheets, B6, 329 (1971).

41. M. B. Lewis, Nucl. Data Sheets, B6, 366 (1971).

42. M. B. Lewis, Nucl. Data Sheets, B6, 370 (1971).

43. P. M. Endt and C. Van Der Leun, Nucl. Phys. A214, 1 (1973).

44. Alburger and Harris, Phys. Rev. 185, 1495 (1969).

45. M. E. Rose, in Alpha-Beta, and Gamma-Ray Spectroscopy, Volume 2, North-Holland Publishing Company, Amsterdam, 1965. p. 887.

46. M. G. Mayer, Phys. Rev. 78, 16 (1950).

47. A. Bohr and B. R. Mottleson, Kgl. Danske. Videnskab. Selskab. Mat. Fys. Medd., 27, No. 16 (1953).

48. S. G. Nilsson, Dan. Mat. Fys. Medd. 29, No. 16 (1955).

49. J. M. Blatt and V. F. Weisskopf, Theoretical Nuclear Physics, John Wiley and Sons, Inc. New York, 1952. p. 627

50. S. A. Moszkowski, in Alpha-, Beta-, and Gamma-Ray Spectroscopy, Volume 2, North-Holland Publishing Company, Amsterdam, 1965. p. 863.

51 Computer program 17, Los Alamos Van de Graaff Facility, written by Dr. R. V. Poore and Dr. J. W. Sunier.

52. W. Herzog and W. Grimm, Z. Physik 257, 424 (1972).

53. W. V. Prestwich, K. Fritze and T. J. Kennett, Nucl. Phys. 37, 45 (1962).

54. D. C. Kocher, Nuclear Data Sheets B8, 527 (1972).

55. J. D. Knight, D. C. Hoffman, B. Dropesky and D. L. D. L. Frasco, J. Inorg. Nucl. Chem. 10, 183 (1959).

56. R. S. Hager and E. C. Seltzer A4, 41 (1968).

57. B. M. Preedom, E. Newman and J. C. Hiebert, Phys. Rev. 166, 1156 (1968).

58. D. J. Hnatowich, E. Hagebo, A. Kjelberg, R. Mohr and P. Patzelt, J. Inorg. Nucl. Chem. 32, 3137 (1969).

59. B. Wannberg, J. O. Jonsson and L. Sanner, Physica Scripta 1, 238 (1970).

60. A. H. Wapstra, G. J. Nijgh and R. Van Lieshout, Nuclear Spectroscopy Tables, North-Holland Publishing Company, Amsterdam, 1959. p. 71.

61. A. Bohr and B. R. Mottelson, Nuclear Structure, Vol. I, W. A. Benjamin, Inc., New York, 1969. pp. 380-389.

62. H. A. O'Brien, Jr. and M. E. Schillaci, Los Alamos Scientific Laboratory Report No. LA-DC-11982 (1971) (unpublished).

63. H. A. O'Brien, Jr. and M. E. Schillaci, Isotop. Rad. Tech. 9, 105 (1971).

64. M. J. Martin and P. H. Blichert-Toft, Nuclear Data Tables 8, 68 (1970).

65. P. M. Grant, M. Kahn and H. A. O'Brien, Jr., J. Inorg. Nucl. Chem., in press.

66. S. R. Garcia, P. M. Grant and H. A. O'Brien, Jr., unpublished work.

67. K. A. Kraus and F. Nelson, Proceedings of the International Conference on the Peaceful Uses of Atomic Energy, Geneva, 1955.

68. R. Gunnink and J. Niday, Lawrence Radiation Laboratory Report No. UCRL-51061 (1971) (unpublished).

69. M. A. Wakat, Nuclear Data Tables A8, 445 (1971)

70. B. J. Dropesky and H. A. O'Brien, Jr. Los Alamos Scientific Laboratory Report LA-5120-PR (1972) (unpublished).

71. G. Friedlander, J. W. Kennedy and J. M. Miller, Nuclear and Radiochemistry, Second Edition, John Wiley and Sons, Inc. New York, 1964. p. 76.

72. J. C. Clark, M. L. Thakur and I. A. Watson, Int. J. Appl. Radiat. Isotop. 23, 329 (1972).

73. P. J. Hurley, M. Cooper, R. C. Reba, K. J. Poggenburg and H. N. Wagner, Jr., J. Nucl. Med. 12, 516 (1971).

74. J. Nucl. Med. 14, (Abstracts) 441, 443, 454, 458 (1973).

75. P. M. Endt and C. Van Der Leun, Nucl. Phys. A214 250 (1973).

76. J. Tabailen, Report No. CEA-N-1466(1) (1971) (unpublished).

77. F. Girardi, R. Pietra and E. Sabbioni, J. Radioanal. Chem. 5, 141 (1970).

78. F. Giardi and E. Sabbioni, J. Radioanal. Chem. 1, 169 (1968).

79. F. P. Treadwell, Analytical Chemistry Volume II. Quantitative, Ninth English Edition, John Wiley and Sons, New York, 1955. p. 494.

80. Bio-Rad Laboratories Chemical Division: Separating Metals Using Chelex 100 Chelating Resin, Technical Bulletin 114, 1972.

81. T. A. Butler, Oak Ridge National Laboratory, November, 1974 (private communication).

☆US GOVERNMENT PRINTING OFFICE 1974—677-177/31